Evolution of upper mantle beneath East Asia and the Tibetan Plateau from P-wave tomography

by

Chang Li

M.S. Geophysics, Peking University, Beijing, China, 2001
B.S. Geophysics, Peking University, Beijing, China, 1998

Submitted to the Department of Earth, Atmospheric, and Planetary Sciences
in partial fulfillment of the requirements for the degree of

Doctor of Philosophy

at the

MASSACHUSETTS INSTITUTE OF TECHNOLOGY

June 2007

Author:.....
Department of Earth, Atmospheric, and Planetary Sciences
May 4, 2007

Certified by: .....
Robert D. van der Hilst
Cecil and Ida Green Professor of Earth Sciences
Thesis Supervisor

Accepted by: .....
Maria Zuber
E. A. Griswold Professor of Geophysics
Head of the Department of Earth, Atmospheric, and Planetary Sciences

Abstract

The main objective of the research presented in this thesis is to improve our understanding for the evolution of the upper mantle beneath East Asia and the Tibetan Plateau through high resolution P-wave tomography. The approach to high resolution tomography is based on (i) the combined use of a large range of different types of seismic data, (ii) the use of approximate finite frequency sensitivity kernels to account for difference in measurement technique and frequency content of the data, (iii) the use of an irregular grid with cell-size adapted to sampling density, and (iv) the use of *a priori* information, e.g., on crustal structure from receiver function analysis. I construct a multi-scale and high resolution seismic tomography model of the upper mantle structure beneath East Asia and the Tibetan Plateau. The new model reveals that the mantle structure associated with the Indian subduction varies considerably along the strike of the collision zone. From west to east, the dip angle of Indian subduction increases and the distance over which the plate underthrusts the Tibetan Plateau decreases. Oblique subduction and changes of dip angle in the central part of the collision zone may cause and determine the location of the north-south trending normal faults in central Tibet. The eastward retreating slabs of western Pacific and Phillipine plates are deflected in the transition zone beneath the Korea, Japan Sea, and East China. Some of Mesozoic subducted slabs have reached as far west as 110°E longitude under the Yangtze Craton, which might have resulted from the Eocene subduction at the South China and Japan trenches. Precambrian continental roots under Ordos block and Sichuan Basin, which extend to 250~300 km depth, may form a boundary of transition in tectonic regimes from the India-Eurasia collision control in the southwest to Pacific, Philippine Sea, and Java-Sumatra subductions control in the east and southeast. I conclude that the (direct) influence of the India-Eurasia collision on the tectonic evolution of East Asia may be confined to the Tibetan plateau and vicinity, whereas the tectonic development of a large area east and southeast of Ordos, Sichuan and Burma is driven by the stress field and 3-D upper mantle processes associated with subductions of Pacific, Philippine Sea, and Indo-Australia plates.

Acknowledgements

Having spent more than five years at MIT I have much to acknowledge.

I would not have been able to complete this thesis without the supervision and support of Professor Robert D. van der Hilst. Rob has been and remains an insightful advisor and a very good friend. I am fortunate to work with him. I thank Prof. Nafi Toksöz, Clark Burchfiel, Leigh Royden, Stéphane Rondenay and Bradford Hager for many constructive discussions. I appreciate Prof. Bob Engdahl for his ongoing research on the EHB dataset and Dr. Ruomei Sun for sharing her data to us. Research support from the U.S. National Science Foundation is gratefully acknowledged.

The biggest harvest of my wife Xue and I was that our son Andrew (Haoming) came to our family last year. He brings lots of happiness to us and is our hope for the future. My deep gratitude goes to my parents-in-law and my parents. Without their help, it would have been impossible for us, two MIT students, to take care of a baby while pursuing PhD degrees.

Ping Wang and I are the first two Chinese students of Rob. We have been classmates for more than fifteen years since 1992 at Peking University. And Ji Li was my first roommate at MIT. The friendship with them and their family makes the greater Boston area a place to live rather than to work.

My appreciation also goes to my former and current officemates, Maureen Long and Erwan Mazarico. Maureen was my English teacher in speaking and writing. Erwan is a great guy to share an office with.

I thank my fellow students in the Green Building and ERL, Hrafnkell Kárason, Sergei Lebev, Frederik Simons, Einat Lev, Youshun Sun, Huajian Yao, Rongrong Lu, Chin-wu Chen, Scott Burdick, Kyle Straub and many more people who, through formal or casual interactions, helped shape and refine my ideas. I also thank the big Chinese community in EAPS and ERL.

I dedicate this work to my motherland, the People's Republic of China.

Contents

List of Figures

Chapter 1

Introduction

Abstract

The high resolution P-wave tomography is crucial for understanding large scale three dimensional (3-D) tectonic evolution of East Asia. This thesis improves the resolution of P-wave tomography by combining the P-wave travel times from global and regional catalogs as well as temporary array networks and using advanced methodology. In this chapter, I summarize the general motivation of this study and the main content of the thesis.

1.1 Motivation

East Asia is a tectonically diverse and active region. There is ongoing subduction of the Western Pacific and Philippine Sea plates with east-direction slab rollback in the east and continental collision between Indian and Eurasian plates in the west. These geodynamics systems form a large scale clockwise rotation in East Asia. The tectonics of East Asia was affected and continues to be shaped by this large scale 3-D flow/rotation in the upper mantle. The Tibetan plateau was generated by the collision and subsequent convergence of the Indian plate into the Eurasian plate beginning about between 50 and 65 million years ago. The plateau is bounded by the deserts of the Tarim Basin to the north, the Himalayas, Karakoram, and the Pamirs mountain chains to its south and west, but its eastern margin is more diffuse. Following the India-Eurasia collision, the crust

under the central and northern parts of the Tibetan Plateau has approximately doubled in thickness to its current thickness of ~70 km, while its elevation has increased by ~4-5 km (Molnar and Tapponnier, 1975; Coward *et al.*, 1988; Dewey *et al.*, 1988).

The Cenozoic Tibetan Plateau has long been regarded as a natural laboratory for studies of continental dynamics. Over the last two decades, a series of key observations of various disciplines from the plateau and surrounding areas have given us a basic concept of how the convergence between Indian and Eurasian plates is being accommodated and the mechanism for having crustal thickness of the Tibetan Plateau nearly twice as thick as most continental crust. Beneath southern Tibet, a weak, probably partially molten, mid-crustal layer has been produced by crustal thickening and behaves as a fluid on the time scale of Himalayan deformation (INDEPTH II, Nelson *et al.*, 1996). Within large parts of the eastern plateau and its margins, crustal thickening has occurred without appreciable shortening of the upper crust (Burchfiel *et al.*, 1995; Wang *et al.*, 1998). Geodynamic modeling suggests that crust at the margins of the plateau is thickened from below by differential flow of the lower and middle crust from the central portions of the plateau towards the margins, rather than shortening and thickening by thrusting in the upper crust (Clark and Royden, 2000).

However there are still many controversies regarding the dynamics of collision (Tapponnier *et al.*, 1982; England and Houseman, 1988; Houseman and England,

1993; Chemenda *et al.*, 2000; Clark and Royden, 2000). In all these models the upper mantle structure and its relationship with the crust are enigmatic. Especially, how far and how deep the Indian lithosphere subducts northward under the Tibetan Plateau is largely unknown. Moreover, the large scale high wavespeed anomalies in the lower mantle and their relationship to regional dynamics remain enigmatic (Van der Voo *et al.*, 1999). Indeed, in order to understand the large scale lithosphere dynamics of East Asia, we need to consider 3-D mantle processes associated with both the continental collision in the west and the subduction of Pacific and Philippine Sea slabs in the east. However the resolution of existing seismic models is not sufficient enough to reveal the interaction between these dynamics systems.

The general motivation of this research is threefold. First, I want to improve our capability for flexible, high resolution tomographic imaging of the lithosphere and the upper mantle. Second, I want to apply this new technique to spectacular new data sets in order to delineate mantle heterogeneity at different length scales beneath East Asia, in general, and beneath the Tibetan Plateau, in particular. Third, along with the evidence from seismicity, geochemistry, and geology, the new models will be used to investigate the tectonics and geodynamics of the geographical region under study.

I- high resolution seismic tomography. The increasing access to seismological data from dense (temporary and permanent) regional seismograph networks, on

the one hand, and the desire to image structure from a global to a regional and local scale, on the other hand, call for more powerful approaches to tomographic imaging than is currently available. Resolving structure on a large range of length scales requires the integration of (independent) *a priori* knowledge of the structure and the use of data from a range of different seismic phases. Our study will build and expand our expertise on travel time tomography (that is, in the future the constraints from travel times need to be integrated with information from surface wave propagation, but that is beyond the scope of this thesis in part because 3-D models from surface wave tomography are currently of much lower resolution than our P-wave model). In particular, I need to be able to (1) add independent constraints when they become available (e.g., the constraints on crustal structure from receiver function analysis and/or active source reflection experiments), and (2) adapt our model if new data sets become available. Our approach to high resolution tomography will be based on (i) the combined use of a large range of different types of seismic data, both from global catalogs as well as from provincial or temporary seismograph networks, (ii) the use of approximate finite frequency sensitivity kernels to account for differences on measurement technique, (iii) the use of an irregular grid with cell-size adapted to sampling density, and (iv) the use of *a priori* information, e.g., on crustal structure from receiver function analysis.

The envisaged improvements have general applicability: they have enabled high resolution of the upper mantle beneath North America using USArray data, and companies like Shell are interested in our approach for "first order exploration" of remote regions that may have promise for future development. Here, however, our prime interest is to improve the constraints on understanding the 3-D structure of the upper mantle beneath East Asia and the Tibetan Plateau.

II- Mantle structure beneath East Asia and the Tibetan Plateau. The main motivation for improving our tomographic method is to make better use of *a priori* information and various new seismological data sets for the construction of a detailed seismic tomography model of the crust and upper mantle structure beneath East Asia and, in particular, the Tibetan Plateau. For this effort I can use several unique data sets. First, with automated procedures I picked the arrival time from temporary seismic arrays in and near the Tibetan Plateau. They are the MIT array in the eastern margin of the plateau; Lehigh university array in southeastern Tibet; Sino-American PASSCAL experiment in central Tibet; arrays from International Deep Profiling of Tibet and the Himalayas (INDEPTH) project and Himalayan Nepal Tibet Experiment (HIMNT) in the southern plateau (Appendix I). Furthermore, through collaborating with Chinese scientists, I have gained access to the wealth of teleseimic and regional data recorded (since 1967) at ~1200 stations of the Chinese Seismography Network (CSN). With these unique data sets I have constructed a higher resolution model than is currently available. Indeed,

inversion of this data set could revolutionize our knowledge of the upper mantle structure beneath East Asia.

III- Improved understanding of tectonics and dynamics evolution of East Asia and the Tibetan Plateau. The large scale geological features and upper mantle structure of East Asia are influenced by two large scale geodynamic systems: the eastward rollback of the subducted slabs beneath the western Pacific and Philippine arcs in the east, and the collision of the Indian continental lithosphere with the continental Eurasia in the west. By delineating the upper mantle structure and in combination with results from other lines of research (e.g., field mapping, seismicity and geochemistry studies), our tomographic models can provide key constraints on effects and relative roles of these geodynamic systems.

With the improved tomographic models I can address several questions:

a) On the large-scale, what is the effect on tectonic features in East Asia of India-Eurasia collision in the west and the subduction of Pacific and Philippine slabs in the east? What is the structure of the upper mantle of East Asia between these two geodynamic systems?

b) How far northward does the Indian mantle lithospheric mantle subduct beneath the Tibetan Plateau? How deep does it go? When and where did it break off with the old oceanic slabs ahead of it? And what is their significance for tectonic evolution of the Tibetan plateau?

c) What is the structure of curst and upper mantle beneath the eastern Tibetan Plateau and surrounding regions? Is the mantle lithosphere beneath the eastern plateau strong or weak as compared to the overlying crust? Is there correlation between mantle structure and surface deformation and active fault systems?

1.2 Thesis structure

After the introduction in this chapter, a global model for P wavespeed variations in Earth's mantle is presented in Chapter 2. I generally describe whole datasets and methodology of this research and focus on a large scale structure of Earth's mantle, such as slab, upwelling, and upper mantle structure beneath continents.

In Chapter 3, I explore in detail how to design and implement an accurate and efficient correction for crust structure that we cannot resolve with the data used (Li *et al.*, 2006) and zoom in the global P-wave model beneath the southeastern Asia.

In Chapter 4, I focus on the upper mantle structure beneath the Tibetan Plateau and surrounding regions. I investigate the Indian subduction beneath Himalayas and Burma, low velocity anomalies beneath Tengchong volcanic area and Red River fault/Ailao Shan range, and high velocity anomaly beneath the Sichuan Basin. The relationship between the Indian lithospheric subduction in the upper mantle and Tethys oceanic slabs in the lower mantle also have been investigated

In Chapter 5, I construct a large scale 3-D picture for the evolution of East Asia's upper mantle through high resolution P-wave tomography. I emphasize the large scale clockwise rotation set up by the continental collision in the west and slab rollback in the east and their relationship with recent tectonic processes in East Asia.

The conclusions of this thesis are presented in Chapter 6. Our understanding for the mantle evolution of East Asia, in general, the Tibetan Plateau, in particular is summarized. Future work related to this research is discussed.

With the exception of Chapter 1 and 6, each of the body chapters of this thesis is written for separate publications. As such, there is some unavoidable overlap among the papers. Chapter 2 will be submitted to *Geochemistry, Geophysics, Geosystems* and Chapter 3 has been published at *Physics of Earth Planetary Interior*. Chapter 4 is in preparation for submission to *Earth and Planetary Sciences Letters* and Chapter 5 is in preparation for submission to the *Journal of Geophysical Research.*

References

Burchfiel, B.C., Chen, Z., Liu, Y., and Royden, L.H., 1995, Tectonics of the Longmen Shan and adjacent regions, Central China: International Geology Review, 37, no. 8, 661-736

Chemenda A.I., Burg J.P., Mattauer M., 2000. Evolutionary model of the Himalaya -Tibet system: geopoembased on new modelling, geological and geophysical data. Earth and Planetary Science Letters: 174, 397-409.

Clark M.K. and Royden L.H., 2000. Topographic Ooze: Building the Eastern Margin of Tibet by Lower Crustal Flow, Geology, 28, 703-706.

Coward M.P., Kidd W.S., Shackleton R.M., Zhang H., 1988, The structure of the 1985 Tibet Geotraverse, Lhasa to Golmud; in Chang C., Shackleton R.M., Dewey J.F. and Yin J., (eds) The Geological Evolution of Tibet: Phil. Trans. R. Soc. London, A 327, 207-336.

Dewey J., Shackleton R.M., Chang C., Sun, Y., 1988. The tectonic evolution of the Tibetan Plateau; In Chang C., Shackleton R.M., Dewey J.F. and Yin J., (eds) The Geological Evolution of Tibet: Phil. Trans. R. Soc. London, A 327, 379-413.

England P.C. and Houseman G.A., 1988. The mechanics of the Tibetan Plateau: Philosophical Transactions of the Royal Society of London A, 326, 301-320.

Houseman G.A. and England P.C., 1993. Crustal thickening versus lateral expulsion in the Indian-Asian continental collision, JGR, 98, 12233-12249.

Li, C., van der Hilst, R.D., and Toksöz, M.N., 2006. Constraining spatial variations in P-wave velocity in the upper mantle beneath SE Asia, Phys. Earth Planet. Inter., 154, 180-195.

Molnar P. and Tapponnier P., 1975. Cenozoic tectonics of Asia: Effects of a continental collision. Science, 189, 419-426

Nelson K.D., et al., 1996. Partially Molten Middle Crust Beneath Southern Tibet: Synthesis of Project INDEPTH Results, Science, 274, 1684-1688.

Replumaz A. and Tapponnier P., 2003. Reconstruction of the Deformed Collision Zone Between Indiaand Asia by Backward Motion of Lithospheric Blocks, JGR, 108(B6), 2285.

Tapponnier P, Peltzer G, Le Dain AY, Armijo R, Cobbold P. 1982. Propagating extrusion tectonics in Asia: new insights from simple experiments with plasticine. Geology 10: 611-16

Van der Voo R, Spakman W, Bijwaard H. 1999. Tethyan subducted slabs under India. Earth Planet. Sci. Lett. 171: 7-20

Wang, E., Burchfiel, B.C., Royden, L.H., Chen, L., Chen, J., and Li, W., 1998, Late Cenozoic Xianshuihe-Xiaojiang and Red River fault systems of southwestern Sichuan and central Yunnan, China: Geol. Soc. America Special Paper 327, 108 pases

Chapter 2

A new global model for P wavespeed variations in Earth's mantle[1]

Abstract

We present a new global tomographic model of three dimensional (3-D) variations in mantle P-wave velocity. The model is parameterized by means of rectangular cells in latitude, longitude, and radius, the size of which reflects the density of sampling by high frequency travel times. The main data source is short period (1 Hz) *P*, *Pn*, *pP* and *pwP* from the catalogue by *Engdahl et al.* (1998), which is based on phase arrival information reported to the International Seismological Centre (ISC) during 1964~2004 with phases re-identified and earthquakes re-located. In order to improve the resolution in the deepest mantle we use short period (1Hz) differential times of core phases, PKP_{DF} - PKP_{AB} and $PKP_{BC} - PKP_{AB}$ and a low frequency (50mHz) dataset of P_{diff} - PKP_{DF} (*Wysession, 1996*). Furthermore we use low frequency *PP-P* differential times (*Woodward and Masters, 1991*) to improve the resolution in the upper mantle under the region with few stations and low seismicity. Approximate 3-D finite frequency kernels are used to integrate the long period data (P_{diff}, *PP*) and short period (*P*, *pP*, *PKP*) data. This global data set is augmented with several regional catalogs and temporary seismic arrays. These include the Chinese Seismography Network and temporary arrays in Tibet and Australia. We implement a crust correction to avoid crustal smearing into the upper mantle. In inversion, we use the iterative LSQR method with norm and gradient regularization. Spatial resolution is ~100 km in

[1] Li, C., van der Hilst, R.D., and Engdahl, E., A new global model for P wavespeed variations in Earth's mantle, in preparation for submission to Geochemistry, Geophysics, and Geosystems.

best sampled upper mantle regions. The model reveals relatively narrow fast structures around mid-mantle depths that have been linked to ancient subduction zones, and display varying styles of subduction in the upper mantle. The model shows upwelling structures beneath hotspots, such as Iceland and Hawaii.

2.1 Introduction

Global tomography has been producing spectacular images of the Earth's interior structure and it provides increasingly detailed constraints on the mantle structure and the nature of the mantle (see reviews by, e.g., *Dziewonski and Woodhouse, 1987; Masters, 1989; Montagner, 1994; Dziewonski, 1996; Kárason and van der Hilst, 2000; Fukao et al., 2001; Trampert and van der Hilst, 2005*). Although increasingly consistent spatial patterns of wavespeed variations on the large scale have emerged, at length scales less than ~1000 km conspicuous discrepancies still exist. These differences limit our understanding of large scale geological processes. The need of high quality tomographic models continues to drive improvement of inversion technique as well as data coverage adequacy.

With ever increasing quality and quantity of seismic data from global and regional seismograph networks and temporary array deployment, global tomography now resolves structure in the Earth's mantle with unprecedented high resolution. In this paper, we present a new global P-wave model. Compared with our old model (*van der Hilst et al., 1997; Kárason and van der Hilst, 2001*) and other P-wave global models (*Zhao, 2004; Montelli, et al., 2004*), we increase the resolution by using: (1) updated global datasets of seismic waves (*P, PP, pP, PKP,*

Pdiff) that sample Earth's mantle in different ways; (2) data from regional networks and temporary seismic arrays; (3) 3-D sensitivity kernels to account for effects of different frequencies – also *Montelli et al. (2004)* did this; (4) an adaptive parameterization to enhance resolution locally – also *Kárason and van der Hilst (2001)* did this; and (5) a correction that reduces the artificial mapping of crustal heterogeneity into the upper mantle.

As an example of the multi-scale aspect of our global tomography, Figure 2-1a shows P wavespeed variations on the global scale at 100 km depth, and Figure 2-1b shows a zoom-in of the global model to illustrate structure beneath eastern Tibetan Plateau and southwestern China, along with relief topography and major active fault systems. Locally, fine structures in the upper mantle have been resolved thanks to the addition of regional networks. As another example of high resolution that can be attained locally, Figure 2-1c depicts slabs of subducted lithosphere under South America. With more data from regional networks and temporary arrays, multi-scale mantle structure resolved by global tomography can help us to further understand the evolution of tectonic processes.

2.2 Data

We use travel time residuals with respect to the reference model *ak135* (*Kennett et al.*, 1995). We use 3 types of data: 1) routinely processed travel times picked from global networks; 2) differential times measured by waveform cross-

correlation; and 3) phases arrivals at regional networks and temporary arrays. The number of phase data is summarized in Table 1. The catalogue of *Engdahl, van der Hilst* and *Buland* (1998) (hereinafter referred to as the EHB dataset) is the largest single source of routinely processed global data. *Engdahl et al.* used arrival times reported to the international Seismographic Centre (ISC) and calculated travel-time residuals by the non-linear earthquake re-location and phase re-identification. The global data coverage by the EHB is augmented by data from regional networks and temporary arrays that do not report to the ISC. Figure 2-3A shows global distribution of stations in the combined dataset.

Phases	# records	# comp. ray	Cent freq.	Forw. Mod.	Source
P	9.4×10^6	2.7×10^6	1 HZ	Rays	EHB
Pn	1.2×10^6	1.8×10^5	1 HZ	Rays	EHB
Pg	9.8×10^5	3.7×10^4	1 HZ	Rays	EHB
pP and *pwP*	6.8×10^5	3.7×10^5	1 HZ	Rays	EHB
PKP_{AB}-$PKP_{DF/BC}$	2.3×10^5	8.8×10^4	1 HZ	Rays	EHB
PKP_{AB}-$PKP_{DF/BC}$	1,383	N/A	1 HZ	Rays	McSweeney
PKP_{diff}-PKP_{DF}	543	N/A	50 MHZ	Kernels	Wysession
PP-P	20,266	N/A	40 MHZ	Kernels	Masters
P	4.7×10^5	2.2×10^5	1 HZ	Rays	CSN+Array
Pn	6,600	3,300	1 HZ	Rays	CSN+Array

Table: Data source: EHB: *Engdahl et al. (1998)* (EHB); McSweeney: *McSweeney (1995)*; Wysession: *Wysession (1996)*; Masters: *Woodward and Masters (1991)*; CSN: *Chinese Seismography Network*; Array: *arrays in Tibet and Australia.*

2.2.1 Routinely processed travel times (the EHB dataset)

The EHB dataset is regularly updated and previous versions have been used in regional (e.g. *van der Hilst et al., 1991; Li et al., 2006*) and global studies (e.g., *van der Hilst et al. 1997; Widiyantoro, 1997; Bijwaard et al., 1998; Kárason and van der Hilst, 2000, 2001; Zhao, 2004*). The EHB dataset used here contains about

ten million travel time residuals associated with more than four hundred thousand well constrained regional and teleseismic earthquakes from 1964 to 2004 (see Table 1 and Figure 2-2b, c, and e). From the EHB catalog, we use *P*, *pP* and *pwP* (for details see *van der Hilst et al., 1991; van der Hilst and Engdahl, 1991; van der Hilst et al., 1997*) and *PKP* (*Kárason and van der Hilst, 2001*), and - for the first time - *Pg* and *Pn* (Figure 2-2c). The *Pg* phase propagates in the crust and gives more constrains on shallow structure. In the EHB catalogue, *P* phases with turning points less than 410 km are labeled as '*Pn*'. In order to select turning rays and omit *Pn* proper (that is, the 'head wave'), we use phases labeled as '*Pn*' in the EHB (and treated it as a turning P-wave) only if their focal depths are larger than 80 km or if their turning points are larger than 100 km depth. The depth phase *pP* bounces off Earth's surface and *pwP* propagates also through water and bounces off the surface of the ocean. Following *Kárason and van der Hilst (2001)*, we use the EHB *PKP* data for records that have two or more *PKP* arrivals so that the construction of differential times ($PKP_{DF} - PKP_{AB}$ or $PKP_{BC} - PKP_{AB}$) is possible. This appears to be a good quality control because most of *PKP* arrivals can only be seen on the later quality data, but - as a consequence - only a fraction of the available EHB *PKP* data is used. In particular, we do not use PKP_{DF} beyond a distance of ~150°; they do not add much to the sampling of the deepest mantle and they are sensitive to inner core structure and anisotropy. To complement the EHB dataset, we also used high frequency *PKP* differential travel times (Mc*Sweeney*,

1995) measured by cross-correlation of the observed *PKP* waveform with a synthetic signal calculated from theoretical predictions.

The ray coverage could be improved further by including later arriving phases from the EHB, but since most of them are harder to read in the coda, they are typically much noisier and the improved coverage would merely give a false impression of improved resolution, because the so-called checkerboard tests that are often used to assess (qualitatively) resolution do not account for realistic errors in the data. For this reason, we do not use EHB data of *PcP* and *PP*. Instead, to complement the EHB dataset we use waveform based differential times that were carefully measured, for instance, by cross-correlation, from digital records.

2.2.2 Waveform based differential times

To improve the sampling of deep mantle structures we use PKP_{DF} - P_{diff} differential times (*Kárason and van der Hilst, 2001*). These data are measured at relatively low frequency (central frequency ~0.05 Hz) by *Wysession* (1996). The P_{diff} phases are diffracted along the core-mantle boundary (CMB) and their differential travel time residuals are very sensitive to structure near the base of the mantle (*Kárason and van der Hilst, 2001*).

To increase our ability to resolve structures in the upper mantle of intra-plate regions with few earthquakes and stations, we use long period *PP-P* data, measured at a frequency ~0.04 Hz. The measurement is made by cross-correlating the Hilbert transform of *P* arrival with the *PP* arrival while accounting for attenuation (*Woodward and Masters, 1991*).

2.2.3 Regional networks and temporary arrays (e.g., PASSCAL)

Data from regional networks and temporary arrays are not always reported to the ISC, but have much potential for improving resolving of the upper mantle structure. As a specific example of the former, we augmented the EHB dataset with data from the Chinese Seismography Network (CSN). This produces a large amount of data at stations not represented in the standard ISC catalogs (Figure 2-3B, C), while data from stations already in the EHB dataset were removed.

As an example of the latter, we add data from arrays in Tibet and Australia. Data from the temporary arrays of the SKIPPY project (van der Hilst *et al.*, 1994) helps resolve the upper mantle structure under Australia. These data was already used in the previous global inversion (van der Hilst *et al.*, 1997). For temporary arrays on the Tibetan Plateau, we measured P-wave travel time using a phase picker designed by *Aldersons* (*2003*). After the station and ellipticity correction to the raw data, we incorporate the new residuals into the EHB dataset with the earthquake re-location (*Engdahl et al., 1998*).

2.3 Methodology

2.3.1 Ray tracing, composite rays, and weighting

The center frequency of the routinely processed travel time data is ~1 Hz, and for the linearized tomographic inversion we back-project the data along ray paths calculated in the one dimensional (1-D) *ak135* reference model for mantle P-wave

speed (also see, *Nolet, 1987; Spakman and Nolet, 1988*). For the EHB dataset, we use weighted composite rays to reduce the size of the sensitivity matrix. To balance the small, but high quality waveform datasets against the much larger, but noisier EHB dataset we give them extra weights (*Kárason and van der Hilst, 2001*).

2.3.2 Sensitivity kernels

Ray theory is not appropriate for the long period data that are measured by waveform cross-correlation (*Dahlen et al., 2000*; *De Hoop and van der Hilst*, 2005), such as differential travel times P_{diff}-PKP_{DF} and *PP-P* here. For these data we use 3-D sensitivity kernels, which effectively smoothes the part of the model space constrained by the low frequency data without degrading the resolution in regions of dense sampling by high frequency data.

The core-diffracted P_{diff} is an evanescent wave and the magnitude of the associated particle motion, consequently the sensitivity to structure decreases with increasing distance from the interface. This decay is frequency dependent. To account for this in the inversion we distribute the sensitivity over a finite mantle volume. The sensitivity kernels for the P_{diff} phase are calculated from normal model theory to estimate for exact kernels (*Zhao and Jordan, 1998; Zhao et al., 2000*). The resulting kernels show that the sensitivity is distributed over a large irregularly shaped volume (Figure 2-4a). Following the work by *Kárason and van der Hilst (2001)*, we project the 3-D kernels onto the basis function used for model parameterization.

For the low frequency *PP-P* differential time we follow *Kárason (2002)* and use single scattering theory to calculate kernels as shown in Figure 2-4b; we only include the first *Fresnel* zone with the maximum sensitivity at the geometrical ray and assume the travel time sensitivity to structure is zero outside the first *Fresnel* zone. Figure 2-4b depicts the absolute travel time surfaces for *P* and *PP*, respectively. The yellow surface represents the first *Fresnel* zone calculated from the dominant frequency of the *PP-P* data. The differential *PP-P* kernel is obtained by subtracting the *P* from the *PP* kernel. We project 3-D kernels onto the constant slowness cells (2.8° by 2.8° by 90 km) and then interpolate them on adaptive grids that are used to parameterize the mantle.

Montelli *et al.* (2004) use Banana-Doughnut kernels for the inversion of long period *PP-P* data. However *De Hoop and van der Hilst* (2005) and *van der Hilst and De Hoop* (2006) argue and show that the effect of the use of such kernels is small. Indeed, from a series of inversions we concluded that, with the current data coverage, the actual distribution of sensitivity over the *Fresnel* zone is of little importance. Therefore we implement the 'fat' ray here with the maximum sensitivity is at the geometrical ray.

2.3.3 Adaptive parameterization

The uneven sampling of mantle structures by seismic waves results in significant lateral variations in resolution. The use of a regular grid would either over-parameterize poorly sampled regions (also be computationally inefficient) or average out small scale structures. An advantage of use of local basis functions is

that they can be adjusted to expected resolution *(Abers and Roecker, 1991; Bijwaard et al., 1998)*. We follow *Kárason and van der Hilst (2000)* to construct an adaptive parameterization scheme on the basis of sampling density (hit counts). In this algorithm, adaptive grid is assembled of one or more cells from the base grid to reach the ray density criterion in each cell. The base grid is approximately 0.7° in latitude and longitude and 45 km in depth throughout the mantle. The maximum size of adaptive grid is less than the wavelength of long period data to assure the resolution for the large scale structures resolved by the low frequency data.

2.3.4 Crust correction

The small incidence angles of teleseismic P-waves may map unresolved crustal heterogeneity to larger depths in the model. Following *Li et al. (2006, Chapter 3)*, we correct for crustal structure by means of regularization to an *a priori* 3-D crustal model. We select the global CRUST 2.0 (*Bassin et al., 2000*) combined with higher resolution regional models where available as the *a priori* 3-D crustal model. Addition to the simplicity of implementation, the correction in the model space can balance the crust and upper mantle contribution to a misfit and recover the big velocity variations in the *a priori* crustal model. Furthermore, later addition of data with complex ray path, such as *PP* phase or updates of the reference crust model, does not require further calculations since all are accounted for in the model space.

2.3.5 Regularization and inversion

As in our previous studies, we apply a combination of norm damping, which tends to minimize the amplitude of the model, and gradient damping, which produces smooth variations, both laterally and radially. We perform experiments with synthetic data from known input models to find appropriate values for the damping parameters, but the choice of the parameters remains subjective. In inversion, the norm damping is small. We keep the gradient damping in the radial direction as small as possible to reduce the vertical smearing. We also account for effects of earthquake mislocation on the travel time residuals. We use the iterative method *LSQR* (*Paige and Saunders, 1982*) to minimize the objective function. The results presented here were obtained after 200 iterations, even for LSQR most of the convergence is achieved within a small number of iterations.

2.4 Results

Figure 2-5 depicts the P wavespeed variations at selected depths in the mantle. The new results are consistent with earlier studies (e.g. *van der Hilst et al., 1997; Kárason and van der Hilst, 2000, 2001)* but locally show more detail. At shallow depths, slow back arc regions and fast subduction zones as well as craton signatures are prominent. The model is marked by long and narrow traces of fast material from the upper mantle transition zone to mid-mantle depths beneath North, South America and southern Asia. These structures have been associated with plate motion history and are thought to be the remnants of old subducted

slabs (*van der Hilst et al., 1997; Grand et al., 1997*). As noticed before, e.g. *Su and Dziewonski (1992)*, at a few hundred kilometers above the CMB, long wavelength structures emerge.

In many regions the data resolve structure on much smaller scales than can be appreciated from the global perspective in Figure 2-5, but a comprehensive discussion of the new model is beyond the scope of this paper. Here we just present a few examples to illustrate the new model.

2.4.1 Improvement in the upper mantle

In this section, we compare the new model (referred to as MIT-P07) with our previous model (referred to as MIT-P02) and current P-wave travel time model using the finite-frequency sensitivity kernels (updated from *Montelli et al. 2004*, referred to as PRI-P06) in the shallow upper mantle (at 150 km) beneath East Asia and North America (Figure 2-6).

Compared to MIT-P02, MIT-P07 has a significant improvement in upper mantle beneath East Asia owing to data from Chinese Seismograph Network (CSN) and temporary Tibetan arrays (Figure 2-3C, see also Chapter 4). The new model reveals more detail in the upper mantle, which generally correlate well with geological processes (A1 and B1 in Figure 2-6). For example, the high velocity anomalies are located beneath the Himalaya and the southwestern margin of the Tibetan Plateau, associated with the subducted Indian lithosphere. The moderate low velocity anomalies are prominent beneath most of the Tibetan Plateau. The pronounced high velocity anomalies are dominant beneath the Precambrian

Sichuan Basin. Although the general pattern of MIT-P07 and PRI-P06 is similar (B1 and C1 in Figure 2-6), MIT-P07 has significantly higher resolution and reveals more interesting structures.

The improvement in upper mantle beneath North America is not as much as beneath East Asia (A2 and B2 in Figure 2-6) because fewer new data were added. The high velocity anomalies beneath the Rocky Mountains in the new model are stronger than before; but in general MIT-P02 and MIT-P07 are very close to each other. PRI-P06 does not resolve the high velocity anomalies in the upper mantle beneath the Rocky Mountains and the west coast of North America (C2 in Figure 2-6).

2.4.2 Several subduction zones

As in our previous models (*van der Hilst et al., 1997; Kárason and van der Hilst, 2000, 2001)*, the slabs are well resolved in the new model because the ray coverage from intensive earthquakes in subduction zones is very dense. We illustrate this for four active subduction systems in Figure 2-7.

In Figure 2-7a, we display cross sections through Central and South American arcs. Sections (1)-(3) show variations in the upper mantle part of the slabs from north to south. In section (1) the subducted slab seems connected to the surface, deflected in the transition zone, but disconnected from the high velocity anomalies in the lower mantle. In contrast, in section (2) and (3) the slabs continue into the lower mantle but there is somewhat of a detachment with lithosphere at the surface. (see also *van der Hilst 1990; van der Hilst and Engdahl 1991; Engdahl et*

al, 1995). Section (4) reveals the deep part of the slab and suggests that subduction has been going on for a long time (see also *van der Hilst et al. 1997; Grand et al., 1997*). Section (5) reveals an interesting subduction pattern beneath Caribbean Sea. In the east, the slab stays in the upper mantle with a western dip angle. In contrast, the slab in the west continues into the lower mantle with an eastern dip angle (*van der Hilst, 1990*). In South America (section (6) to (9)), intervals of detached and continuous slabs are observed and seem to be fairly well resolved. As is the case for the southern Hemisphere in general, the resolution deteriorates when going south and the subducted slab beneath south sandwich island is poorly resolved (section (10)).

In Figure 2-7b, we show continuous subduction in the western Pacific Ocean, which stretches from the Kamchatka Peninsula in the north, through the Kuril islands and Japan, and ends south in the Mariana Trench. The style of subduction varies dramatically along these trenches and is consistent with previous studies (*see also, van der Hilst et al., 1991; Fukao et al., 1992; Fukao et al., 2001*). In the north, the slab is rather steep and seems directly connected to lower mantle structures and some earthquakes reached to the boundary of upper and lower mantle (section (11), (12)). To the south, the dip angle gradually decreases to ~30^{o} for central Japan and the slabs appear largely stagnant in the mantle transition zone (section (13)-(15)). The stagnant slabs seem to extent far beyond the *Wadati-Benioff* zone defined by seismicity and go further to the east coast of China (Section (14), (15)). Further south, the subduction of Pacific and Philippine Sea

plates at the Izu Bonin and Ryukyu trenches, respectively, are clearly visible (section (16)). Both of them are stagnant in the mantle transition zone. The stagnant slabs subducted from the Izu Bonin trench are much more than that subducted from the Ryukyu trench (section (16)). Further towards the Mariana Trench, the vertical slab seems to sink directly into the lower mantle and lose the connection to the surface (section (17)) (See detailed discussion in the Chapter 5).

In Figure 2-7c, we show Andaman-Sumatra subduction system (*see also Widiyantoro and van der Hilst, 1996; Replumaz et al. 2004*). The subduction zones beneath the Celebes Sea (section (21)) and through the Philippine trench (section (22)) are more clearly defined in the new model and reach down to the lower mantle. Beneath Indonesia the subduction is continuous to larger depth (section (19), (20)), with an up to 1000 km thick mass of fast material in the lower mantle. To the northwest the accumulation in the lower mantle becomes less and the slab becomes steeper but seems to be confined to the upper mantle and the mantle transition zone (section (18)).

In Figure 2-7d, we show major circum Pacific Ocean subduction systems.

2.5 Discussion

2.5.1 Resolution of large scale structures

In Figure 2-8 we show results of the checkerboard resolution test. The input pattern has a half wavelength of ~5° and the constant amplitude of 1.5% in the

upper half of the mantle. In the lower half of the mantle, the half wavelength is ~10°. This way the real length (500-600km for half wavelength) of input pattern is similar for near-surface and lowermost mantle. The input structure was put in each depth at a time. Noiseless synthetic travel times were created and inverted using the same inversion scheme as used in constructing the model.

Although the resolution is still spatially limited in the upper mantle due to the uneven distribution of stations and zones of active seismicity, we recovered more input fields in the upper mantle than before owing to more samplings from regional networks and low-frequency *PP-P* differential data (Figure 2-8a,b). However, due to the scarcity of stations, large areas beneath the Southern Hemisphere are poorly resolved at all depths. The input pattern is better recovered several hundred kilometers above the CMB owing to the high quality core phase data. The amplitude of the recovery is significantly less than that of the input structure, even where the pattern is retrieved well, mainly because we implement a relatively high damping to suppress the large noises in the datasets.

2.5.2 Resolution tests for slabs

In Figure 2-9, we show some target resolution tests to assess the resolution in several selected slabs. The left column displays four randomly selected slabs in the model (cross sections (5), (9), (15), (20) in Figure 2-7). In order to investigate how much anomalies in the upper mantle could be smeared into the lower mantle, we set velocity anomalies in the lower mantle at zero and keep the anomalies in the upper mantle unchanged (the middle column in Figure 2-9). With the synthetic

tests, we find that the amplitude of the recovery will be decreased about 50%. In order to mimic the real smearing effect, we set the input signal in the upper mantle at 1.5 times the amplitude of that in the global model. We also input a big positive anomaly in the lower mantle (cross section (20)) to asses our ability to resolve slabs in the lower mantle.

We calculate the synthetic data multiplying the same sensitive matrix (that is, forward propagation) as in the real data inversion with the input model. Then we implement the same damping factors to invert the synthetic data. The recovery model is shown in the right column in Figure 2-9. In general, we recover most of input signals, especially the slabs where the ray coverage is dense. The amplitude of recovery is typically decreased about 50% compared to the input signal. This implies that the real amplitude of velocity anomalies in the Earth might be about 50% larger than what we observe in the model. The smearing effect in the lower mantle is very small compared to the amplitude we observed in the model. The input signal in the lower mantle (cross section (20)) can also be recovered very well. This indicates that the high velocity anomaly in the lower mantle is not an artifact due to smearing of strong anomalies in the upper mantle, which supports the interpretation that some slabs have directly sunk into the lower mantle.

2.5.3 Upwelling structures in the upper mantle

We resolve the upwelling structures beneath hotspots such as Iceland, Hawaii, and Yellowstone. However, due to relatively sparse sampling, the resolution

beneath hotspots is generally low. Here we show resolution tests beneath Iceland (Figure 2-10) and Hawaii (Figure 2-11).

Pronounced low velocity anomalies beneath Iceland are only visible in the upper mantle (Figure 2-10a). To test if with the data used we could resolve part of a deeper structure, we generated synthetic data from an input column anomaly of negative 2% amplitude, from the surface down to 1700 km depth (Figure 2-10b). With current data coverage, we have no ability to resolve most of the low velocity anomaly input in the lower mantle (Figure 2-10c). The main reason is that most stations are located in Iceland. With this limited station aperture, the ray paths of earthquakes in Europe and North America do not sample the upper part of the lower mantle. Thus, we cannot exclude the existence of deep mantle plumes beneath Iceland. Deploying more Ocean Bottom Seismometers in the Atlantic Ocean would help address this issue.

In our model, a low velocity anomaly is also detected beneath Hawaii. The main anomaly is confined in the upper mantle and the amplitude is relatively small compared to that of Iceland (Figure 2-11A1, B1). In the upper part of the lower mantle, a low velocity anomaly appears beneath the west of Hawaii (Figure 2-11 B1; Figure 2-5e). The model also shows the low velocity anomaly in a few hundred kilometers above the CMB beneath the north of Hawaii (Figure 2-11A1 and Figure 2-5j). We implement the same resolution test as for Iceland. With the current data coverage, we cannot resolve the input field in the lower mantle (Figure 2-10A3, B3). Thus, we cannot reject the low velocity anomaly in the lower

mantle. The more high quality data from the permanent stations and Ocean Base Seismometers is required to further explore the low velocity anomalies in the upper mantle under Hawaii.

2.5.4 Velocity anomalies above the CMB

In Figure 2-12, we compare the lower-most mantle parts of MIT-P07, MIT-P02, PRI-P06 and recent shear wave model (updated from *Grand (2002)*, referrer to as Grand-S06). The general pattern of the different models is similar. Pronounced high velocity anomalies are beneath Asia, western Pacific Ocean, and North America. Low velocity anomalies prevail beneath central Pacific Ocean, Africa and east Atlantic Ocean. However, controversies on small scale remain in the different models. For example, the low velocity anomalies are located beneath southern Africa in the PRI-P06 model, beneath east Atlantic Ocean in the MIT-P07 model, and beneath both regions in the Grand-S06 model.

We assess our resolution beneath southern Africa with a synthetic test. The column input field -2.0% velocity anomalies extends upward ~600 km from the CMB (the left column in Figure 2-13). The recovery patterns are shown in the right column of Figure 2-13. The input field is well recovered, especially at the bottom of the mantle. This indicates that we can resolve the low velocity anomalies at the bottom of the mantle under southern Africa if any. Our model suggests that there might be no strong low African supper plume from the CMB. Instead, a large area low velocity anomalies prevail at the bottom of the mantle under east Atlantic Ocean.

2.6 Conclusions

More high quality data and advances in methodology play equally important role in improving the resolution in the global tomographic model. To improve sampling, we augment our dataset with both more P-wave data from the regional networks and temporary arrays and more seismic phases that are sensitive to different parts of the mantle. To treat low frequency datasets properly, we apply a practical calculation for the 3-D sensitivity kernels. The results prove that this method is appropriate for the current datasets. More sophisticated theory and calculation is needed for the refined datasets in the future (*De Hoop and van der Hilst, 2005; Tromp et al., 2005; Dahlen et al., 2000*). Variable resolution has allowed us to extract more from our current data. We believe that this model is well balanced with respect to the different data sets and, in the aggregate, a significant improvement over our previous models.

The new model is available at http://quake.mit.edu/hilstgroup/robspage/ftp.

Acknowledgements:

This work would not have been possible without the data generously providing by Gay Masters, Michael Wysession, Tom Mcsweeney, and Ruomei Sun. This research is funded by NSF grant 6892042.

References:

Abers, G.A. and Roecker, S.W., 1991, Deep-structure of an arc-continent collision: Earthquake relocation and inversion for upper mantle P and S wave velocities beneath Papua New Guinea, *J. Geophys. Res.*, 96, 6379-6401.

Aldersons, F., Ben-Avraham, Z., Hofstetter, A., Kissling, E., and Al-Yazjeen, T., 2003. Lower-crustal strength under the Dead Sea basin from local earthquake data and rheological modeling. *Earth Planet. Sci. Lett.*, 214 (1-2), 129-142.

Bassin, C., Laske, G., and Masters, G., 2000. The Current Limits of Resolution for Surface Wave Tomography in North America, *EOS Trans AGU*, 81, F897.

Bijwaard, H., Spakman, W., and Engdahl, E.R., 1998. Closing the gap between regional and global travel time tomography. *J. Geophys. Res.*, 103 (B12): 30055-30078.

Dahlen, F., Hung, S.-H., and Nolet, G., 2000. *Frechet* kernels for finite-frequency traveltimes–I. Theory. *Geophys. J. Int.*, 141, 157–174.

De Hoop, M. and Van der Hilst, R., 2005. On sensitivity kernels for 'wave equation' Tomography. *Geophys. J. Int.*, 160, 621–633.

Dziewonski, A.M. and Woodhouse, J.H., 1987. Global images of the Earth's interior. *Science*, 236, 37-48.

Dziewonski, A.M., 1996. Earth's mantle in three dimensions, in: Boschi, E. et al. (Editors), Seismic modeling of Earth structure, Instituto Natzionale di Geofisica, Rome, pp. 507-572.

Engdahl, E.R., van der Hilst, R.D. and Berrocal, J., 1995. Imaging of subducted lithosphere beneath South America. *Geophys. Res. Lett.*, 22, 2317-2320.

Engdahl, E.R., van der Hilst, R.D., and Buland, R., 1998. Global teleseismic earthquake relocation with improved travel times and procedures for depth determination. *Bull. Seism. Soc. Am.*, 88, 722-743.

Fukao, Y., Obayashi, M., Inoue, H., and Nenbai, M., 1992. Subducting slabs stagnant in the mantle transition zone. *J. Geophys. Res.*, 97, 4809-4822.

Fukao, Y., Widiyantoro, S., and Obayashi, M, 2001. Stagnant slabs in the upper and lower mantle transition region. *Rev. Geophys.*, 39, 291-323.

Grand, S.P., 2002. Mantle shear-wave tomography and the fate of subducted slabs. Philosophical Transactions of the Royal Society of Engineering Sciences 360 (1800): 2475-2491.

Grand, S.P., van der Hilst, R.D., and Widiyantoro, S. 1997. Global seismic tomography: A snapshot of convection in the earth, *GSA Today*, 7, 1-7.

Gudmudsson O. and Sambridge M., 1998. A regionalized upper mantle (RUM) seismic model, *J. Geophys. Res.*, 103, 7121-7130.

Kárason, H. and van der Hilst R.D., 2000. Constrains on mantle convection from seismic tomography, in History and Dynamics of Plate Motion, Geophys. Monogr. Ser., vol. 121, edited by Richards M.A., Gordon R., and Van der Hilst R.D. pp. 277-288, AGU, Washington, D.C..

Kárason, H. and van der Hilst, R.D., 2001. Tomographic imaging of the lowermost mantle with differential times of refracted and diffracted core phases (PKP, Pdiff), *J. Geophys. Res.*, 106, 6569-6588.

Kárason, H., 2002. Constrains on mantle convection from seismic tomography and flow modeling, Ph.D. thesis, 228 pp., M.I.T., Cambridge, MA, USA.

Kennett, B.L.N., Engdahl, E.R., and Buland, R., 1995. Constrains on seismic velocities in the Earth from travel times. *Geophys. J. Int.*, 122, 108-124.

Li, C., van der Hilst, R.D., and Toksöz, M.N., 2006. Constraining P-wave velocity variations in the upper mantle beneath Southeast Asia. *Phys. Earth Planet. Inter.*, 154, 180-195.

Masters, G., 1989. Low frequency seismology and the three-dimensional structure of the Earth. Philos. Trans. R. Soc. Lond. A, 328, 479-522.

McSweeney, T.J., 1995. Seismic constraints on core structure and dynamics, Ph.D. thesis, Univ. of Wash., Seattle.

Montelli, R., Nolet, G., Dahlen, F.A., Masters, G., Engdahl, E.R., and Hung, S.H., 2004. Finite-frequency tomography reveals a variety of plumes in the mantle. *Science*, 303 (5656): 338-343.

Montagner, J.P., 1994. Can seismology tell us anything about convection in the mantle? *Rev. of Geophys.* 32 (2): 115-137.

Nolet, G., 1987. Seismic wave propagation and seismic tomography, in Seismic tomography, with Application, in Global Seismology and Exploration Geophysics, edited by Nolet G., pp 1-27, Reidel D., Norwell, Mass..

Paige, C.C., and Saunders, M.A., 1982. LSQR: an algorithm for sparse linear equations and sparse least squares. *ACM Trans. Math. Soft.* 8, 43–71.

Replumaz, A., Kárason, H., van der Hilst, R.D., Besse, J., and Tapponnier, P., 2004. 4-D evolution of SE Asia's mantle from geological reconstructions and seismic tomography. *Earth Planet. Sci. Lett.*, 221 (1-4): 103-115.

Spakman, W. and Nolet, G., 1988. Imaging algorithms, accuracy and resolution in delay time tomography, in Mathematical Geophysics: A survey of Recent Developments in Seismology and Geodynamics, edited by Vlaar N.J., pp. 155-188, Reidel D., Norwell, Mass..

Su W.J. and Dziwonski, A.M., 1992. On the scale of mantle heterogeneity, *Phys. Earth Planet. Inter.*, 74, 29-54.

Tromp, J., Tape, C., and Liu, Q., 2005. Seismic tomography, adjoint methods, time reversal and banana-doughnut kernels. *Geophys. J. Int.*, 160, 195–216.

Trampert, J. and van der Hilst, R.D., 2005. Towards a quantitative interpretation of global seismic tomography, in: van der Hilst R.D., Bass J., Matas J., Trampert J. (Editors), Earth's Deep Mantle: Structure, Composition, and Evolution, American Geophysical Union, Washington, pp. 47-62.

Widiyantoro, S. and van der Hilst, R.D., 1996. Structure and evolution of lithosphere slab beneath the Sunda arc, Indonesia, *Science*, 271, 1566-1570.

Widiyantoro S., 1997. Studies of seismic tomography on regional and global scale, Ph.D. thesis, 256 pp., Aust. Nat. Univ., Canberra.

Wysession, M.E., 1996. Large-scale structure at the core-mantle boundary from diffracted waves. *Nature*, 382 (6588): 244-248.

Woodward, R.L. and Masters, G., 1991. Global upper mantle structure from long-period differential travel-times. *J. Geophys. Res.*, 96 (B4): 6351-6377

Van der Hilst, R.D., 1990. Tomography with P, PP and pP delay time data and the three dimensional mantle structures below the Caribbean region, Ph.D. thesis, Utrecht University.

Van der Hilst, R.D., Engdahl, E.R., Spakman, W., and Nolet, G., 1991. Tomographic imaging of subducted lithosphere below northwest Pacific island, *Nature*, 353, 37-43.

Van der Hilst, R.D. and Engdahl, E.R., 1991. On ISC PP and pP data and their use in delay-time tomography of the Caribbean region, *Geophys. J. Int.*, 106, 169-188.

Van der Hilst, R.D., Kennett, B.L.N., Christie, D., and Grant, J., 1994. Project SKIPPY explores the lithosphere and mantle beneath Australia, *Eos Trans. AGU*, 75, 177-181.

Van der Hilst, R.D., Widiyantoro, S., and Engdahl, E.R., 1997. Evidence for deep mantle circulation from global tomography, *Nature*, 386, 578-584.

Van der Hilst, R.D. and De Hoop, M.V., 2006. Reply to comment by R. Montelli, , G. Nolet, and F. A. Dahlen on "Banana-doughnut kernels and mantle tomography", *Geophys. J. Int.*, 167, 1211-1214.

Zhao, L. and Jordan, T.H., 1998. Sensitivity of frequency-dependent travel times to laterally heterogonous, anisotropic Earth structure. *Geophys. J. Int.*, 133, 683-704.

Zhao, L., Jordan, T.H., and Chapman, C.H., 2000. Three-dimensional Frèchet differential kernels for seismic delay times. *Geophys. J. Int.*, 141 (3): 558-576.

Zhao, D., 2004. Global tomographic images of mantle plumes and subducting slabs: insight into deep Earth dynamics. *Phys. Earth Planet. Inter.*, 146, 3-24.

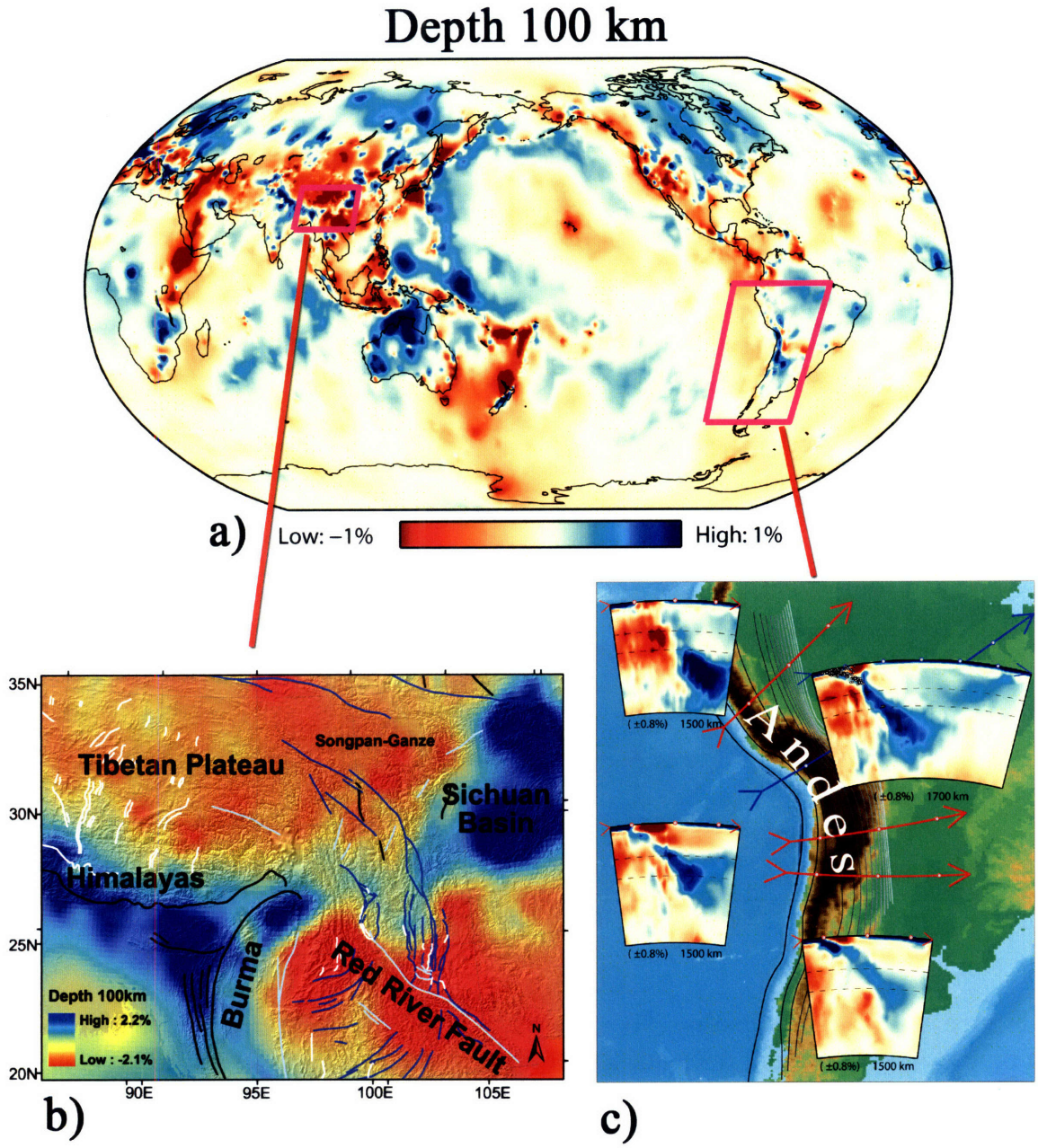

Figure 2-1. Multi-scale global tomography. a) Global P-wave velocity variations at 100 km depth. b) Regional wavespeed heterogeneity at 100 km in eastern Tibetan plateau and southwestern China with topography and major active faults, where black, white, blue and grey lines represent thrust, norm, left strike slip, and right strike slip faults respectively. c) Four cross-sections down 1500 km depth through the Andean subduction zone in South America. The dash lines on images represent 410 km and 660 km discontinuities. Gray circles in the blue cross-section show earthquake distribution. Grayscale contours display the outline of the subduction zone, as defined by slab-related seismicity (Gudmundsson and Sambridge 1998).

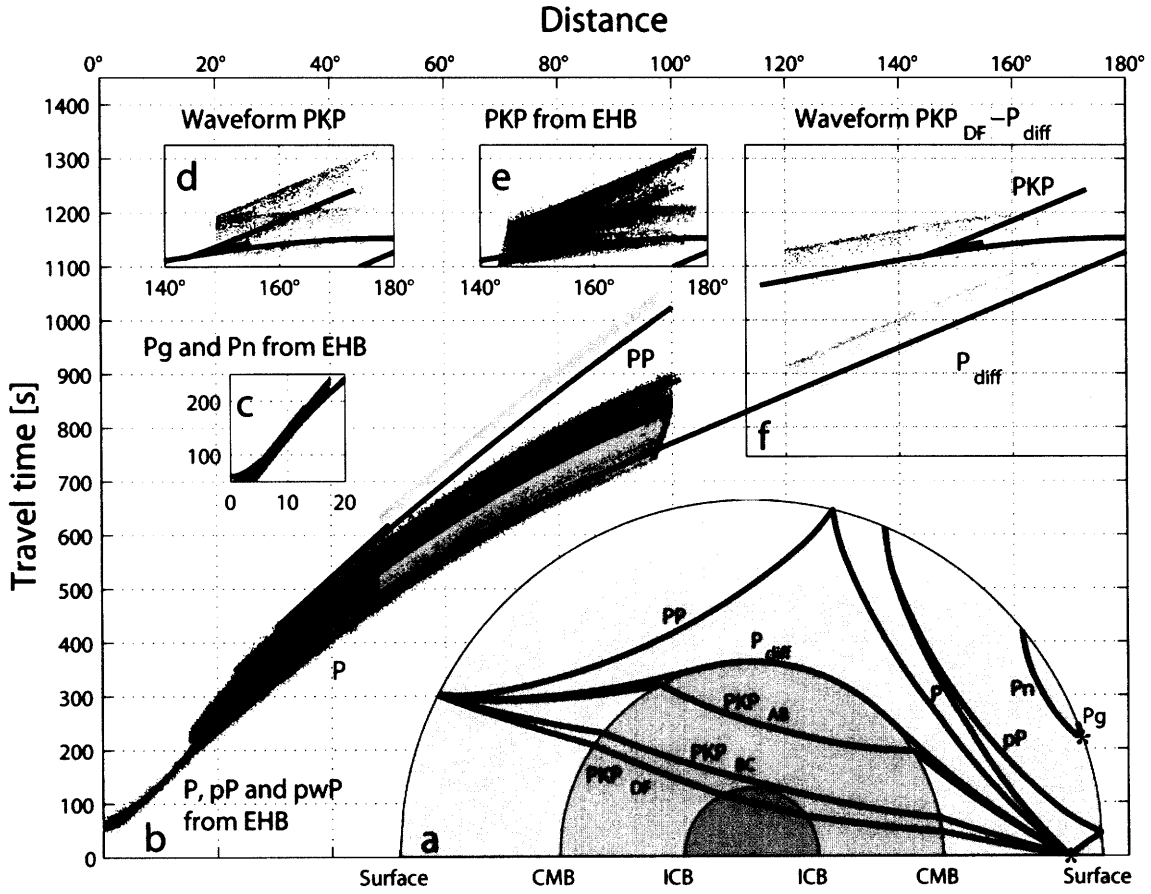

Figure 2-2. a) Ray paths. The red stars represent sources. '*P*' is the direct compression wave and does not travel through the core. '*pP*' is up-going from the source while '*PP*' is down-going, both bounce once off the Earth's surface. '*Pg*' propagates in the curst. We define '*Pn*' as having a focal depth larger than 80 km or a turning point deeper than 100 km. 'PKP_{AB}' and 'PKP_{BC}' travel through the outer core, while 'PKP_{DF}' travels both through the outer and inner cores and '*Pdiff*' grazes the core. b) Theoretical travel time versus distance curves (solid lines). Also shown are scatter plots for *P* (light shading) and *pP* (dark shading) from EHB and waveform *PP* (light shading). c) *Pg* and *Pn* from the EHB. d) Waveform $PKP_{AB} - PKP_{DF/BC}$. e) $PKP_{AB} - PKP_{DF/BC}$ from the EHB. f) Waveform PKP_{DF} - *Pdiff*.

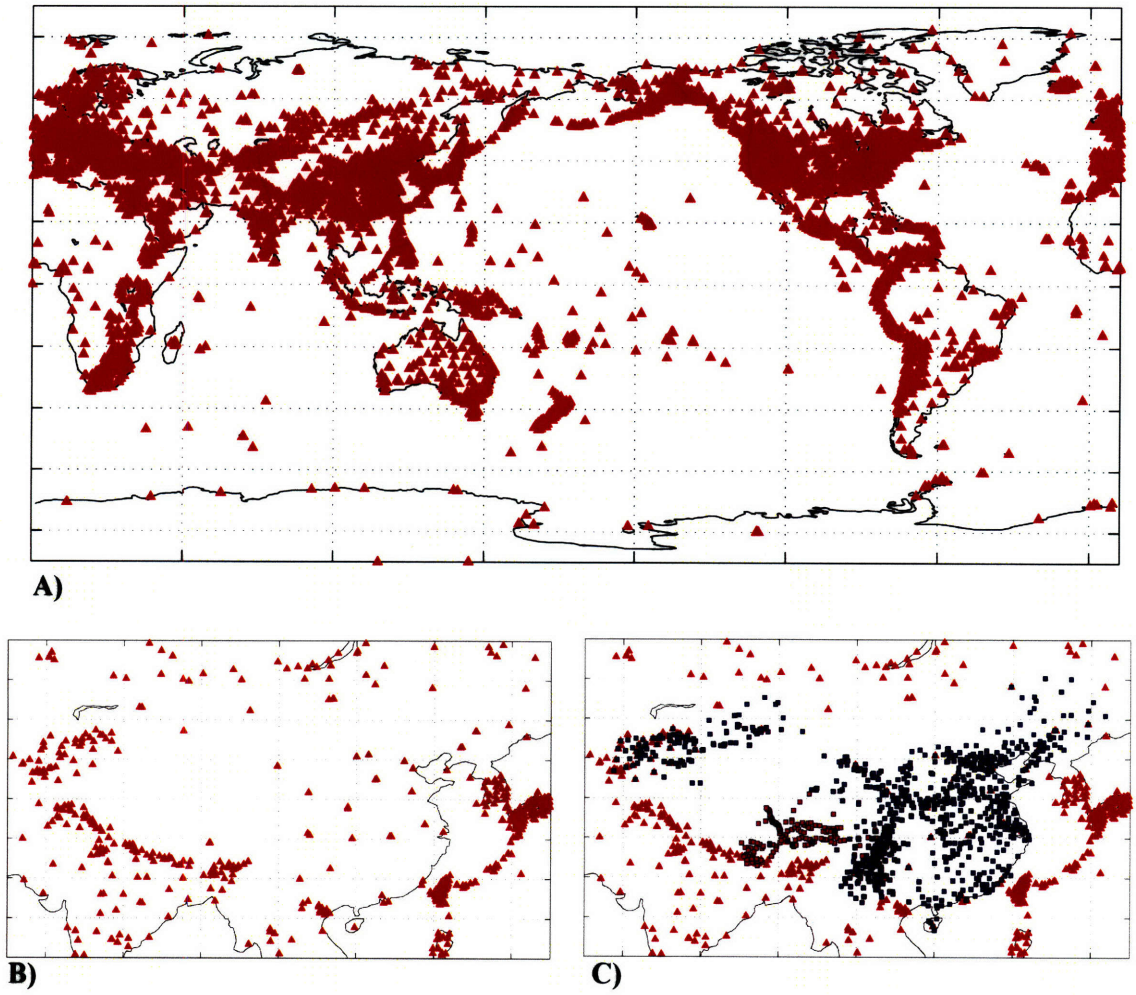

Figure 2-3. A) Global distribution of stations (red triangles) B), C) Station coverage before and after adding data from Tibetan arrays (magenta squares) and Chinese Seismography Network (blue squares).

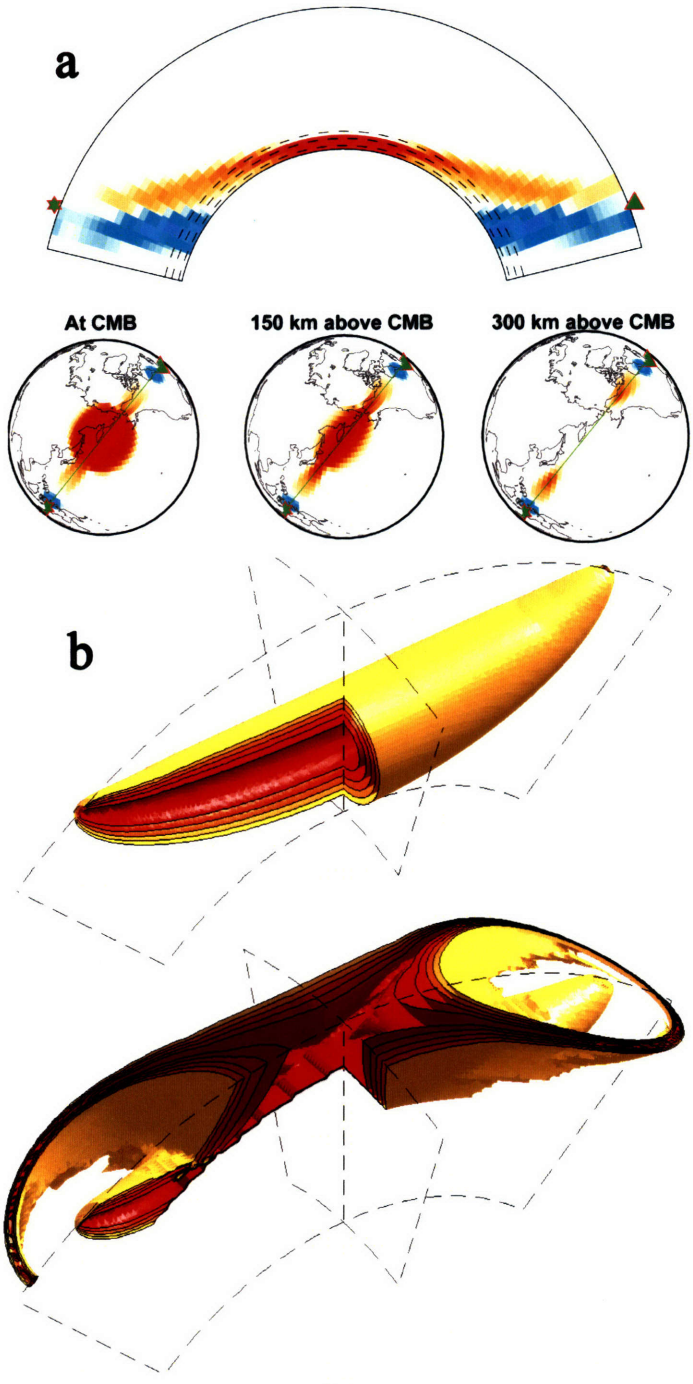

Figure 2-4. 3-D finite frequency kernels. a) Sensitivity to slowness variations within the Earth for low frequency $PKP_{DF} - P_{diff}$ differential times. Red and blue indicate negative and positive sensitivities, calculated by subtracting P_{diff} from PKP_{DF}. b) Surfaces representing constant travel time deviations, using single scattering for *P* and *PP* respectively. One quadrant is cut out to see the interior of the 3-D kernels. Redder colors correspond to smaller travel time deviations. We assume zero sensitivity outside of the yellow surface which represents the first *Fresnel* Zone.

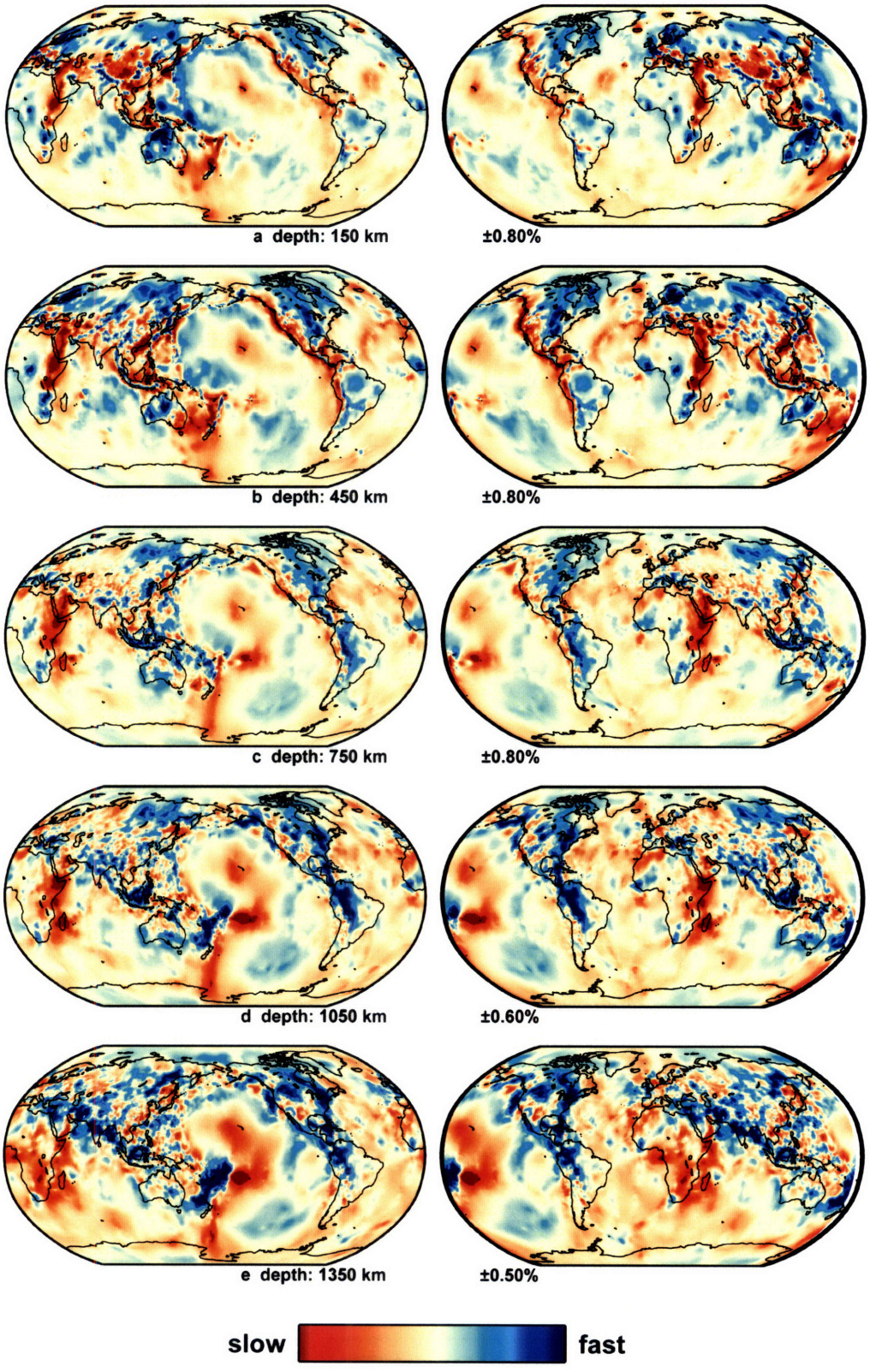

Figure 2-5. Global P wavespeed heterogeneity at several selected depths with the Robinson projection centered on the Pacific Ocean (left column) and on Africa (right column).

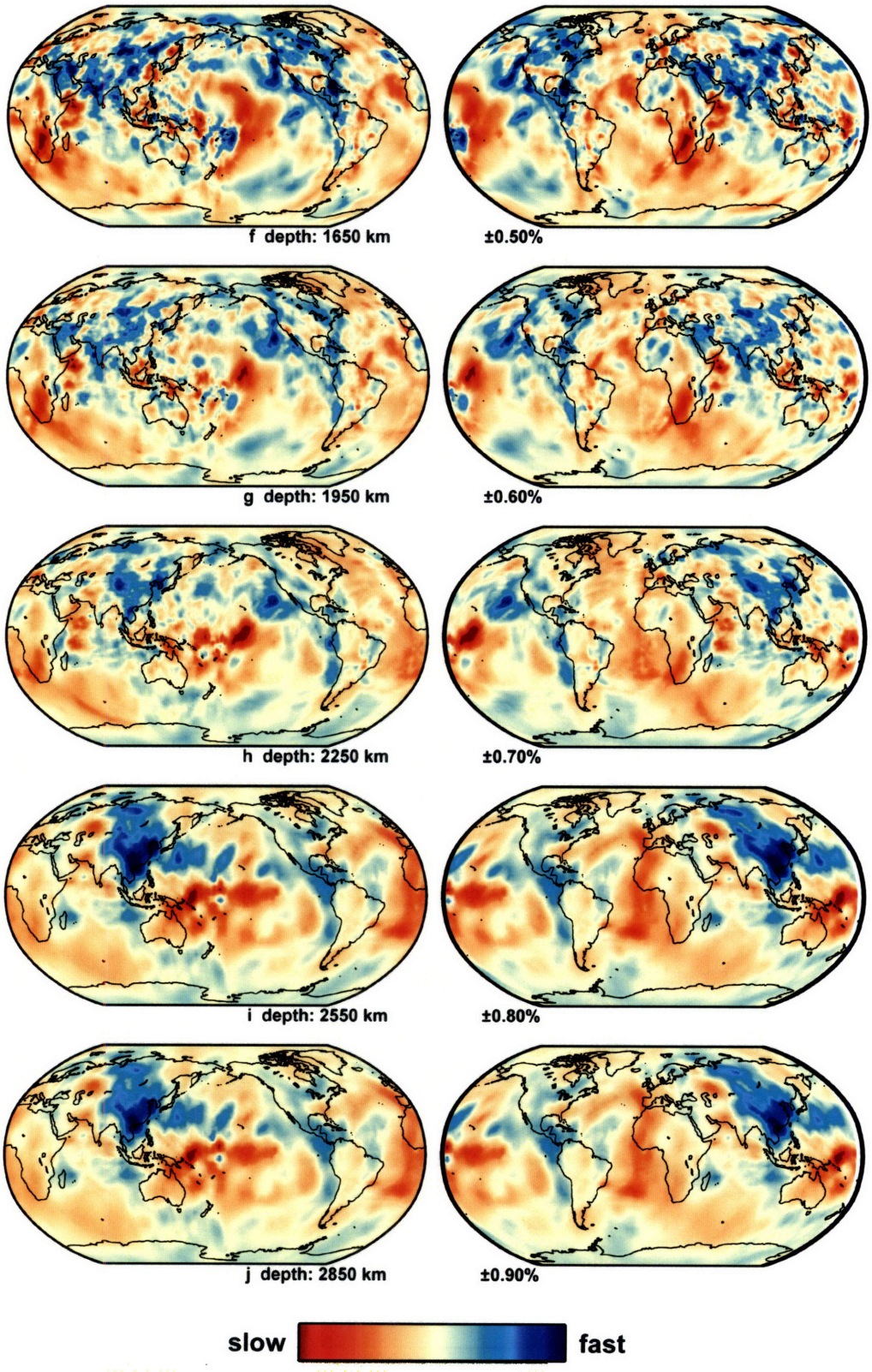

Figure 2-5. Continued.

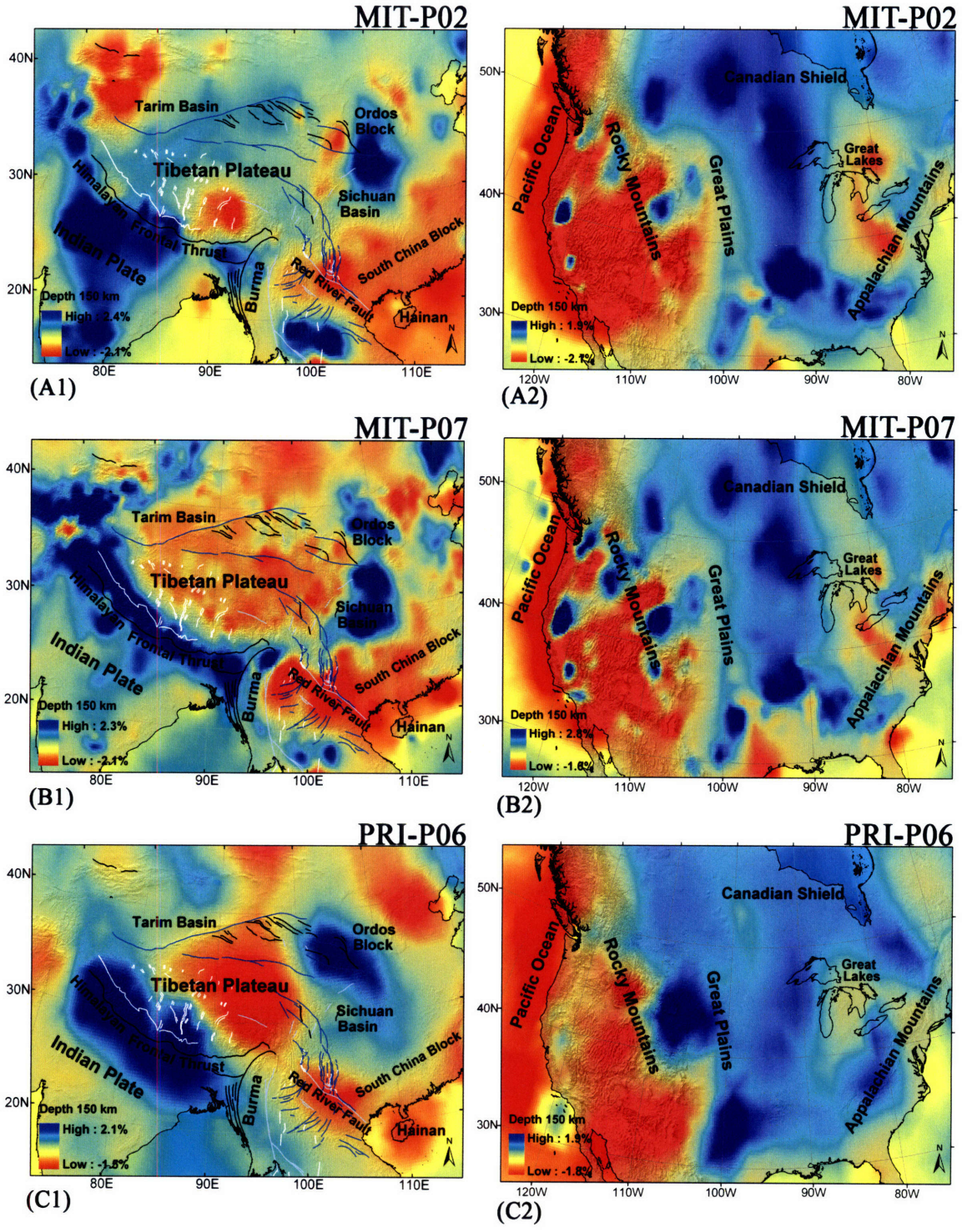

Figure 2-6. Model comparison at 150 km depth in the Tibetan plateau and North America. A) MIT-P02, MIT 2002 model, *Kárason H. (2002)*; B) MIT-P07, this study; C) PRI-P06, updated from *Montelli et al. (2004)*.

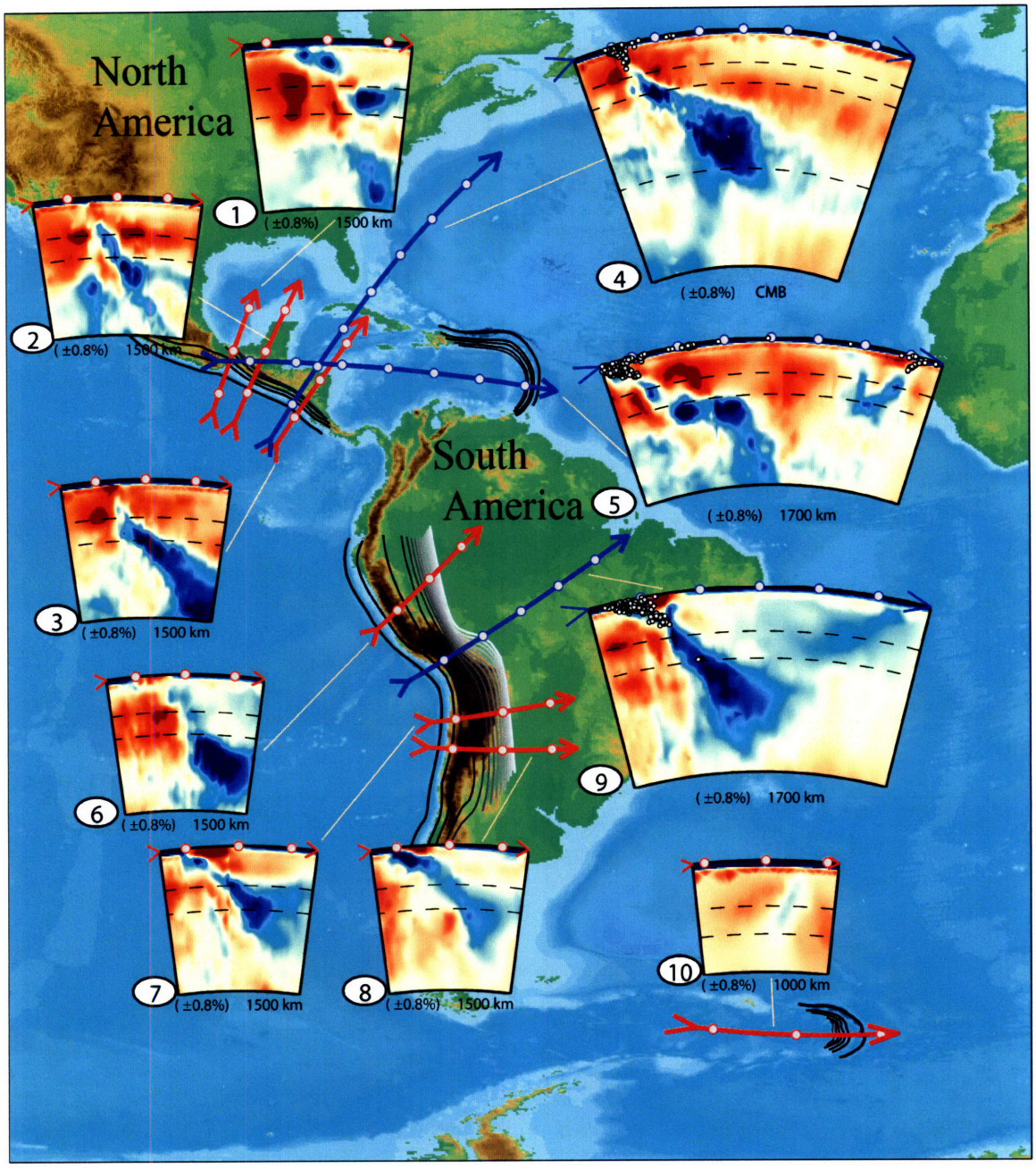

Figure 2-7a. Subduction through Central America and South America. Same as in Figure 2-1, the gray circles on cross section show the earthquakes and the grayscale contours show the outline of the subduction zone.

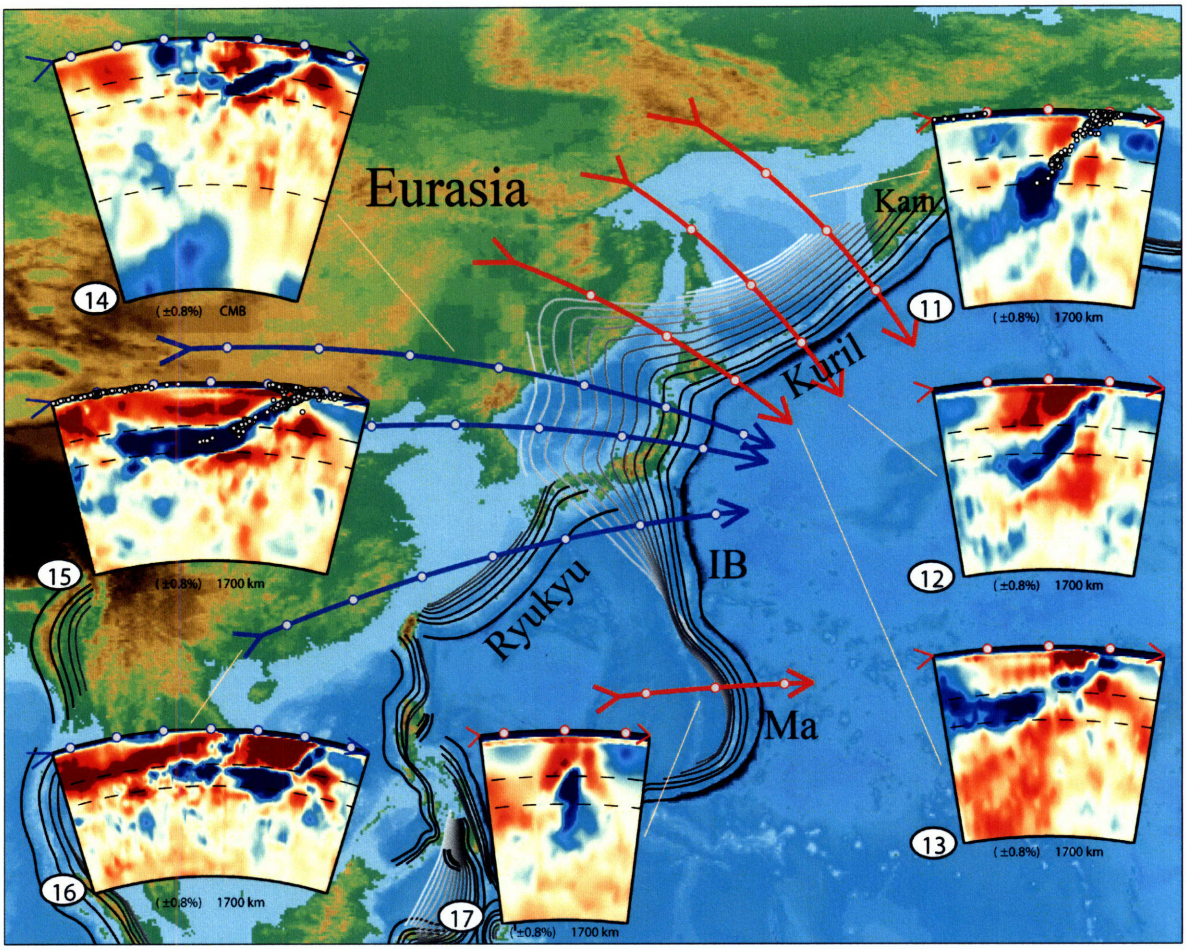

Figure 2-7b. Northwestern Pacific and Philippine Sea subduction, where Kam - Kamchatka; IB - Izu Bonin; Ma – Mariana.

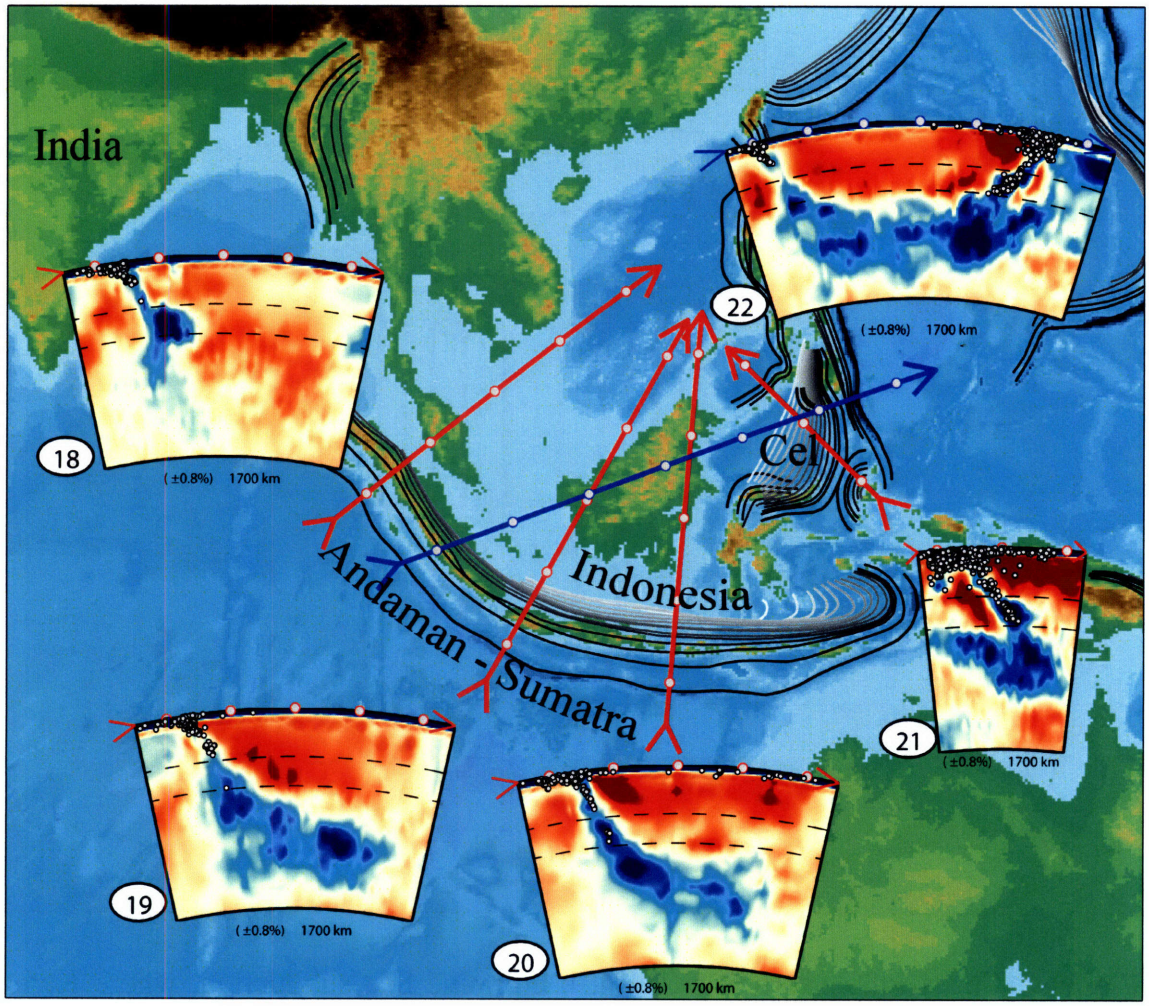

Figure 2-7c. Andaman-Sumatra subduction, where Cel - Celebes Sea.

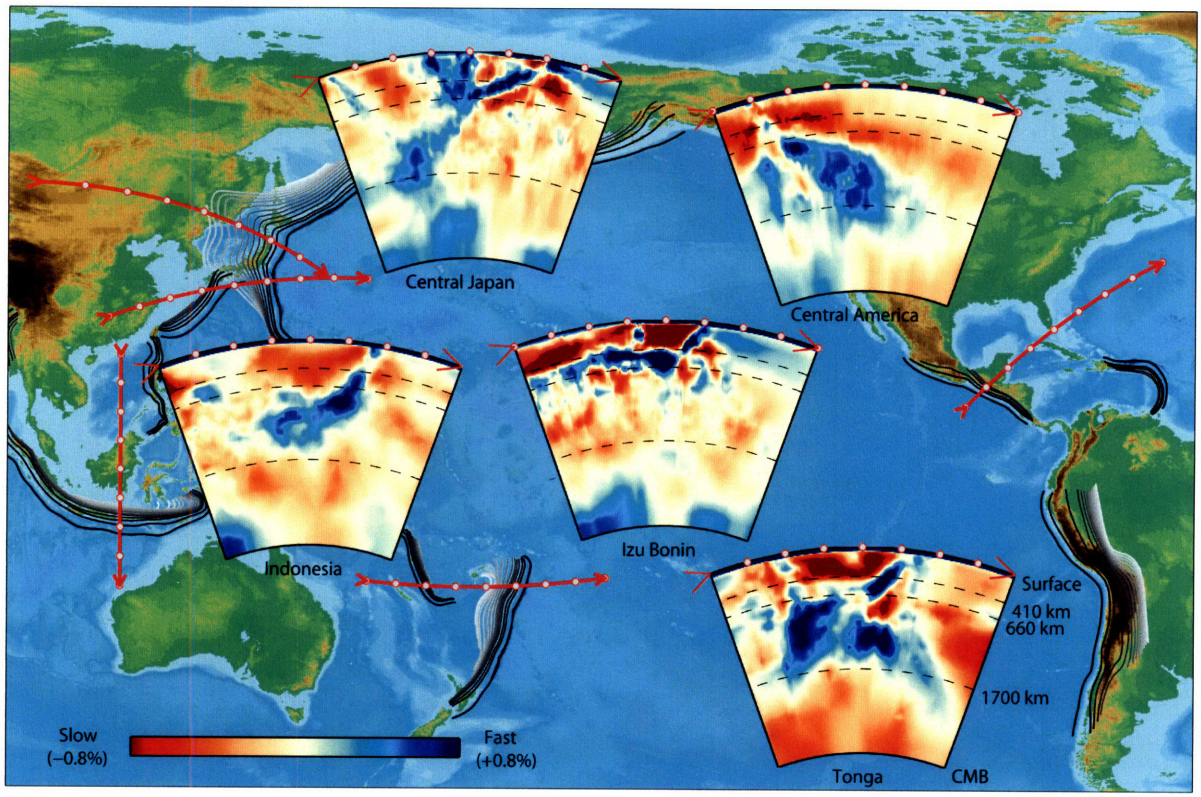

Figure 2-7d. Circum Pacific Ocean subduction.

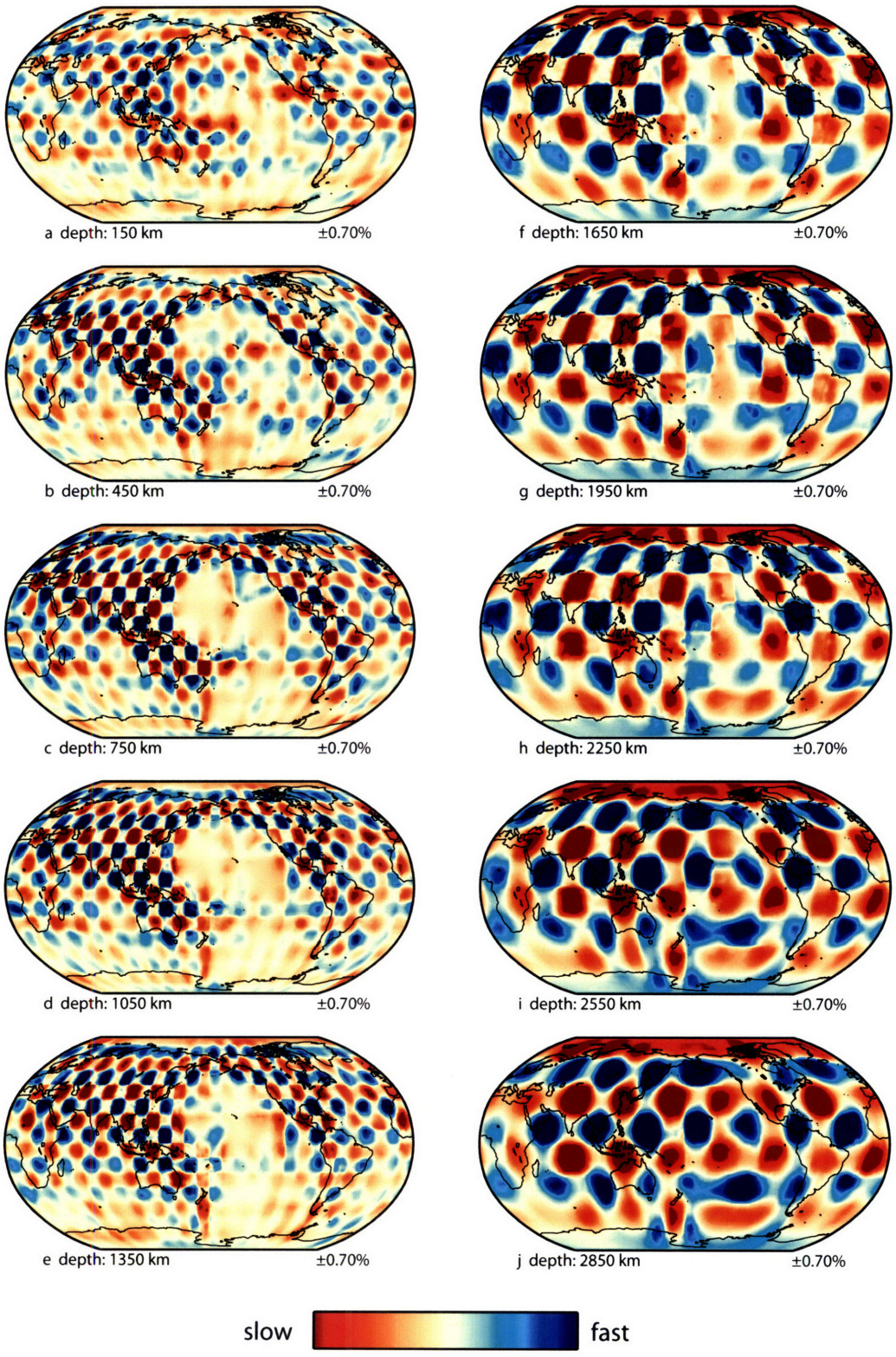

Figure 2-8. Recovery fields of global resolution tests, using harmonic input patterns with constant amplitude ±1.5% throughout the mantle. (a-e) Half-wavelength of ~5° (spatial wavelength of ~550 km at the surface). (f-j) Half-wavelength of ~10° (~600 km at the CMB).

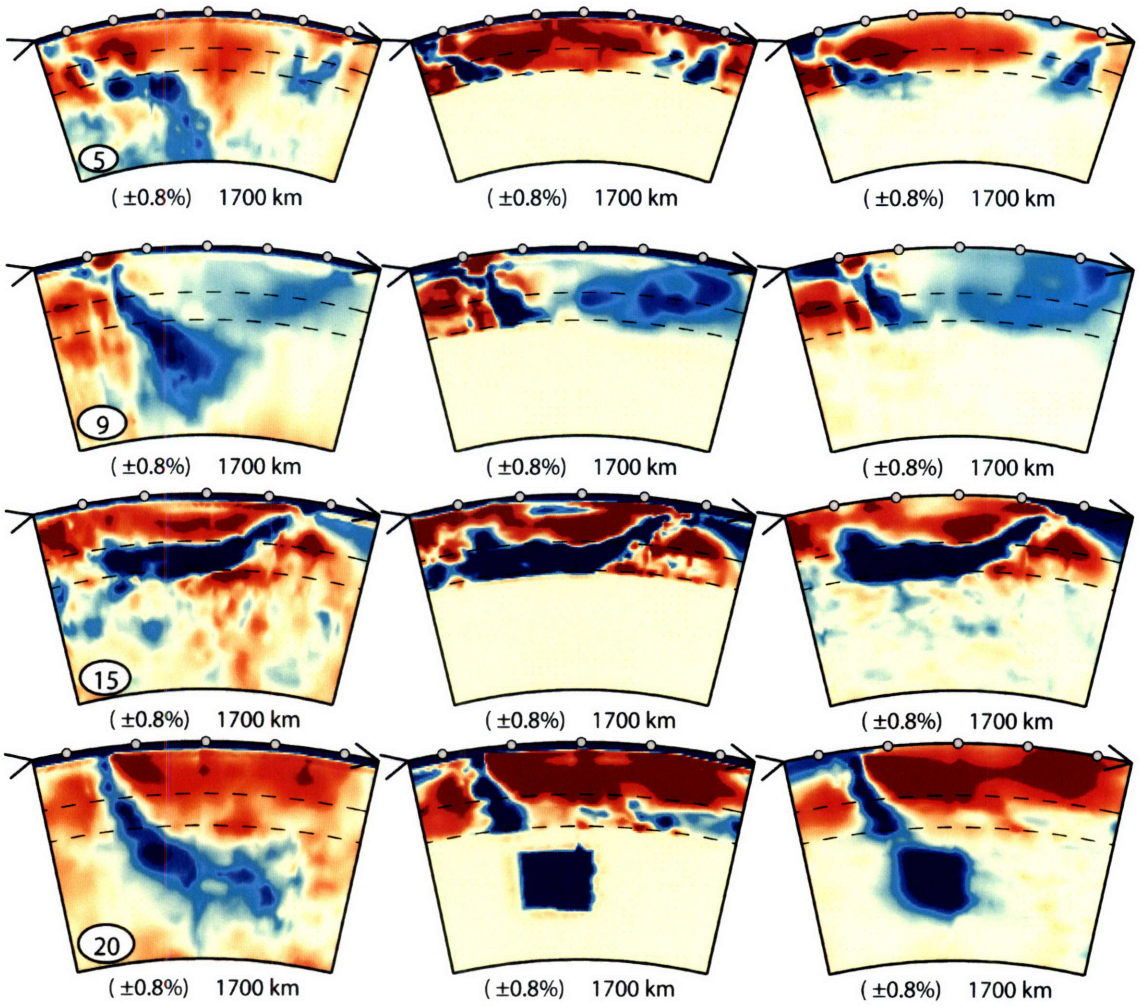

Figure 2-9. Synthetic tests for several slabs. Left: four selected cross-sections from the global model. Middle: input P-wave field, with anomalies above 660km increased by 50% and set to zero below. For cross-section 20, we added a large fast anomaly in the lower mantle. Right: recovered field inverted by the (non-noisy) synthetic data.

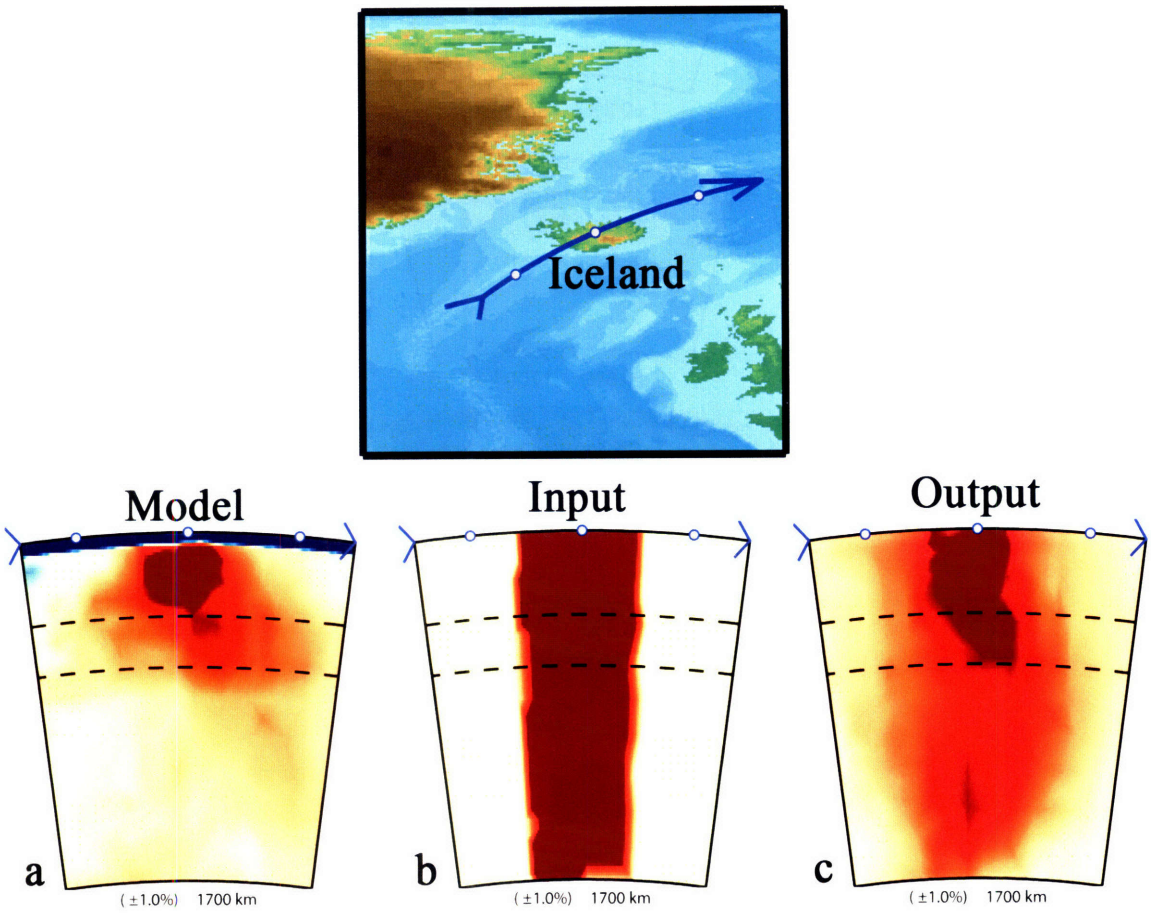

Figure 2-10. Synthetic test for the Iceland plume. Left: MITP07 model beneath Iceland. Middle: an input column structure with negative 2.0% anomalies, from surface down to 1700 km depth. Right: the recovered field.

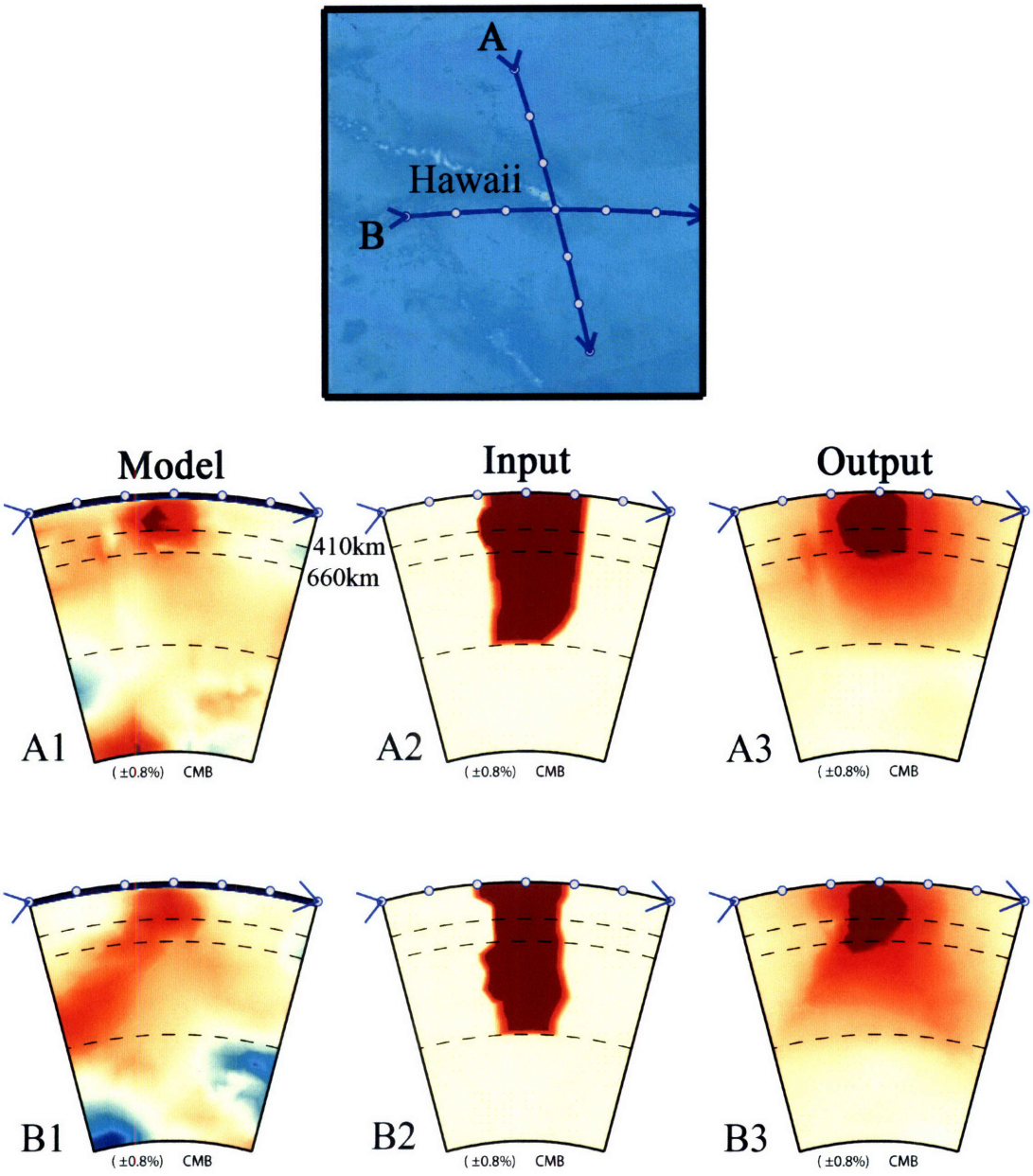

Figure 2-11. Synthetic test for the Hawaii plume. The test design is the same as for the Iceland plume (see Figure 2-10).

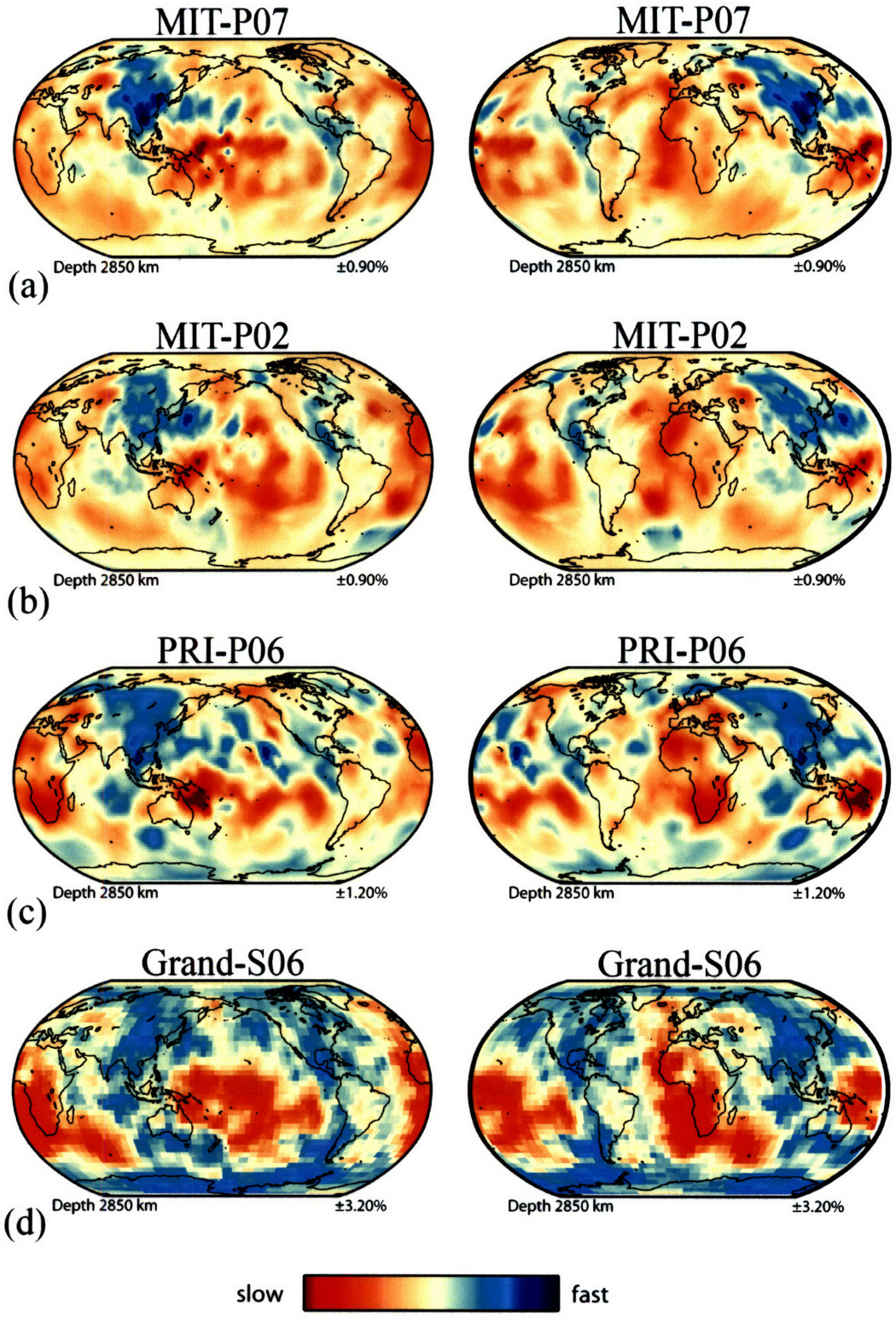

Figure 2-12. Comparison of different velocity models at the bottom of the mantle. (a) MIT-P07; (b) MIT-P02; (c) PRI-P06 updated from *Montelli et al. (2004)*; (d) the shear wave model updated from *Grand (2002)*.

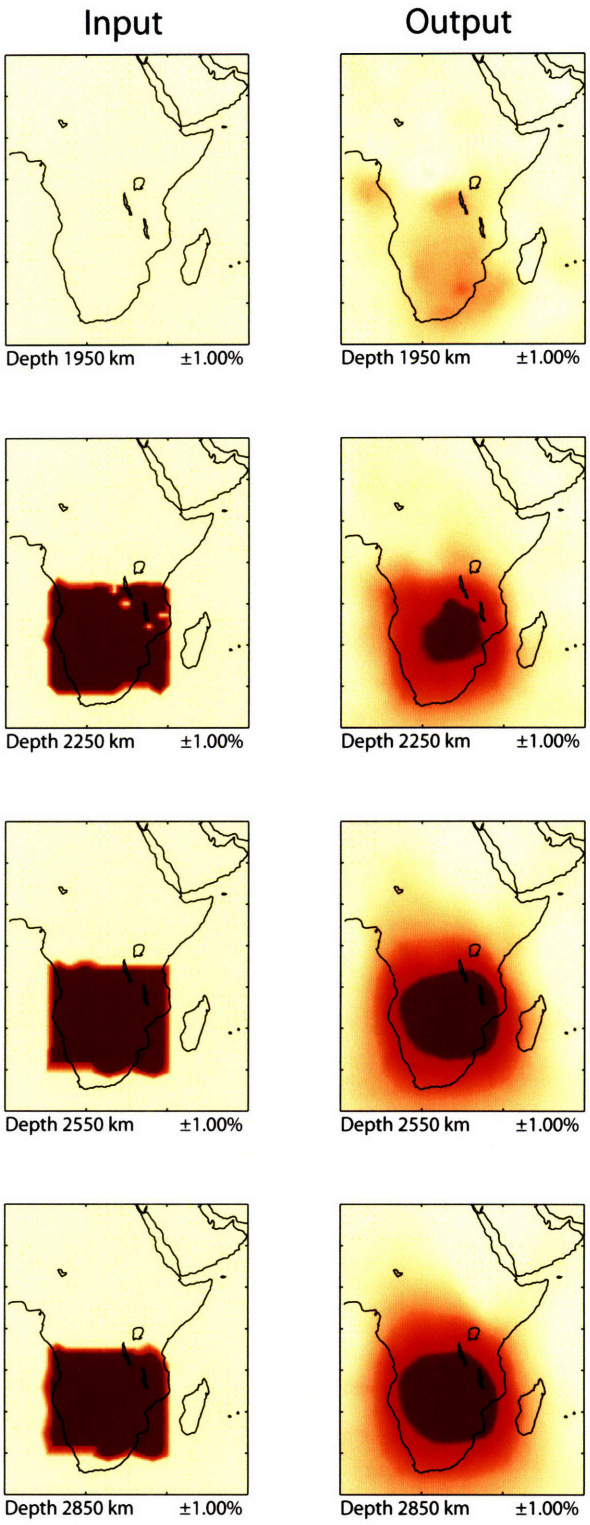

Figure 2-13. Synthetic test for the African super plume in the lower mantle. -2.0% velocity anomaly column extends from 2250 km to 2850 km depth (left). The recovery pattern is shown at the right column.

Chapter 3

Constraining P-wave velocity variations in the upper mantle beneath Southeast Asia[2]

Abstract

We have produced a *P*-wave model of the upper mantle beneath Southeast (SE) Asia from reprocessed short period International Seismological Centre (ISC) *P* and *pP* data, short period *P* data of the Annual Bulletin of Chinese Earthquakes (ABCE), and long period *PP-P* data. We used 3D sensitivity kernels to combine the datasets, and mantle structure was parameterized with an irregular grid. In the best-sampled region our data resolve structure on scale lengths less than 150 km. The smearing of crustal anomalies to larger depths is reduced by a crustal correction using an *a priori* 3D model. Our tomographic inversions reveal high-velocity roots beneath the Precambrian Ordos Plateau, the Sichuan Basin, and other continental blocks in SE Asia. Beneath the Himalayan Block we detect high seismic velocities, which we associate with subduction of Indian lithospheric mantle. This structure is visible above the 410 km discontinuity and may not connect to the remnant of the Neo-Tethys oceanic slab in the lower mantle. Our images suggest that only the southwestern part of the Tibetan plateau is underlain by Indian lithosphere and, thus, that the upper mantle beneath northeastern Tibet is primarily of Asian origin. Our imaging also reveals a large-scale high-velocity structure in the transition zone beneath the Yangtze Craton, which could have been produced in multiple subduction episodes. The low *P*-wave velocities beneath the Hainan Island are most prominent in the upper mantle and transition

[2] Published as: Li C., van der Hilst R.D., Toksöz M.N., Constraining P-wave velocity variations in the upper mantle beneath Southeast Asia, *Phys. of Earth and Planet. Inter.*, 154 (2006) 180-195

zone; they may represent counter flow from the surrounding subduction zones, and may not be unrelated to processes beneath eastern Tibet.

3.1 Introduction

Southeast Asia is a tectonically diverse and active region. Continental collision in the west and eastward retreating slabs of subducting lithosphere in the east set up a large-scale clockwise rotation (black arrows in Figure 3-1). The major large-scale features produced by the collision and post-collisional convergence of the Indian and Eurasian plates include the Tibetan Plateau, where the continental crust has approximately doubled in thickness (Molnar and Tapponnier, 1975; Tapponnier et al., 2001; Rapine et al., 2003). Offshore, oceanic lithosphere is predominantly of early Cenozoic age, and there is ongoing subduction of the Pacific, Philippine Sea, and Indo Australian plates beneath Eurasia (van der Hilst et al., 1991; Fukao et al., 1992; Widiyantoro and van der Hilst, 1996) with eastward slab roll back since at least Oligocene times (van der Hilst and Seno, 1993; Northrup et al., 1995). Between these active plate boundary zones the continental lithosphere was subjected to extension during early Cenozoic time (Tapponnier and Molnar, 1977; Zhang et al., 1984; Li, 1998). The extensional features are usually regarded in the context of the Indian-Eurasian collision (Molnar and Tapponnier, 1975). However, both the collision and the subduction processes, along with their impact on mantle (return) flow beneath the region, must be taken into account in order to obtain a complete understanding of the

dynamics and the tectonic evolution of SE Asia. It can be expected that this complex tectonic environment has produced significant structural heterogeneity in the upper mantle. Understanding this relationship is the main long-term objective of our study; here we present preliminary results of seismic travel time tomography.

Southeast Asia is characterized by relatively high levels of seismicity, but the distribution of seismological stations from which data are openly available is rather sparse (red triangles in Figure 3-2). This puts restrictions on the type of seismic imaging that can be performed and the scale of the structure that can be resolved. Surface wave tomography studies show pronounced high-velocity continental roots beneath several Precambrian tectonic units (e.g. Ordos Plateau, Songliao Basin, Sichuan Basin) of SE Asia (Lebedev and Nolet, 2003; Debayle, et al., 2005; Lebedev, et al., 2005) and a seismically fast Indian lithosphere under southeastern Tibet (Friederich, 2003). These features can also be inferred from global shear-wave velocity models (e.g., Trampert and Woodhouse, 1995; Ekström, et al., 1997; Shapiro and Ritzwoller, 2002). However, the relatively low frequency of surface wave data put limits the structural wavelengths that can be resolved in the upper mantle.

In regions with good data coverage short-period travel times can provide higher resolution than the surface wave inversions. A number of *P*-wave tomographic studies have concentrated on complex morphology of the subducting oceanic lithospheric slabs beneath the western Pacific, the Philippine Sea, and

Indonesia (e.g. Van der Hilst et al., 1991; Fukao et al., 1992; Widiyantoro and van der Hilst, 1996). Using data from temporary seismic arrays, receiver function studies have focused on the crust and shallow mantle beneath central Tibet (e.g., Kind et al., 1996; Kosarev et al., 1999; Kind et al., 2002). Regional and local *P*-wave tomography has focused on the crust and uppermost mantle (e.g. Sun et al., 2004; Hearn et al., 2004; Liang et al., 2004; Huang et al, 2002; Wang et al, 2003). Global tomography has long been inadequate for detailed studies of the upper mantle beneath China and the broad realm of continental collision. In part this is due to the paucity of data from the numerous stations in China. But this situation is changing. There are promising signs that data from Chinese networks may become more openly available, and also data from temporary arrays will continue to fill in gaps in data coverage. For example, data from arrays deployed by MIT in collaboration with the Chengdu Institute of Geology and Mineral Resources (CIGMR), and by Lehigh University - CIGMR (Sol, et al., 2004) are now being processed and will soon be incorporated into the inversions.

With a better *P* wave velocity model of the upper mantle beneath Southeast Asia we hope to answer specific questions, for instance: How far does the Indian lithospheric mantle underthrust beneath the Tibetan plateau? What is the relationship between recent tectonic processes and structures deeper in the mantle? Which structures in the transition zone (TZ) are related to the underthrusting of Indian lithosphere and which are due to the subduction of the Pacific, Philippine Sea, and Indo-Australian plates? To improve the tomographic images of mantle

structure in this region we (i) combine *P* data from the Annual Bulletin of Chinese Earthquakes (ABCE) (a national earthquake catalog compiled by the Institute of Geophysics, China Seismological Bureau), *P* and *pP* data from Engdahl et al, (1998), and *PP-P* differential travel time data from Bolton and Masters (2001), (ii) use an irregular grid parameterization to enhance local parameter estimation, and we (iii) correct for the large regional variations in crustal structure using an *a priori* 3D crustal model. As regards the latter, we present a simple approach that reduces artifacts caused by errors in the *a priori* crust models.

The results presented here are a subset of the new *P*-wave global model; compared to our previous results – see, for instance, Kárason & van der Hilst (2001) –the use of an irregular grid, the addition of *PP-P* and ABCE (*P*) data, and the crustal corrections combine to provide more detail in the upper mantle region of our current interest. The global model will be presented elsewhere (Li, van der Hilst, and Engdahl, in preparation) but is freely available upon request.

3.2 Data

The travel time data used in our study comes from three sources. The first is the International Seismological Centre (ISC) data that have been reprocessed by Engdahl, van der Hilst, and Buland (1998) (hereinafter referred to as EHB). Engdahl et al. used arrival times reported to the ISC and calculated travel-time residuals using a non-linear process earthquake relocation and phase re-

identification scheme. In our global inversion we used ca. 9,400,000 *P* and 680,000 *pP* EHB residuals of well-constrained regional and teleseismic earthquakes that occurred between 01/01/1964 and 15/09/2004.

As a consequence of many Chinese stations not reporting to ISC the station coverage of EHB is not very good in SE Asia, especially in China. In order to improve data coverage, we augmented the EHB data with Annual Bulletin of Chinese Earthquakes (ABCE) data. This database contains nearly 670,000 *P*-wave travel time residuals from 220 stations in China and surrounding areas. Combining datasets has to be done with care. Relative to the *ak135* reference velocity model (Kennett et al. 1995), the ABCE residuals have an offset of more than 2 s. There are two contributions to this baseline problem. One is the effect of crustal structure in the region. If the crust is thicker than that of the reference model the arrival time will be greater than the reference travel time, resulting in positive travel time residuals. For example, the 0.5 s offset at Lhasa station is most likely due, in part, to the thick crust of Tibet. We account for this in the inversion. The second and larger effect concerns the source locations used in the EHB and ABCE catalogs; they can differ substantially, in particular for events in the Wadati-Benioff zones beneath the northwest Pacific island arcs. Calculating the ABCE residuals with respect to the EHB hypocenters reduces the baseline to less than 0.2 second. Prior to inversion we eliminated data for the 113 ABCE stations that are already included in EHB. The study area comprises 1223 EHB stations (44 of which are

mainland China, red triangles in Figure 3-2) and 107 Chinese ABCE stations that have not been reported to ISC (blue square in Figure 3-2).

The subset of the global model presented here also includes ~22,000 *PP-P* low frequency differential times measured by waveform cross-correlation (Bolton and Masters, 2001). We account for sensitivity to structure away from the optical ray path with 3D Fréchet derivatives (sensitivity kernels) estimated from single forward scattering; for details see Kárason (2002) and Van der Hilst et al., (in preparation). For the spatial resolution sought here these low frequency data may seem superfluous, but the *PP-P* differential times constrain large wavelength variations in the region under investigation.

3.3 Methodology

3.3.1 Adaptive Grid

Uneven data coverage can produce significant lateral variation in resolution of tomographic models. We mitigate effects of uneven data coverage by means of an adaptive parameterization based on the sampling density of the high frequency data (Abers and Roecker, 1991; Bijwaard and Spakman, 1998; Kárason and van der Hilst, 2000). Each block in the grid used in the inversion consists of one or more base blocks of 45 km × 0.7^{o} × 0.7^{o}. The total number of free parameters (that is, the sampled irregular blocks and the event relocation parameters) is slightly less than 0.5 million. As an example, Figure 3-2 (green lines) displays the irregular

grid at 200 km depth. The relatively fine grid near the subduction zones of the Indian and Philippine Sea plates, the Sichuan Basin, and Tian Shan suggests that in these regions we can image finer structures. In contrast, the grids beneath Mongolia, the Tarim Basin, and the center of Philippine Sea is relatively coarse, which, of course, limits the spatial resolution beneath these regions.

For the calculation of the sensitivity matrix associated with short period data we use a high-frequency approximation and trace optical rays (in the radially stratified reference model). We use weighted composite rays (Kárason and Van der Hilst, 2001) to better balance the sampling and further reduce the size of the sensitivity matrix. Because of noise in the data, we apply norm and gradient damping: norm damping favors a result that is close to the reference model and thus tends to minimize the amplitude of the model, while gradient damping reduces the differences between adjacent blocks and thus produces smooth variations, both laterally and radially. We perform experiments with synthetic data and known input models to find appropriate values for the damping parameters, but the choice of the parameters remains subjective. In our inversions, the norm damping is small. We use the iterative method LSQR (Paige and Saunders, 1982) to minimize

$$\varepsilon = \| Am - d \|^2 + \lambda_1 \| Lm \|^2 + \lambda_2 \| m \|^2 \quad , \tag{3.1}$$

where A is the sensitivity matrix, d is the vector of travel time residuals, and m is the vector of model parameters (which include slowness perturbations and

hypocenter mislocations). L is a smoothing operator, and λ_1 and λ_2 are the weights for gradient and norm damping, respectively. The results presented here were obtained after 200 iterations, but for LSQR most of the convergence is achieved within a small number of iterations: ~ 98% of the total variance reduction is obtained within the first 25 iterations. In order to visualize the values determined for the irregular blocks we projected and interpolated them on a regular ($0.5^{\circ} \times 0.5^{\circ} \times 50$km) grid.

3.3.2 Crust correction

The small incidence angles of the *P*-waves may combine with strong crustal heterogeneity to cause crustal anomalies to be 'smeared' (mapped) to larger depths in the model. This could be a significant problem if the actual crust is very different from that in the 1D reference model, as is the case here. Application of crustal correction in global surface wave tomography is common practice, see, e.g. Boschi & Ekström (2002), but such corrections are not yet routinely considered in regional and global travel time tomography.

In SE Asia, the lateral variation in crustal thickness is considerable. For instance, crust of the Tibetan plateau is at least 70 km thick compared to just several kilometers for the oceanic crust in the Philippine Sea (Figure 3-3a, from (59°E, 35°N) to (134°E, 14°N)). As an estimate of the 3D crustal structure we embed the regional model by Sun et al. (2004) into the global CRUST 2.0 (Bassin et al. 2000), calculate the difference in wavespeed with respect to *ak135,* and project this *a priori* crustal model onto our grid (Figure 3-3b). In order to evaluate

if and how this crustal heterogeneity would "smear" into the model if unaccounted for, we use a resolution experiment with synthetic data. The response to such a crustal model, including all its artifacts, is shown in Figure 3-3c. Obviously, the crust cannot be resolved by the data used, and crustal structure may be smeared to depths of at least 200 km. Moreover, the retrieved anomalies are much smaller than those in the input models. We try to remedy this with a crustal correction.

Crustal corrections can be done in several ways. One could calculate travel times through the 3D crustal model, subtract these from the observed times, ray-trace to the bottom of the 3D crust, and then solve for the structure beneath the crust while leaving the crustal model unchanged (e.g., Waldhauser et al., 2002; Weidle & Widiyantoro, 2005). While straightforward and intuitive, without an explicit method for confining crustal anomalies to the crust, the relatively large anomalies of the 3D crust can still smear into the upper mantle. Moreover, artifacts due to errors in the crustal models are not mitigated. A practical drawback is that later data addition and (crustal) model updates require repeated ray tracing, which comes at considerable computational cost. Furthermore, calculating explicit time corrections is not straightforward for phases with complicated sampling properties, such as *PP*.

In view of these disadvantages, we correct for crustal structure by means of regularization; this is accomplished through a simple modification of (3.1):

$$\varepsilon = \| AM - d \|^2 + \lambda_1 \| LM \|^2 + \lambda_2 \| M \|^2 + \lambda_3 \| C - M_c \|^2 \quad , \qquad (3.2)$$

where C is the *a priori* 3D crustal model and M_C is the crustal part of the model space M. We determine λ_3 through tests with synthetic data. Through such regularization in the model space we can balance the crust and upper mantle contribution to misfit ε and recover the *a priori* crustal model (Figure 3-3d). Later addition of data sets does not require further calculations since all is accounted for in the model space.

These methods of crust correction produce the same result, but because of the ease of implementation we use the regularization approach for the inversions discussed below.

3.4 Results

3.4.1 Model improvements

The addition of the ABCE data and the correction for the crust improve the 3D mantle model (Figure 3-4). For 60 and 200 km depth, Figure 3-4A (1 and 2) depicts the model derived from the EHB and PP data. The addition of the ABCE data, and concomitant adjustment of the grids, increases our ability to resolve the small-scale structure (Figure 3-4B1, B2). In the mainland of China, where the extra ABCE stations are located, more detail is recovered than before. For example, we now begin to observe a high velocity structure beneath the eastern part of the Sichuan Basin and the Songliao Basin and a low velocity structure beneath the Songpan Ganzi Foldbelt (Figure 3-4B1, B2). As expected, outside the

mainland of China, for instance beneath the Indian continent and the Philippine Sea, the improvements are small. The crustal thickness of central Tibet (~70-90 km) differs significantly from the 35 km in *ak135*, but the application of our crust correction reduces the smearing of unresolved shallow structures (compare, e.g., Figure 3-4 C2 and B2).

3.4.2 Resolution tests

Resolution test with synthetic data confirm that the addition of the ABCE data increases our ability to resolve 3D structure. In Figures 2-5 and 2-6 we show the retrieved structure from a checkerboard resolution test at different depths for box sizes of $5^{o}\times5^{o}$ and $3^{o}\times3^{o}$, respectively. The input structure of ±1% velocity variation (Figures 2-5.0 and 2-6.0) was computed one layer at a time, and noiseless synthetic travel times were created and inverted using the same inversion scheme and sampling (that is, sensitivity matrix) as used in the inversion of the earthquake data.. In the shallow mantle, spatial resolution remains a concern. At 200 and 300 km depth the pattern is smeared beneath Philippine Sea, South China Sea, and most of Mongolia, but in areas of our particular interest, such as mainland China, and the Himalayas the recovery is somewhat better (Figure 3-6.3 and 6.4). The $5^{o}\times5^{o}$ pattern can be recovered beneath China (Figure 3-5.1 and 2-5.2), but smaller anomalies are not likely to be resolved beneath the Tarim Basin and the northern part of Tibet (Figure 3-6.1 and 2-6.2). At depths below 400 km, both the $5^{o}\times5^{o}$ and $3^{o}\times3^{o}$ input patterns are recovered beneath most parts of our study region (Figures 2-5.5~2-5.9; 2-6.5~2-6.9).

The near vertical incidence of rays reduces the radial resolution in the shallow mantle. The checkerboard tests of two input patterns (400×400 km and 280×280 km) in Figure 3-7 help us evaluate the vertical resolution of structure in the four slices that will be discussed later. These slices are about 4000 km long and extend from Earth's surface to 1700 km depth. In general, the recovery of the input models is adequate below 400 km depth. At shallower depth, small scale structure cannot be recovered well in many areas beneath the study region, but larger scale variations can be recovered reasonably well.

From our lateral checkerboard test we conclude that below 200 km depth most of the $3^{o}\times3^{o}$ input signal could be recovered, so the average resolution length at these depths is the half of input signal dimension (Lebdev and Nolet, 2003), that is, about 150 km. At shallow depths, the smaller scale pattern is only recovered beneath a few densely sampled regions, such as the Yangtze Craton, the Sino-Korean Craton, and the Himalayas (Figure 3-6.1), where we estimate the resolution length to be of the order of 100 km. At the Tarim Basin and the north part of Tibet, the estimated lateral resolution is ca. 200 km (Figure 3-6.2). The vertical resolution length is about 150 km below 400 km depth (Figure 3-7).

3.4.3 Structure of the upper mantle beneath SE Asia

We show the P-wave velocity variations in map view from the surface to about 700 km depth (Figure 3-8) and in four vertical cross sections (Figure 3-9). For presentation purpose we label the major structures as 1, 2, 3 and so on. The major features of the model are discussed below.

3.4.3.1: Upper mantle structure beneath India and central Tibet:

A pronounced high-velocity anomaly (labeled as 1) is visible to a depth of ~300 km beneath the region of the Precambrian Indian continent (Figures 2-8a-d). In cross section this structure appears to dip northeastward with the flexure starting near the foreland basin about 200 km to the south of the Himalaya Frontal Thrust (Figure 3-1, 2-9a). Even though it is not yet well resolved, we interpret this dipping structure as the subducting slab of Indian continental lithosphere, and perhaps part of the Tethyan oceanic lithosphere in front of it. From Figures 2-8b~e and 2-9a we infer that only the southwestern part of the Plateau, the Himalayan Block and the western Lhasa Block, is directly underlain by the Indian lithosphere, the northern limit of Indian lithosphere beneath Tibet is marked by the thick blue line in Figure 3-1. Our result is consistent with the image presented by Shapiro and Ritzwoller (2002), but since they used fundamental mode surface waves they could only map the structure to ca. 200 km depth. In our images the dipping structure is detected to at least 400 km depth, and possibly continues to ~ 660 km depth. At depths greater than about 660 km another high-velocity anomaly is observable beneath north-central India (structure 2 in Figure 3-8h). In Figure 3-9a, this structure extends just near the 660 km discontinuity to deep in the lower mantle with a south-dipping angle, where it forms part of the large scale structure that has been interpreted as a remnant slab of late Mesozoic Neo-Tethys oceanic lithosphere prior to the India-Eurasia collision (van der Hilst et al., 1997; Van der voo et al., 1999; Replumaz et al., 2004). The spatial resolution of the current data

coverage does not yet allow us to establish the structural relationship between the northward dipping structure 1 and the southward dipping structure 2.

3.4.3.2: Upper mantle structure beneath eastern Tibet:

Our results suggest that the shallow mantle beneath the southeastern part of Songpan Ganzi Foldbelt and eastern parts of the Tibetan Plateau is marked by very slow *P* wavespeeds (structure 3 in Figure 3-8b). The wavespeeds would be artificially low if the actual crust is even slower than that in the *a priori* model used, but the resolution of shallow mantle structure is adequate (Figure 3-6.2~2-6.4) so that leakage to large depths is unlikely. The slow velocity structure continues to 300-400 km depth (Figures 3-8b~d, 3-9d). These results also suggest that this slow velocity structure may extend beyond the eastern margin of Tibet and to depths well in excess of the thick crust. In fact, our images suggest that these slow structures may connect to the slow wavespeeds in the upper mantle further SE beneath South China Sea coast and, in particular, Hainan Island (Figures 3-8d~e).

3.4.3.3: Tian Shan and Tarim basin:

Slow velocities beneath the Tian Shan and western part of the Tarim Basin seem to continue to at least 300 km depth (Structure 4 in Figures 3-8a~d and 3-9c). In this depth range, no prominent high wavespeed feature is detected beneath the Tarim Basin, but the resolution beneath Tarim Basin is relatively poor. The shallow mantle beneath the Junggar Basin is marked by high *P* wavespeeds

propagation (Structure 5 in Figures 3-8b~d). Figure 3-9a suggests that this structure may be dipping to the south.

3.4.3.4: Mantle structure beneath the Precambrian cratons:

Beneath the Sino-Korean Craton the most prominent feature is the high-velocity root extending down to 200 km beneath the Precambrian nucleus of the Ordos Basin (Structure 6 in Figures 3-8a~d and 3-9b,e). This anomaly seems to be confined within the Ordos Basin boundary. Another high-velocity root, extending down to 200 km, underlies the eastern half of the Sichuan Basin (structure 7 in Figures 3-8a~c and 3-9c). Below 200 km, this high-velocity root fades and changes to slow velocity structures. The resolution in the Sichuan and Ordos Basin is high (Figure 3-6.2, 3-6.3), so the high velocity roots are not artifacts. Eastern migration of high-velocity root beneath the Sichuan Basin may be affect of the collision between Indian and Eurasia plates. A large scale high velocity anomaly appears in transition zone (410-660 km) beneath the Yangtze Craton (structure 8 in Figures 3-8f~g and 3-9c, d) and the resolution in the transition zone is good (Figure 3-6.5~6.8).

3.4.3.5: South East China, Hainan Island:

Beneath Southern and Southeastern China, and beneath Hainan Island, in particular, the *P* velocity is very low. At shallow depths the slow anomaly may connect westward, across the Youjiang Block, to the low wavespeeds beneath the Red River fault and the southeastern part of the Songpan Ganzi Foldbelt (Figures

3-8a~c). At larger depth, a pronounced slow velocity feature is detected beneath the Hainan Island and the southern coast of China (structure 9 in Figure 3-8d~g, 9d, e). Near 660 km depth, the wavespeed is not significantly different than the reference wavespeed according to *ak135* (Figures 3-8h, 3-9d, e), in the top of the lower mantle a slow velocity feature appears again. This deeper structure is much weaker than the upper mantle and transition zone anomalies, and it is not distinctly slower than nearby slow anomalies. Other studies have argued for a lower mantle origin of the Hainan structure (e.g., Montelli et al., 2004), but the observations presented here suggest that the most prominent part is confined to the upper mantle and transition zone.

3.4.4 Comparison to the other global model in the region

The model by Montelli et al. (2004) is more similar to our results than any other *P*-models that are publicly available. For this comparison we use their latest model (Montelli et al., in preparation), which has a different crust correction and, therefore, has a better upper mantle structure than the one used for their 2004 publication. Figures 3-10a, b depicts the anomalies at 140 and 400 km depth, and in Figures 3-10c, d we show it for cross sections BB' and DD'. The long wavelengths patterns agree quite well, although there are substantial differences in amplitude (with our amplitudes almost certainly too low). At shallow depth (Figures 3-8b and 3-10a) we recognize similar fast anomalies beneath the boundary of Indian and Eurasian plates, north-eastern and central China, and to the north of Japan, and slow anomalies beneath the Tibetan Plateau, Hainan Island,

and the coast of the South China Sea and to the south of Japan. At larger depth (Figure 3-8e and 2-10b) both models shows fast anomalies around western Pacific plate boundaries, but differences occur that could be due to the different types of regularization employed in these studies. These difference merit further investigation, but since our main interest is in the sub continental mantle this is beyond the scope of this paper. On smaller length scales our model reveals more detail than the model by Montelli et al., which we attribute in part to our use of ABCE data and a higher resolution model for regional variations in crust structure.

3.5 Discussion

3.5.1 The seismic evidence for subduction of Indian lithosphere

The regional tomographic image of the upper mantle beneath central Tibet from the INDEPTH array has revealed a subvertical high velocity zone from 100 to 400 km depth (Tilmann and Ni, 2003), which has been interpreted as the downwelling Indian lithosphere. This regional image covers the area from 29°N to 33.5°N, and therefore does not completely image the whole underthrusting Indian lithosphere beneath the Himalayan Frontal Thrust and the Tibetan plateau. In our model, the high wavespeeds associated with what is presumably subducted lithosphere is clearly visible beneath the boundary of Indian and Eurasian plates at 140 and 200 km depths (structure 1 in Figures 3-8b and 3-8c). At larger depths, it trends further northward and mainly underlies beneath the western part of

Himalayan Block and Lasha block (Figures 3-8d and 3-8e). This is also visible in AA' (Figure 3-9A). Although the relatively poor resolution beneath the northern Tibet leaves some room for alternate interpretations, our images suggest that the Indian lithosphere subducts from the foreland basin and underlies only the southwestern margin of the Tibet Plateau (thick blue line in Figure 3-1), implying that much of the Tibet Plateau is not underlain by Indian but by Asian lithosphere (Tapponnier, 2001). This conclusion may be refined by analysis of the data from the MIT-CIGMR and Lehigh-CIGMR arrays, but if confirmed it has important implications for evolutionary models of the Tibetan plateau. The southward dipping high-velocity structure 2 in the lower mantle (Figures 3-9a and 3-9b), interpreted as Neo-Tethys oceanic lithosphere (van der Hilst et al., 1997; van der Voo et al., 1999; Replumaz et al., 2004), seems to be separated from the subducted Indian lithosphere as it sinks below 660 km discontinuity, but this relationship will be subjected to further study.

3.5.2 Fast velocity structure within the TZ beneath Yangtze Craton

Our images show that there is a significant high-velocity anomaly beneath the Yangtze Craton in the transition zone (structure 8 in Figures 3-8f~h, Figures 3-9c,d), which spans almost 2000 km from northeast to southwest (Figure 3-8f). The high resolution at this depth ensures that this fast velocity anomaly is not an artifact. This large-scale high velocity structure may have a complex origin. The eastern part of these anomalies has been well documented in tomographic studies (e.g. van der Hilst et al., 1991; Fukao et al., 1992) and has been interpreted as

"slab deflection" at the 660 km discontinuity as a result of slab roll back ocean ward (van der Hilst and Seno, 1993). The strong anomalies in the transition zone east of ~120°E can probably be explained as the subducted ocean lithosphere of the western Pacific and Philippine Sea plates (Figures 3-8f, g). It has been suggested that also the western part of the anomaly, between ~100°E and ~120°E, has been produced by subduction. Lebedev and Nolet (2003) interpreted the high *S*-wave velocity beneath the Sino-Korean Craton as the subducted continental lithosphere of the Yangtze Craton beneath the Sino-Korean Craton. But perhaps the anomaly between ~110 °E and ~120°E is related in part to the Philippine Sea subduction and the anomaly between ~100 °E and ~110°E might be associated with the eastward subduction of the Indian plate. We thus suggest that the explanation of this transition zone structure may involve other subduction systems than subduction of continental lithosphere alone.

3.5.3 Slow velocity structure beneath Eastern Tibet and South China Sea

In the image of the upper mantle beneath eastern Tibet, the most prominent feature is the large-scale low velocity structure (Structure 3 in Figures 3-8b, c and Figures 3-9b~d) in the depth above 200 km. This structure is probably not an artifact of the thick crust since this contribution is corrected for, although it is possible that the crustal velocities are even slower than in the crustal model used for the correction. Preliminary results of receiver function and surface wave analysis of the MIT-CIGMR array data suggest the presence of slow velocity channels in the crust below the Sichuan and Yunnan provinces (Van der Hilst et

al., 2005). The location of slow wave propagation also coincided with areas of local volcanism and high heat flow; for example, the P wavespeed beneath the Tengchong volcanic area (25°N, 98°E), one of the few recently active volcanic area in mainland China, is anomalously low. Interestingly, this is also the area where the lower crust is thought to be sufficiently hot to undergo large-scale horizontal flow (Clark and Royden, 2000).

Our preliminary results suggest that the low wavespeeds are not confined to the crust but extend much deeper into the upper mantle. The slow velocity asthenospheric mantle beneath eastern Tibet is perhaps involved in large-scale extrusion driven by the Indian-Eurasian collision. Alternatively, it may be related to processes further to the southeast. The large low velocity anomaly beneath Hainan Island and the south coast of China extends down to 660 km (structure 9 in Figures 3-8c~g, 3-9d,e) may represent a regional counter flow in response to subduction beneath nearby convergent margins. The images are suggestive of a connection between this structure and those in the shallow mantle beneath eastern Tibet (Figure 3-8c). This intriguing spatial relationship is a subject of further study since it may suggest a relationship between the tectonics of eastern Tibet and mantle processes beneath the Hainan Island and South China Sea. If corroborated by further study, this connection would have major implications for our understanding of the geological history of the Tibetan plateau.

3.6 Conclusion

We have combined different seismic data sets and implemented a crustal correction in order to improve the tomographic imaging of the upper mantle beneath SE Asia. The images reveal significant heterogeneity in the upper mantle. First, high velocity crustal roots (~ 200 km in thickness) are observed beneath most of the Precambrian Basins (Ordos Basin, Sichuan Basin, and Songliao Basin). Second, our results suggest that only the southwest part of the Tibetan plateau is underlain by lithospheric mantle involved in the subduction of the Indian plate. This implies that most of upper mantle beneath the Tibetan plateau is primarily of Asian origin, in agreement with, for instance, Tapponnier (2001). However, better resolution is required to establish the spatial and temporal relationship between the shallow and deep slabs. Subducted Indian lithosphere is detected to ~400 km depth and may be detached from the sinking ocean slab in the lower mantle. *P*-wave velocity is very slow beneath most of eastern Tibet where the lower crust is thought to be sufficiently hot to undergo large-scale flow (Clark and Royden, 2000). This slow anomaly may extend across the western boundary of the Yangtze Craton and connect with the low velocity structures deeper in the mantle beneath the Youjiang Block and Hainan Island. If confirmed by further study, our results pertaining to the subduction of Indian lithosphere and the possible connection between shallow mantle structures beneath eastern Tibet and the south coast of China may change views about the tectonic evolution of SE Asia.

Acknowledgements

We are indebted to Bob Engdahl for his ongoing research on the EHB dataset. We are also grateful to Raffaella Montelli for kindly providing us her global model and to Youshun Sun for his 3D crust model. We benefited from the constructive discussion with Stéphane Rondenay, Bradford Hager, Leigh Royden, Clark Burchfiel, and Sergei Lebedev. We thank an anonymous reviewer for constructive comments, which have helped us improve the manuscript. This work was funded by NSF grant 6892042 of Collaborative Research in Eastern Tibet and AFRL grant FA8718-04-C-0018.

References

Abers, G.A., and Roecker S.W., 1991. Deep-structure of an arc-continent collision: Earthquake relocation and inversion for upper mantle P and S wave velocities beneath Papua New Guinea. J. Geophys. Res., 96, 6379-6401.

Bassin, C., Laske, G., and Masters, G., 2000. The Current Limits of Resolution for Surface Wave Tomography in North America. EOS Trans AGU 81, F897.

Bijwaard, H., Spakman, W, and Engdahl, E.R., 1998. Closing the gap between regional and global travel time tomography. J. Geophys. Res., 103, 30055-30078.

Boschi L., Ekström G., 2002. New images of the Earth's upper mantle from measurements of surface wave phase velocity anomalies, J. Geophys. Res., 107 (B4), doi: 10.1029/2000JB000059.

Bolton, H. and Masters, G., 2001. Travel times of P and S from global digital seismic networks: implication for the relative variation of P and S velocity in the mantle, J. Geophys. Res., 106, 13527-13540.

Clark, M.K., and Royden, L.H., 2000. Topographic ooze: Building the eastern margin of Tibet by lower crustal flow. Geology, 28, 703-706.

Debayle, E., Kennett, B., and Priestley, K., 2005. Global azimuthal seismic anisotropy and the unique plate-motion deformation of Australia. Nature, 433, 509-512.

DeMets, C., Gordon, R.G., Angus, D.F., and Stein, S., 1990. Current plate motions. Geophys. J. Int., 101, 425-478.

Ekström, G., Tromp, J., and Larson, E., 1997. Measurements and global models of surface wave propagation. J. Geophys. Res., 102, 8137-8157.

Engdahl, E.R., van der Hilst, R.D., and Buland, R., 1998. Global teleseismic earthquake relocation with improved travel times and procedures for depth determination. Bull. Seism. Soc. Am., 88, 722-743.

Friederich, W., 2003. The S-velocity structure of the East Asian mantle from inversion of shear and surface waveforms. Geophys. J. Int., 153, 88-102.

Fukao Y., Obayashi, M., Inoue, H., and Nenbai, M., 1992. Subduction slabs stagnant in the mantle transition zone. J. Geophys. Res., 97, 4809-4822.

Hearn, T. Wang, S., Ni, J., Xu, Z., Yu, Y., and Zhang, X., 2004. Uppermost mantle velocities beneath China and surrounding regions. J. Geophys. Res., 109(B11), doi: 10.1029/2003JB002874

Huang, J., Zhao D. and Zheng S., 2002. Lithospheric structure and its relationship to seismic and volcanic activity in southwest China. J. Geophys. Res., 107, doi: 10.1029/2000JB000137.

Kárason, H., and Van der Hilst, RD, 2000. Constraints on mantle convection from seismic tomography. In M.A. Richards, R. Gordon and R.D. van der Hilst (Editors). History and Dynamics of Plate Motion. Am. Geophys. Union, Geophys. Monogr. Ser., 121, 277-288.

Kárason, H., and van der Hilst, R.D., 2001. Tomographic imaging of the lowermost mantle with differential times of refracted and diffracted core phases (PKP, Pdiff). J. Geophys. Res., 106, 6569-6587.

Kárason, H., 2002. Constrains on mantle convection from seismic tomography and flow modeling, Ph.D. thesis, MIT.

Kennett, B.L.N., Engdahl, E.R., and Buland, R., 1995. Constrains on seismic velocities in the Earth from travel times. Geophys. J. Int., 122, 108-124.

Kind, R., Ni, J., Zhao, W., Wu, J., Yuan, X., Zhao, L., Sandvol, E., Reese, C., Nabelek, J., and Hearn, T., 1996. Mid-crust low velocity zone beneath the southern Lhasa block: Results from the INDEPTH-II earthquake recording program. Science, 274, 1692-1694.

Kind, R., Yuan, X., Saul, J., Nelson, D., Sobolev, S.V., Mechie, J., Zhao, W., Kosarev, G., Ni, J., Achauer, U., and Jiang, M., 2002. Seismic Images of crust and upper mantle beneath Tibet: evidence for Eurasian plate subduction. Science, 298, 1219-1221.

Kosarev, G., Kind, R., Sobolev, S.V., Yuan, X., Hanka, W., and Oreshin, S., 1999. Seismic evidence for a detached Indian lithospheric mantle beneath Tibet. Science, 283, 1306-1309.

Lebedev, S., and Nolet, G., 2003. Upper mantle beneath Southeast Asia from S velocity tomography. J. Geophys. Res., 108, 2048-2074.

Lebedev, S., Nolet, G., Meier, T., and van der Hilst, R., 2005. Automated multimode inversion of surface and S waveforms. Geophys. J. Int., 162, 951-964.

Li, Z.X., Tectonic history of the major East Asian lithosphere blocks since the mid-Proterozoic. In Flower M. et al. (Editors). Mantle Dynamics and Plate Interactions in East Asia, Geodyn. Ser., 27, 211-243.

Liang, C.T., Song, X.D., and Huang J.L. 2004. Tomographic inversion of Pn travel times in China. J. Geophys. Res., 109(B11), doi: 10.1029/2003JB002789.

Molnar, P., and Tapponnier, P., 1975. Cenozoic tectonics of Asia: Effects of a continental collision. Science, 189, 419-426.

Montelli, R., Nolet, G., Dahlen, F.A., Masters G., Engdahl E.R., and Hung S.H., 2004. Finite-frequency tomography reveals a variety of plumes in the mantle. Science, 303, 338-343.

Northrup, C., Royden, L., and Burchfiel B., 1995. Motion of the pacific plate relative to Eurasia and its potential relation to Cenozoic extension along the eastern margin of Eurasia. Geology, 23, 719-722.

Paige, C.C., and Saunders, M.A., 1982. LSQR: an algorithm for sparse linear equations and sparse least squares. ACM Trans. Math. Soft. 8, 43-71.

Replumaz, A., Kárason, H., van der Hilst, R.D., Besse, J., and Tapponnier, P., 2004. 4-D evolution of SE Asia's mantle from geological reconstructions and seismic tomography. Earth Planet. Sc. Lett., 211, 103-115.

Rapine, R., Tilmann, F., West, M., and Ni, J., 2003. Crustal structure of northern and southern Tibet from surface wave dispersion analysis. J. Geophys. Res., 108(B2), 2120, doi:10.1029/2001JB000445

Shapiro, N.M., and Ritzwoller, M.H., 2002. Monte-Carlo inversion for a global shear-velocity model of the crust and upper mantle. Geophys. J. Int., 151, 1-18.

Sol, S.J., A. Meltzer, B. Zurek, X. Zhang, J. Zhang, 2004. Insight into the lithospheric structure and deformation in Eastern Tibet from splitting and travel time variations of core phases, Eos Trans. AGU, 85(47), Fall Meet. Suppl., Abstract, T31A-1279.

Sun, Y., Li, X., Kuleli, S., Morgan, F.D., and Toksöz, M.N., 2004. Adaptive moving window method for 3D P-velocity tomography and its application in China. Bull. Seism. Soc. Am., 94, 740-746.

Tapponnier, P., and Molnar, P., 1977. Active faulting and tectonics in China, J. Geophys. Res., 82, 2905-2930.

Tapponnier, P., Zhiqin, X., Roger, F., Meyer, B., Arnaud, N., Wittlinger, G., and Jingsui, Y., 2001. Oblique stepwise rise and growth of the Tibet Plateau. Science, 294, 1671-1677

Tilmann, F., and Ni, J., 2003. Seismic imaging of the downwelling Indian lithosphere beneath central Tibet. Science, 300, 1424-1427.

Trampert J., and Woodhouse J., 1995. Global Phase-velocity maps of Love and Rayleigh waves between 40 and 150 seconds. Geophys. J. Int. 122: 675-690.

Van der Hilst, R.D., Engdahl, E.R., Spakman, W., and Nolet, G., 1991. Tomographic imaging of subducted lithosphere below northwest Pacific island arcs. Nature, 353, 37-43.

Van der Hilst, R.D., and Seno, T., 1993. Effects of relative plate motion on the deep structure and penetration depth of slabs below the Izu-Bonin and Mariana island arcs, Earth Planet. Sci. Lett., 120, 395-407.

Van der Hilst, R.D., Widiyantoro, S., and Engdahl, E.R, 1997. Evidence for deep mantle circulation from global tomography. Nature, 386, 578-584.

Van der Hilst, R.D., Chen, Z., Li, C., Lev, E., Xu, L., and Yao, H., 2005. Crust and Upper Mantle Structure Beneath Sichuan/Yunnan Provinces, SW China: Preliminary Results of a Joint MIT-CIGMR Broad-Band Seismometry Project. Trans. Am. Geophy. Un. Spring Meeting, Abstract, S41A-01.

Van der Voo, R., Spakman, W., and Bijwaard, H., 1999. Tethyan subducted slabs under India, Earth Planet. Sci. Lett., 171, 7-20.

Waldhauser, F., Lippitsch, R., Kissling, E., and Ansorge, J., 2002. High-resolution teleseismic tomography of upper-mantle structure using an a priori three-dimensional crustal model. Geophys. J. Int., 150, 403-414.

Wang, C.Y., Chan, W., and Mooney, W., 2003. Three-dimensional velocity structure of crust and upper mantle in southwestern China and its tectonic implications. J. Geophys. Res., 108(B9), 2442, doi: 10.1029/2002JB001973.

Weidle, C., Widiyantoro, S., and CALIXTO Working Group, 2005. Improving depth resolution of teleseismic tomography by simultaneous inversion of teleseismic and global P-wave travel time data: application to the Vrancea region in Southeastern Europe. Geophys. J. Int., 162, 811-823.

Widiyantoro, S., and van der Hilst, R.D., 1997. Mantle structure beneath Indonesia inferred from high-resolution tomographic imaging. Geophys. J. Int., 130, 167-182.

Widiyantoro, S., and van der Hilst, R.D., 1996. Structure and evolution of lithospheric slab beneath the Sunda arc, Indonesia. .Science, 271, 1566-1570.

Zhang, Z.M., Liou, J.G., and Coleman, R.G., 1984. An outline of the plate tectonics of China, Geol. Soc. Am. Bull, 95, 295-312.

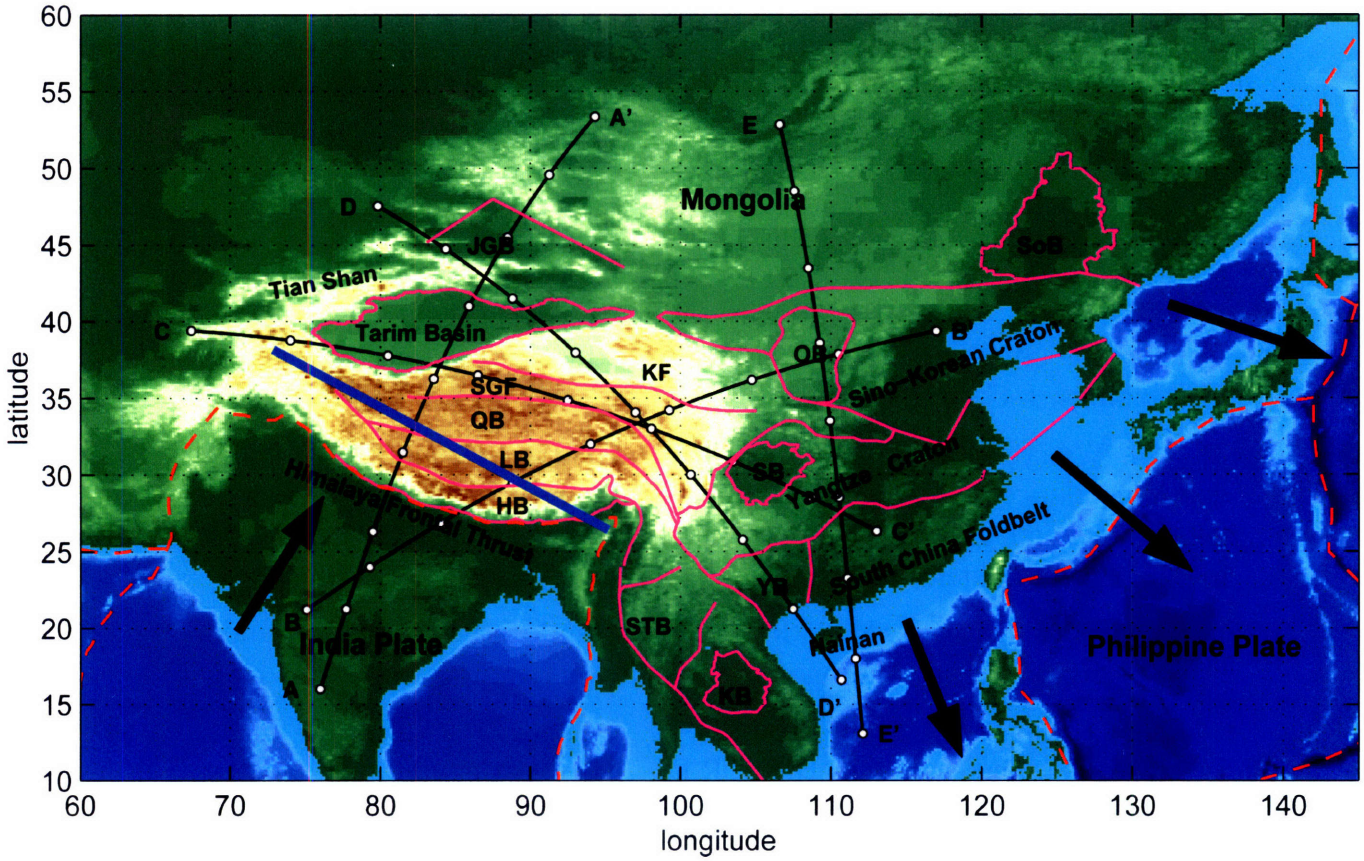

Figure 3-1. The main tectonic elements in the SE Asia. The dashed red lines are plate boundaries, according to NUVEL-1 (DeMets et al., 1990). The thick purple lines denote main tectonic structures, where SoB-Songliao Basin, OB-Ordos Basin, SB-Sichuan Basin, KB-Khorat Basin, STB-Shan Thai Block, YB-Youjiang Block, JGB-Junggar Basin, SGF-Songpan Ganzi Foldbelt, QB-Qiangtang Block, LB-Lhasa Block, HB-Himalayan Block, KF-Kunlun Fault (modified from Li, 1998 and Tapponnier et al., 2001). Black arrows show the continental collision in the west and slab roll back in the east set up the clockwise rotation for the SE Asia. The blue thick line shows the horizontal limit of the Indian lithospheric mantle beneath the Tibetan plateau. The positions of five cross sections in Figure 3-9 are shown by black lines with grey dots.

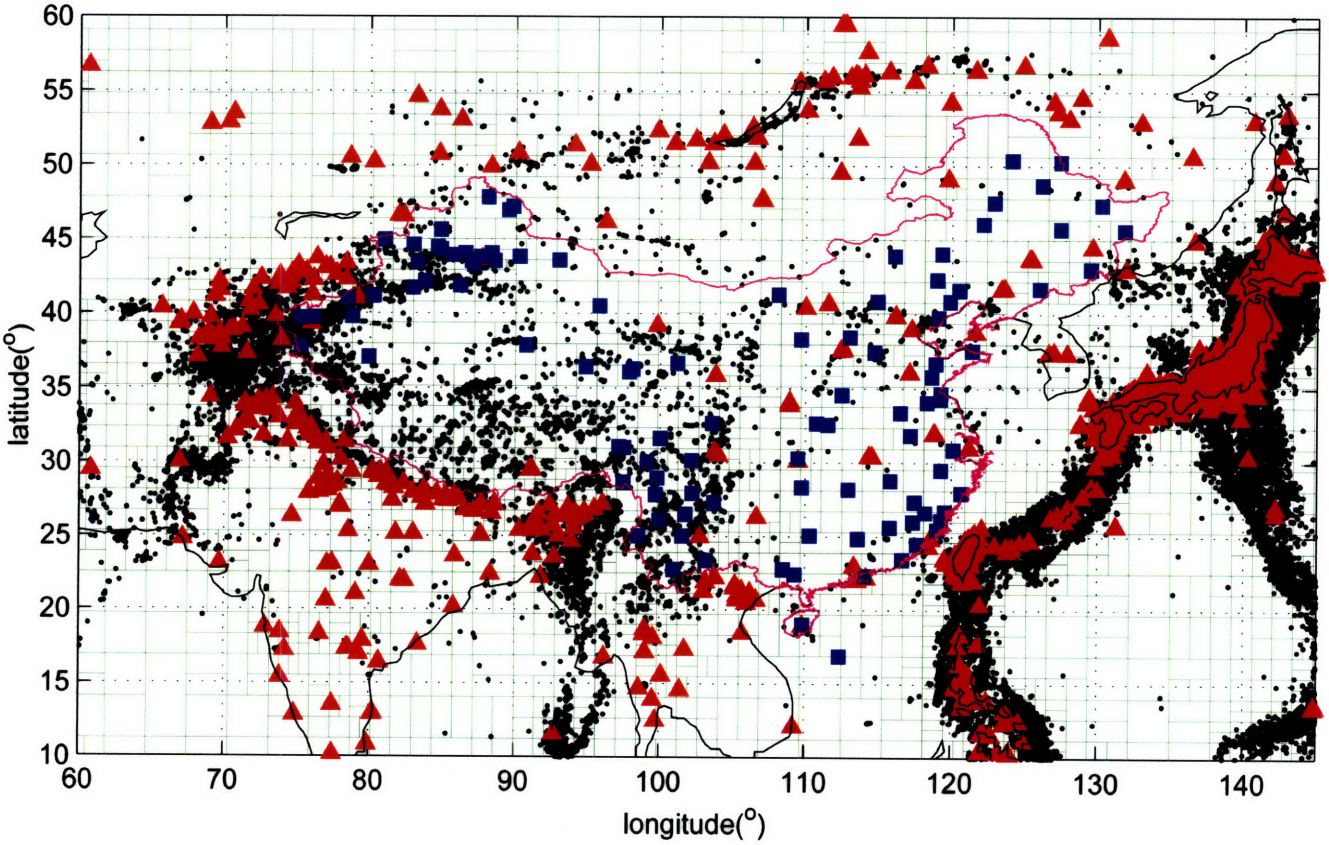

Figure 3-2. The distribution of stations and earthquakes (black dots) in Southeast Asia and the irregular grids at 200km depth. The irregular grid, depicted here with thin green lines for 200 km depth, allows us to resolve the fine structure in regions of dense sampling. Blue squares depict 107 stations of ABCE from which data were not previously reported to ISC. Red triangles depict the 1223 EHB stations in the area of interest, of which 44 stations are located in the mainland China.

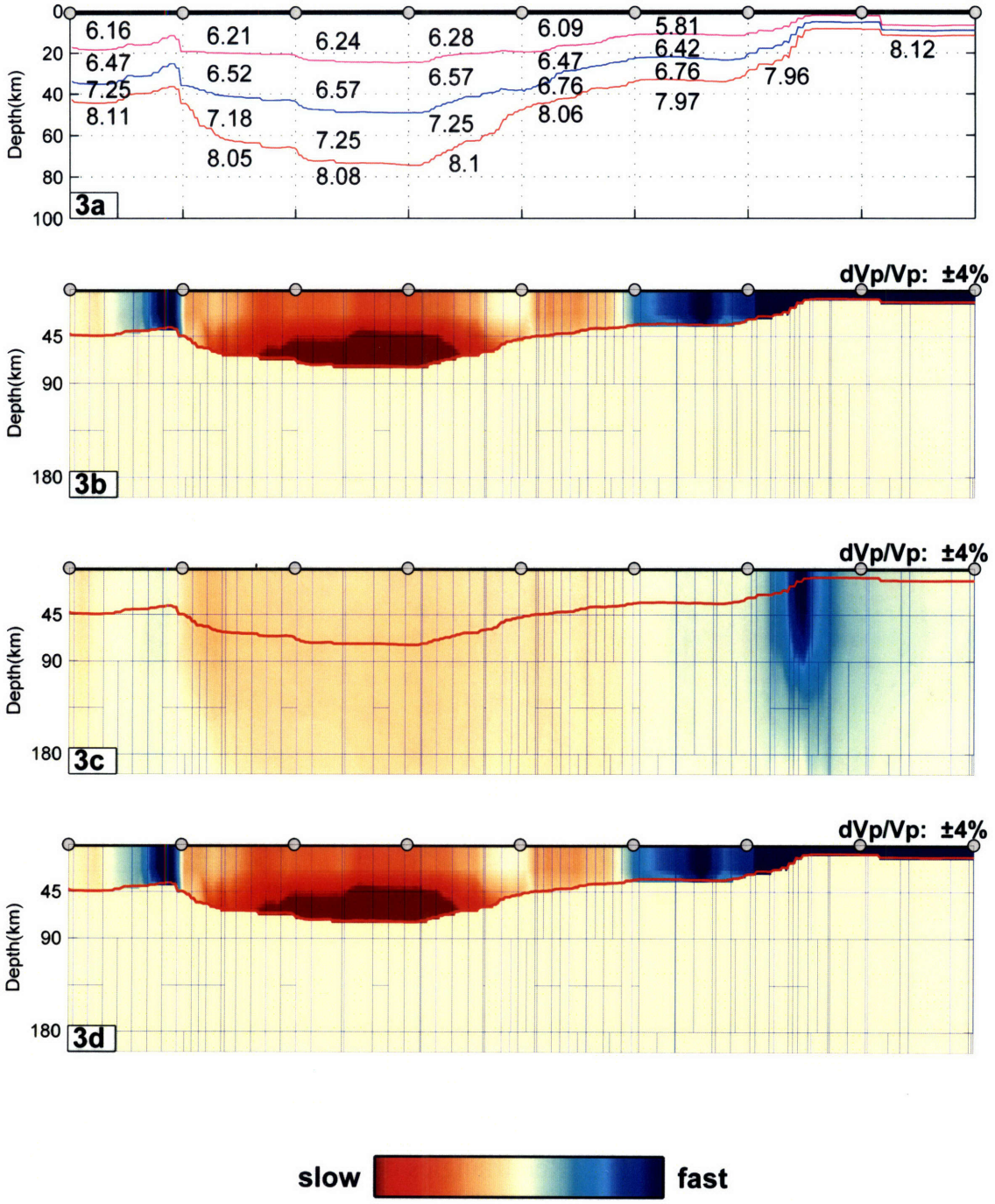

Figure 3-3. Regularization for 3D crust. a) Three layers of crust through the Tibetan plateau and Philippine Sea (From (59°E 35°N) to (134°E 14°N)). *P* wavespeeds of input model (in km/s) for each layer is shown. b) Vertical projection of 3D crust on irregular grid. c) The recovery model using same inversion scheme and sampling as in the construction of the final model. d) The recovery model using the regularization in the model space for crust. After regularization, the big velocity variation of the crust can be confined in crustal blocks. Moho depth (red line) and irregular grid (blue line) are shown in b, c, and d.

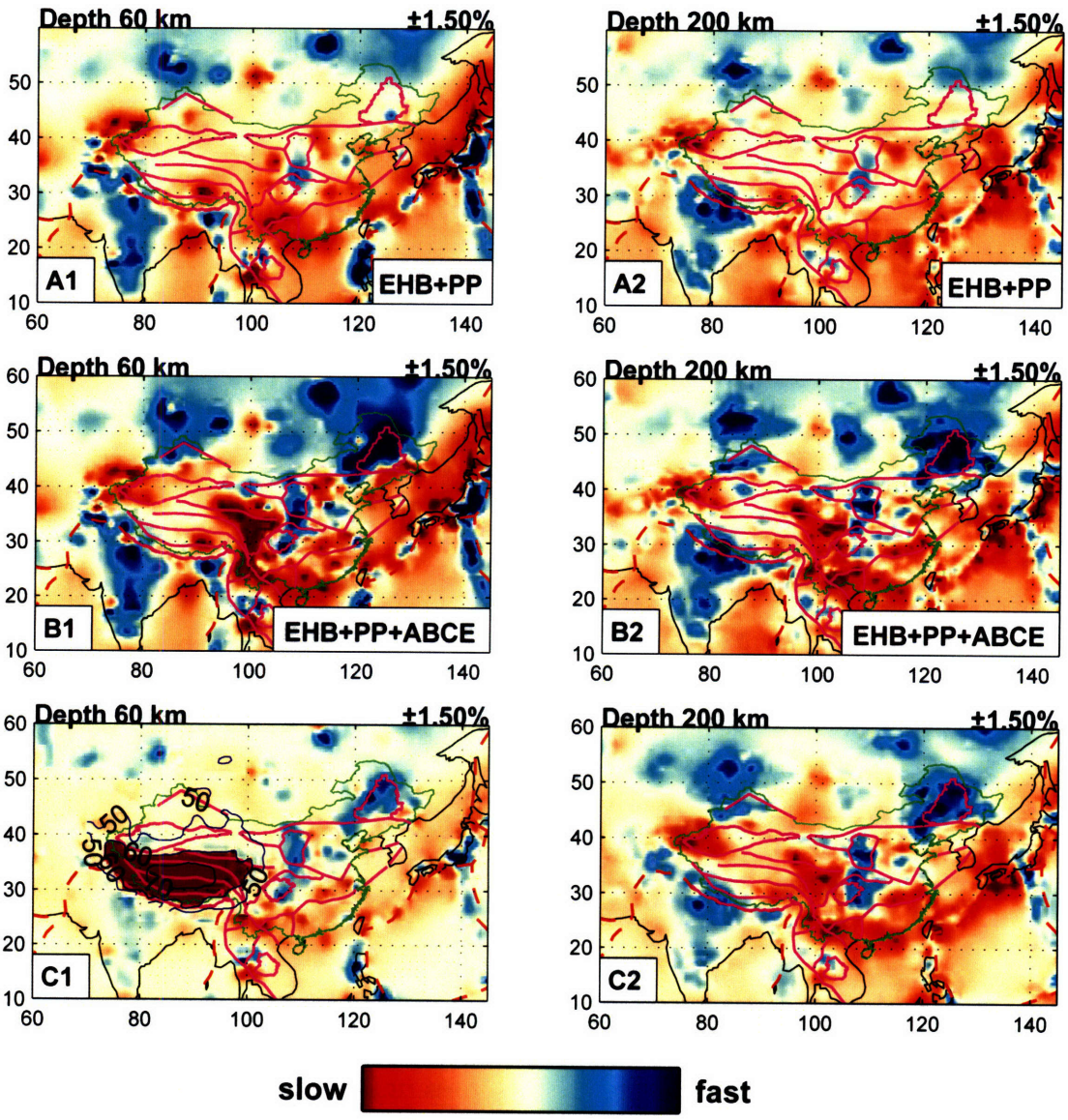

Figure 3-4. Effects of data addition and crust correction; for illustration purposes we only display the models at 60 and 200 km depth. A) Model based on EHB and PP data only. B) EHB + PP + ABCE data. C) EHB + PP + ABCE + 3D crust correction. Regularization in the model space not only recovers the big anomaly in the crust, it can also balance the crust and upper mantle to best fit the travel time residuals. Figure 3-4C1 depicts the 50, 60, and 70 km depth contours of the 3D crust model used; within these contours the wavespeed is much lower than in the reference values (*ak135*), see Figure 3-3b.

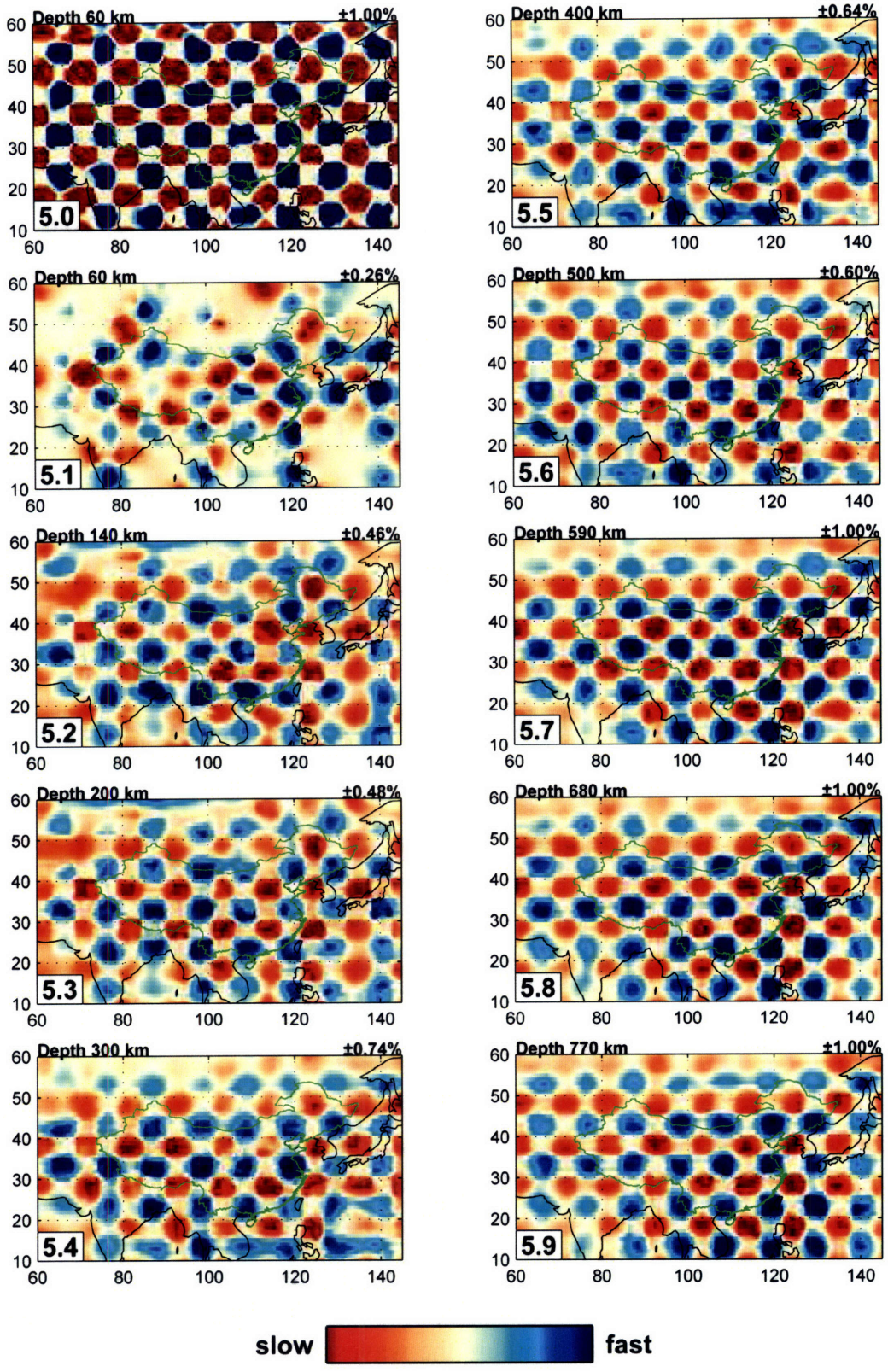

Figure 3-5. Checkerboard resolution test for target anomalies at different depths. Input pattern (5×5 degree) is shown in 5.0.

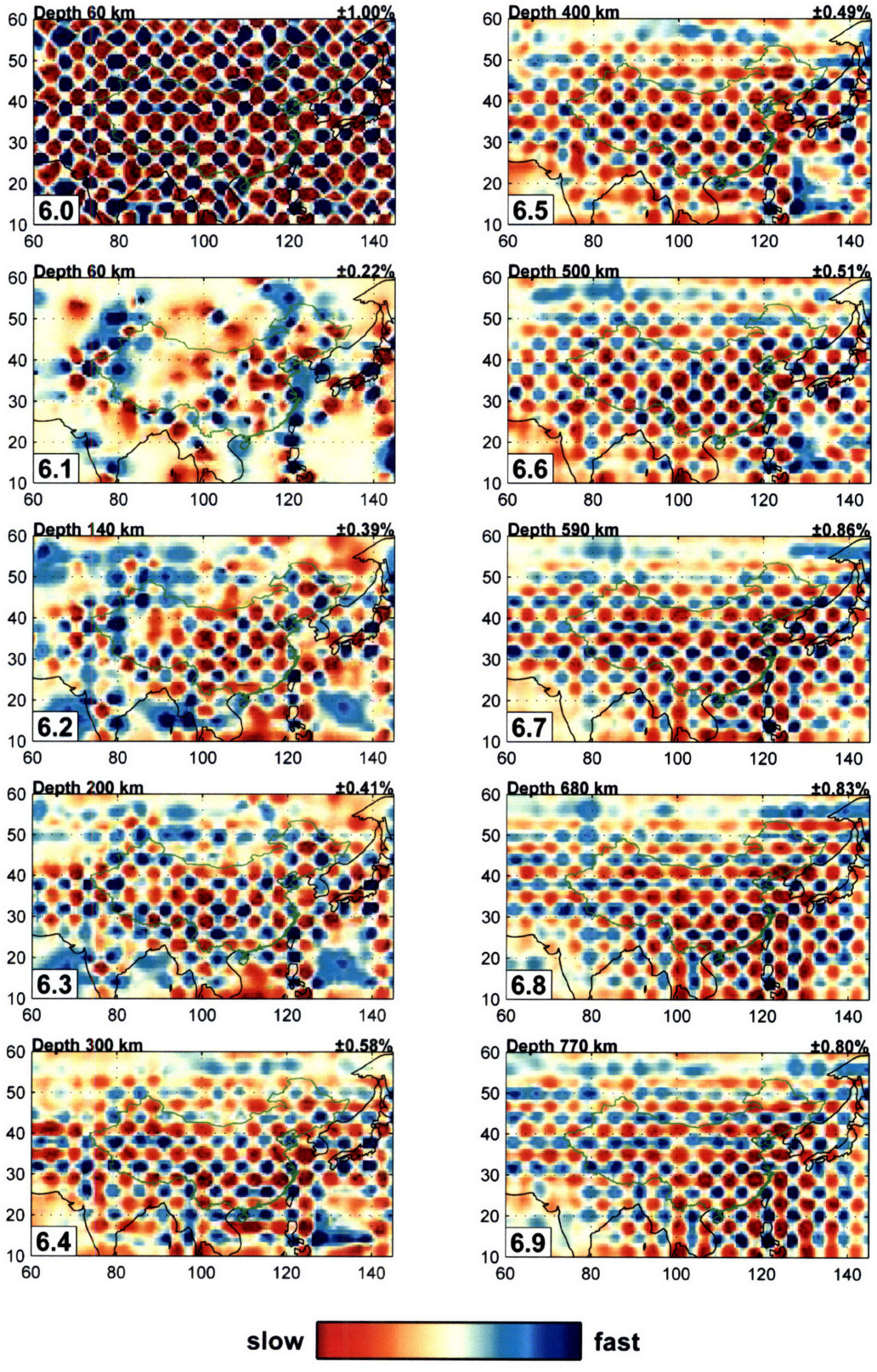

Figure 3-6. Checkerboard resolution test for target anomalies at different depths. Input pattern (3×3 degree) is shown in 6.0.

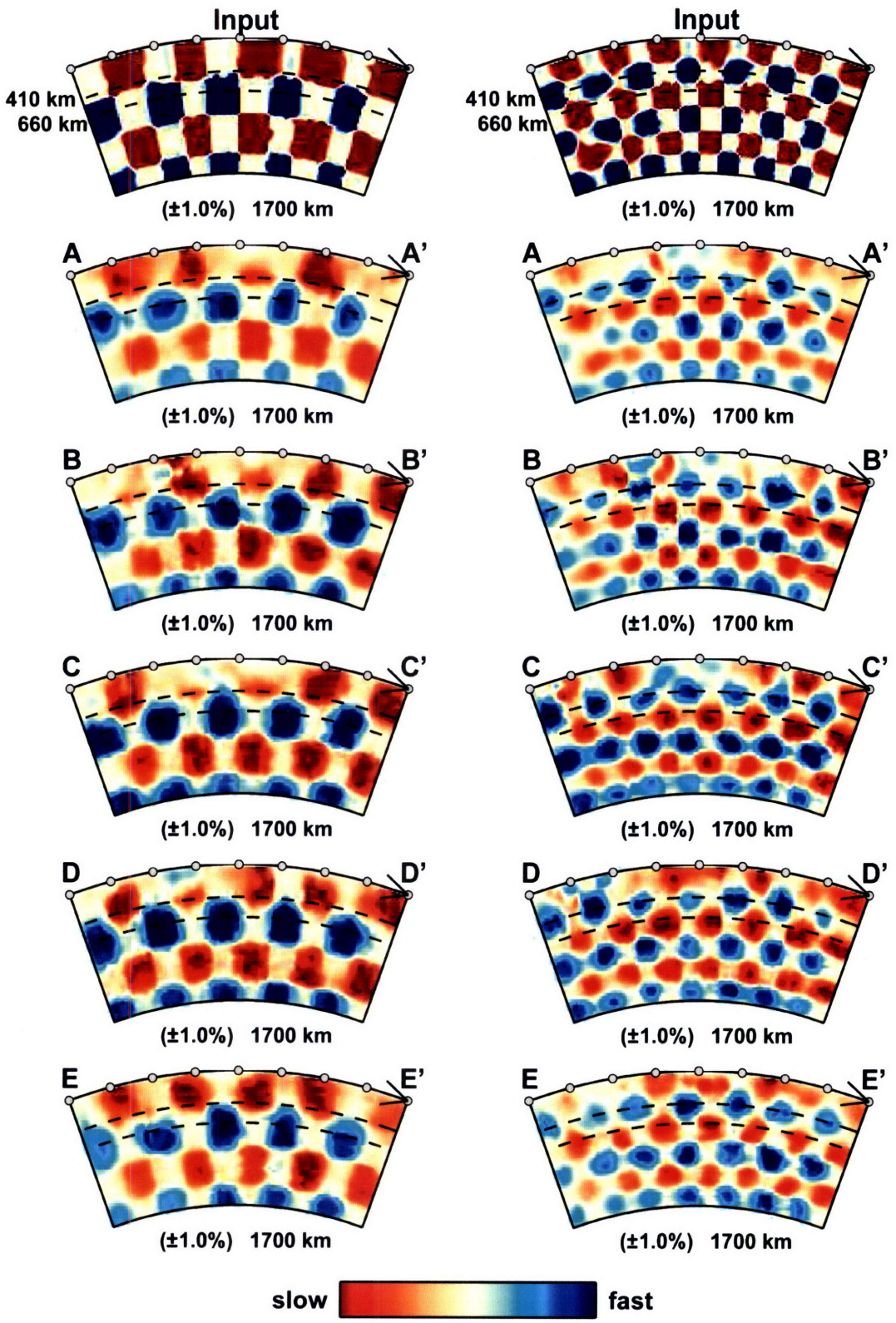

Figure 3-7. Vertical checkerboard resolution tests at five slices, as depicted in Figure 3-1. For each slice we use the same input pattern (show at the top) with target anomalies of 400×400 km (left) and 280×280 km (right).

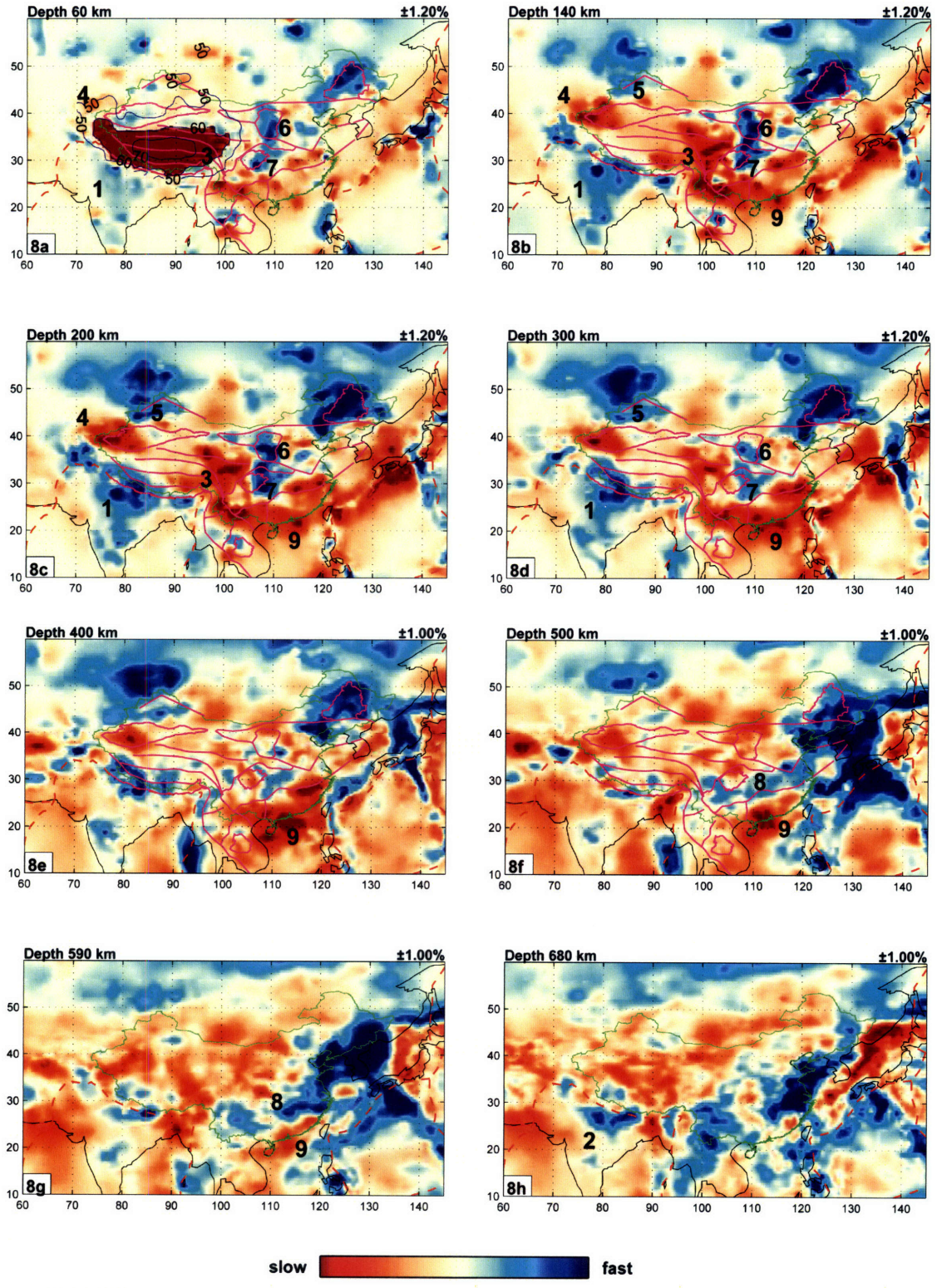

Figure 3-8. Lateral *P* wavespeeds perturbation at different depths as indicated on the left corner. The blue and red represent fast and slow perturbation respectively. The perturbation scale is shown on the right upper corner. The significant structures have labeled as 1, 2, 3, etc.

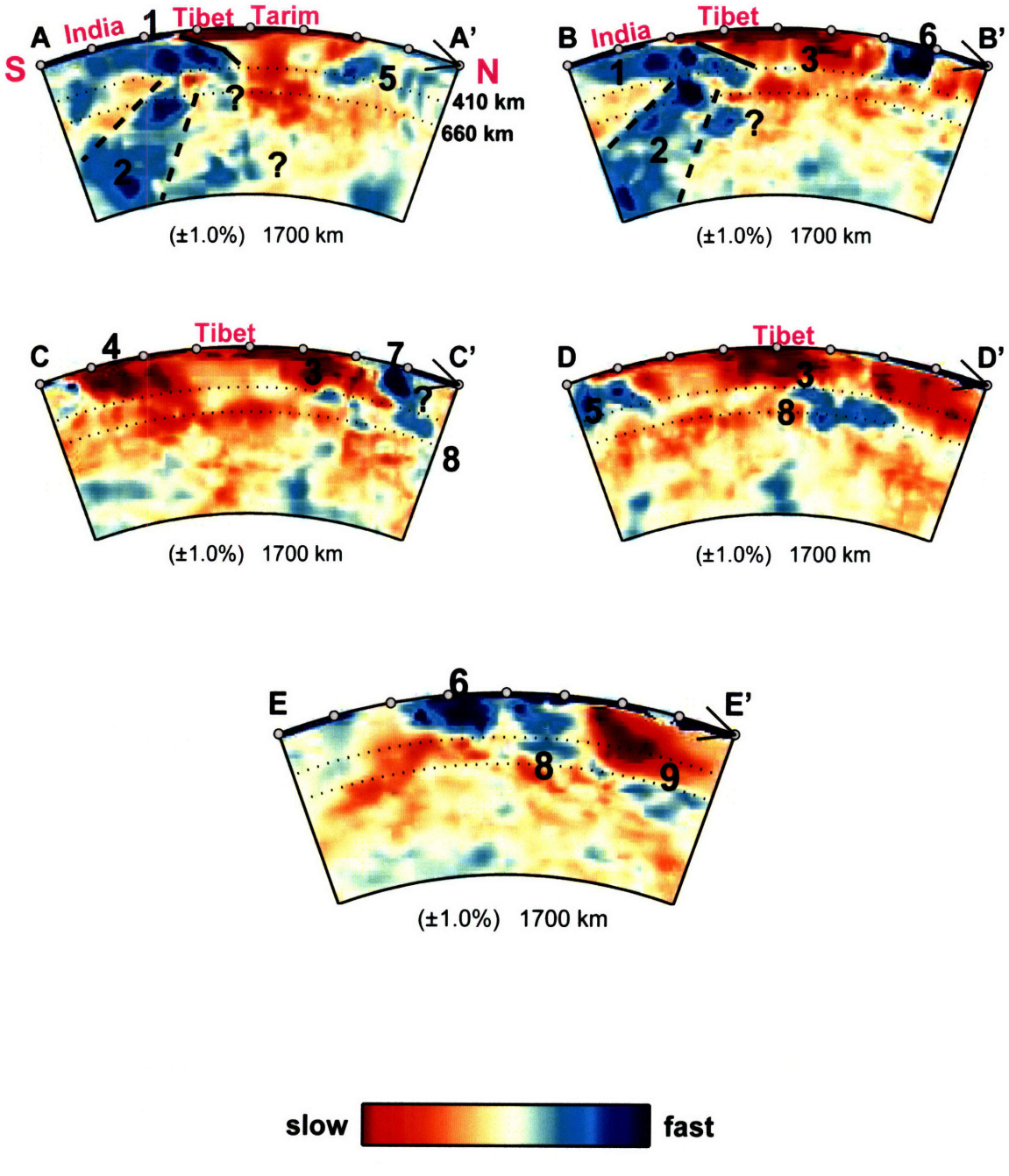

Figure 3-9. Vertical cross sections through some of the main features of the velocity model down to 1700 km depth. The locations of cross sections AA', BB', CC', DD', and EE' are indicated in Figure 3-1.

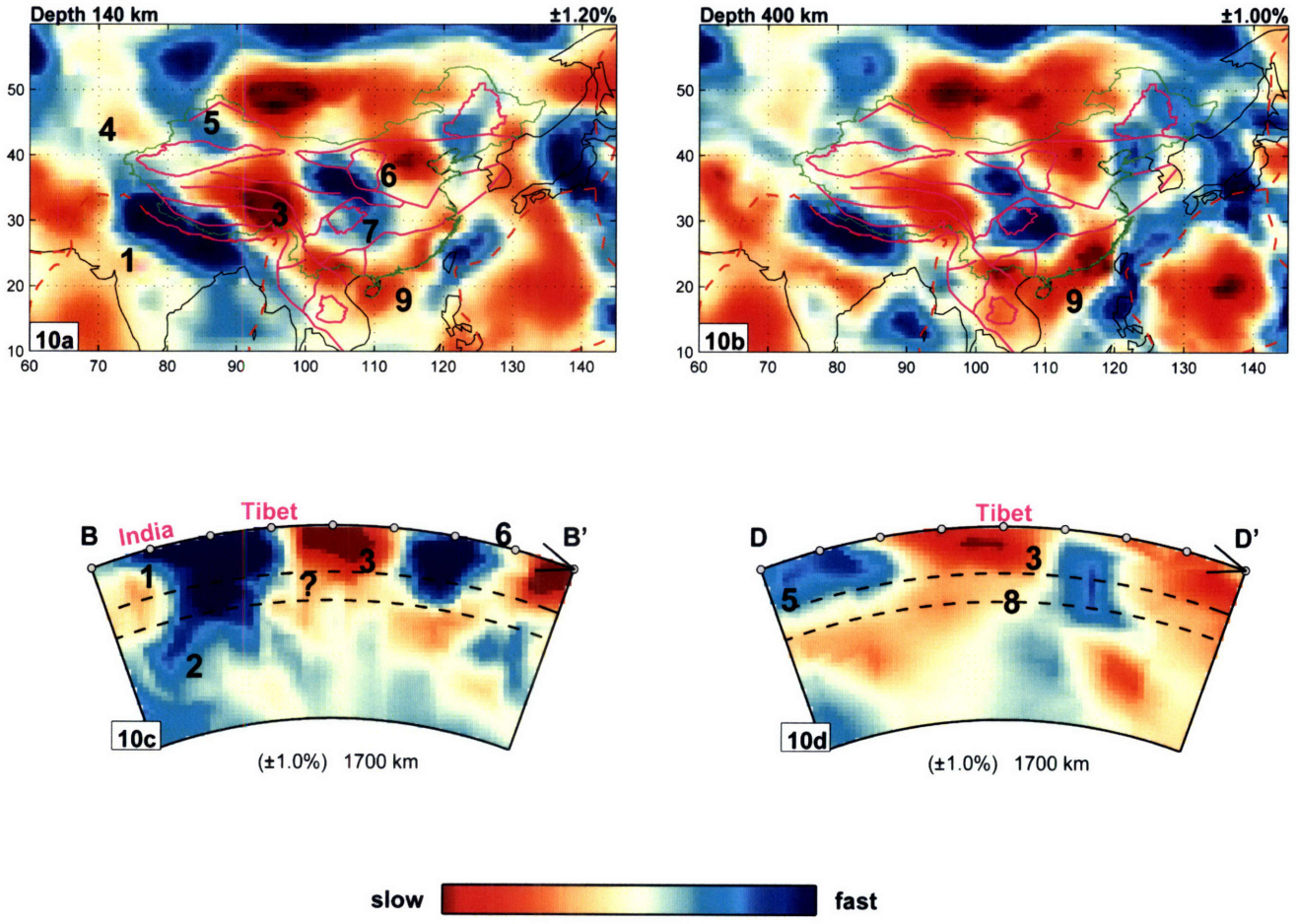

Figure 3-10. (a, b) Lateral *P* wavespeeds perturbation of model from Montelli et al. (2004) at 140 and 400 km depth. (c, d) Vertical cross sections along BB' and DD'.

Chapter 4

Imaging Indian subduction beneath the Tibetan Plateau and Burma[3]

Abstract

The subduction of Indian lithospheric mantle under Eurasia plays an important role in the tectonic evolution of the Tibetan plateau and surrounding regions. Due to limited seismic data coverage, our understanding of upper mantle structure, and hence, the evolution of Indian subduction remains enigmatic. To improve tomographic imaging, we combine P-wave arrival time data from several temporary seismic arrays on the Tibetan plateau and from ~1200 stations of Chinese Seismograph Network with reprocessed data from the International Seismological Centre. The combined datasets ensure unprecedented resolution of structures associated with subducted plates beneath Tibet and surrounding ranges. The dip angle of Indian subducted lithosphere increases from west to east. Beneath western Tibet, the subducted plate underlies the entire plateau, but beneath the center part of the collision zone the subducted Indian plate does not extend beyond the Bangong-Nujiang Suture (~33°N). In contrast to results of surface wave tomography, our results reveal anomalously slow P-wave propagation beneath much of central and eastern Tibet. These observations suggest that much of the Tibetan Plateau is underlain by lithosphere of Asian origin. The seismic images reveal that to 250-300 km depth the Precambrian roots of the Ordos Block and Sichuan Basin are marked by fast P-wave propagation. The Tengchong volcanic area in southwest China is underlain by pronounced low velocity to 200 km depth, suggesting that it is related to the eastward subduction from the Burmese arc.

[3] Li, C., van der Hilst, R., Meltzer, A., Sun, R., and Engdahl E.R.. Imaging Indian subduction beneath the Tibetan Plateau and Burma, in preparation for submission to *Earth Planet. Sci. Lett.*

Another pronounced slow structure is situated beneath the Red River fault region to at least 300 km depth and extending all the way to the South China Sea. It is more likely related to low velocity anomalies beneath the South China Sea induced by the subduction of India-Australia, Philippine Sea and Pacific plates. Observed change in anisotropy, from shear wave splitting, coincides with structure heterogeneity in the upper mantle beneath the Xianshuihe-Xiaojiang fault system (XXFS), in between the Sichuan Basin and Burma range.

4.1 Introduction

The Tibetan plateau was generated by the collision and post-collisional intracontinental deformation of Indian and Eurasian plates beginning between ~50 and ~65 million years ago. Following continental collision, the crust under the central and northern parts of the plateau has approximately doubled in thickness to 70 km, while its elevation has increased to 4-5 km (Molnar and Tapponnier, 1975; Coward *et al.*, 1988; Dewey *et al.*, 1988). North-south trending normal faults and east-west trending fast polarization directions indicate east-west extension in central and southern Tibet (Huang *et al.*, 2000; Sol *et al.*, 2007). Within the southeastern plateau, clockwise rotational deformation suggested from Global Positioning System (GPS) measurements is manifested by active left lateral strike-slip fault systems (Chen *et al.*, 2000). However, complex fast polarization directions in southeast Tibet indicate that structure in the upper mantle is different from active structures observed at the surface (Lev., *et al.*, 2006) (Figure 4-1).

Distinctly different models have been proposed for the tectonic evolution of Tibet, such as uniform thickening and shorting of Asian lithosphere (England and Houseman, 1986), block extrusions along principal strike-slip faults (Tapponnier *et al.*, 1982, 2001), southward subduction of Asian lithosphere under Tibet (e.g., Willett and Beaumont, 1994; Roger *et al.*, 2000; Kind *et al.*, 2002), and thrusting of the Indian lithospheric mantle under Asia (e.g., Argand, 1924; Powell, 1986; Owens and Zandt, 1997; Kosarev *et al.*, 1999; Tilmann *et al.*, 2003). Knowing the 3-D geometry of subduction of Indian lithosphere would help distinguish between these evolutionary models, or inspire new ones, but many of its first order aspects, including its present-day lateral and depth extent and how these may change laterally along the collision boundary have remained largely unknown.

Prior to plate tectonic theory geoscientists thought that the northern edge of the Indian lithosphere underthrust the entire Tibetan plateau and that this had produced the Himalayan Mountains and the Plateau (Argand, 1924; Holmes, 1965). With the advent of plate tectonic theory, a number of studies based on tectonic data have focused on reconstructing the motion of the Indian plate relative to Eurasia since the Late Cretaceous and estimated the magnitude of Indian subduction based on the surface area of the Indian plate before the collision (Patriat and Achache, 1984; Besse and Courtillot, 1988; Lee and Lawver, 1995; Acton, 1999; Replumaz and Tapponnier, 2003). These studies are mainly based on near-surface observations and kinematic plate reconstructions. It is likely that

these processes have created or respond to complicated heterogeneity in the upper mantle, but the relationship between near-surface and deeper mantle processes remains enigmatic. Seismic imaging can provide constraints on deeper structure, but pertinent information has been available only from relatively low resolution global and regional studies or from high resolution studies of limited spatial extent. This has now begun to change.

A number of studies have focused on imaging the upper mantle beneath the Himalaya-Tibet region. Global surface wave studies have suggested that Indian lithospheric mantle has subducted from the Himalayas beneath western Tibet to ~200 km depth (e.g., Shapiro, *et al.*, 2002). Several regional surface wave studies have also shown that at ~150 km depth fast shear wave velocities prevail in western and southern Tibet (e.g., Friederich, 2003). Van der Voo *et al.* (1999) used results from global P-wave travel time tomography to suggest that Indian lithosphere was sinking into the mantle almost directly beneath the Himalayan Mountains. Regional P-wave travel time studies have suggested, however, that the Indian lithosphere subducts as far north as the Bangong-Nujiang suture (~33°N) (Huang and Zhao, 2006) or even further north under the entire plateau (Zhou and Murphy, 2005). In general, poor lateral resolution of surface wave studies and sparse station coverage of body wave studies in Tibet limit the structural wavelengths that can be resolved consequently these studies only provide weak constraints on the subduction of the Indian lithosphere.

In order to image the structure of the crust and mantle beneath Tibet in more detail, a number of seismic experiments have been carried out in the Tibetan plateau. The INDEPTH project (Nelson *et al.*, 1996), for instance, suggested a partially molten zone in the middle crust of southern Tibet. Surface wave dispersion analysis showed that beneath the uppermost mantle fast velocity anomalies prevails in southern Tibet and that slow velocity anomalies are found only beneath northern Tibet (Raphine *et al.*, 2003). Inefficient *Sn* propagation and low *Pn* velocities have been found in the north Tibet and high *Pn* velocities are dominant beneath southwestern Tibet (McNamara *et al.*, 1995; McNamara et al., 1997). Using *P*-to-*S* converted teleseismic waves along a NNE-SSW oriented receiver network in eastern Tibet, Kosarev *et al.* (1999) suggested that a north-dipping Indian lithosphere begins north of the Zangbo suture (~29°N) and continues to a depth of 200 km beneath the Bangong suture (~33°N). Teleseismic P-wave travel time tomography based on the data from the INDEPTH project suggested a subvertical high velocity zone from 100 to 400 km depth beneath the area south of Bangong suture (Tilmann *et al.*, 2003). In summary, studies from the INDEPTH projects suggested that the Indian lithosphere has underthrust Asia to as far north as the Bangong-Nujiang suture. However, due the almost linear seismic network from north to south, these studies give insight only into a two-dimensional (2-D) structure (around 90°E), and lack of full 3-D sampling can produce imaging artifacts.

Recent areal seismic arrays deployed by M.I.T. in collaboration with the Chengdu Institute of Geology and Mineral Resource (CIGMR) and by Lehigh University - CIGMR (2003~2004) provided good coverage in southeastern Tibet. The data from these arrays have already been used for surface wave tomography (Yao *et al.*, 2006), receiver functions (Xu *et al.*, 2007) and shear wave splitting studies (Lev *et al.*, 2006; Sol *et al.*, 2007). Here we combine data from MIT-CIGMR, Lehigh-CIGMR, and previous seismic arrays in Tibet, and the Chinese Seismography Network (CSN, ~1200 stations) with data from the International Seismological Centre (ISC), which has been reprocessed by Engdahl *et al.* (1998, hereinafter referrer as to EHB). The denser and more uniform station coverage of the combined datasets ensures unprecedented resolution in the upper mantle of the plateau and surrounding regions (Figure 4-2).

We focus on 3-D images of the Indian subduction system, from Hindu-Kush, along the Himalayas, to Burma. This study shows significant lateral variations in the Indian subducted lithosphere along the Himalayas. The Indian lithosphere only underlays the western portion of Tibet. The dip angle gradually increases from west to east, which may explain the formation of Cenozoic north-south rifts in the central plateau. Some Indian lithospheric mantle seems to subduct to ~500 km depth under the central plateau, however does not extend north beyond the Bangong-Nujiang suture (~33°N). By implication, most of the Tibetan lithosphere is of Asian origin. The subduction beneath Burma appears to be separated from the

Indian subduction at depths larger than ~200 km and descends to ~500 km depth beneath the active volcanic Tengchong region.

4.2 Data

The data most relevant for this study come from four sources: (1) picked arrival times from regional (temporary) seismic arrays; (2) reports from ~1200 national and provincial stations of the Chinese Seismography Network (CSN) during 1967 to 2004; (3) the EHB dataset reprocessed from the International Seismological Center (ISC) during 1964 to 2004; (4) global *PP-P* dataset

Array data: we pick P-wave arrivals from local, regional, and teleseismic earthquakes recorded at one or more of the ~170 seismometers of MIT-CIGMR, Lehigh-CIGMR, and previous seismic arrays on the plateau (Figure 4-2, see Appendix 1 for more information about the seismic arrays in Tibet). In practice, reliable and accurate automatic picking remains a serious challenge and an experienced human observer might be the best picker engine. However the size of combined datasets prohibits manual processing. Here we apply the automatic picking software MannekenPix (Aldersons *et al.*, 2003) to pick the first arrivals from these arrays data. The picking engine of MannekenPix is the Baer-Kradolfer algorithm (1987) based on the energy ratios of the short term behavior to the long-term trend. To calibrate the algorithm to our data sets, we manually pick ~20 percent of raw data and compare with corresponding automatic pickings, and we

adjust the criteria in the picking engine to ensure accuracy and consistency. In total, we picked ~22,000 *P* and ~13,000 *Pn* arrivals.

Travel time residuals are then computed by subtracting travel times calculated based on the *ak135* reference model (Kennett *et al.*, 1995). In Figure 4-3, we show the geographical pattern of travel time residuals (after elevation correction) of the Tibetan arrays. For most stations we have more than 200 first arrival picks. The pattern of travel time residuals shows a distinct direction-dependent distribution. For all stations, including those on the southern parts of the plateau, arrivals from earthquakes north and northwest of the arrays have large and positive residuals. This is mainly due to propagation through thick Tibetan crust and perhaps relatively low velocity anomalies in the upper mantle under the plateau. In contrast, most arrivals from the south and southeast appear relatively fast. Even without tomographic inversion, the pattern of travel time residuals thus suggests slow P-wave propagation beneath the plateau and higher propagation speed in the south, perhaps related to the Indian subducted lithosphere.

Chinese Seismography Network (CSN): the second part of the data used in this study comes from ~1200 national and regional stations of the CSN, of which about 200 stations are located under the eastern plateau and SW China (red squares on Figure 4-2). We use about 1 million *P* and *Pn* phases from 1967 to 2004, which far exceeds the number of data from the Annual Bulletin of Chinese Earthquake (ABCE) used previously (*Li et al*, 2006).

Global EHB catalog: the third part of our data comes from the global EHB catalog. We use about 10 million *P*, *Pg*, *pP*, *Pn* and *PKP* phases from 1964 to 2004. About 100 stations of the EHB are located within the Indian plate and the Himalayas (yellow triangles in Figure 4-2) and provide key constraints on the Indian subducted lithosphere. Station coverage in the plateau and surrounding regions is thus greatly improved and provides higher spatial resolution in the upper mantle for our region of interest (Figure 4-2).

Global *PP-P* data: we use the differential times of *PP-P*, accurately measured by waveform cross-correlation from digital seismogram (Woodward and Master, 1991), to resolve structures in the upper mantle of region with few earthquakes and stations, such as northern Tibetan plateau and Tarim Basin.

Combining the global, regional and local seismic network data is not trivial, and careful processing is required to avoid internal inconsistencies. After deleting duplicate stations before incorporating all data from EHB, CSN and Tibetan arrays, we calculate new travel time residuals using a non-linear process of earthquake relocation and phase re-identification (Engdahl *et al.*, 1998). This ensures that data from different sources are consistent with each other. To compensate for the relatively small volume but high quality of the datasets compared to the routinely processed global and regional data, however, we apply larger weights to data from the Tibetan arrays.

4.3 Methodology

To mitigate effects of uneven data coverage we use an adaptive parameterization, in which the size of grid block is based on the sampling density of the high frequency data (Abers and Roecker, 1991; Bijwaard *et al.*, 1998; Kárason and van der Hilst, 2000). The size of the blocks is a multiple of 45 km×0.35°×0.35° in depth, latitude, and longitude beneath the Tibetan plateau and surrounding regions (down to 800 km depth) and 45 km×0.7°×0.7° elsewhere. The total number of free parameters (the sampled irregular blocks and the event relocation parameters in the global model) is about 0.5 million.

We use the iterative LSQR algorithm (Paige and Saunders, 1982) to minimize an objective function combining a measure of data misfit and regularization terms:

$$\varepsilon = \| \mathbf{Gm} - \mathbf{d} \|^2 + \lambda_1 \| \mathbf{m} \|^2 + \lambda_2 \| \mathbf{Lm} \|^2 + \lambda_3 \| \mathbf{C} - \mathbf{m}_c \|^2 \qquad (1)$$

In the first term, **m** represents the model vector, including the constant slowness perturbation in each grid cell as well as hypocenter perturbation terms. **G** is the sensitivity matrix, calculated using ray theory for the short period data and 3-D finite frequency kernels estimated from single scattering for long period *PP-P* data (Kárason, 2002). We use weighted composite rays (Kárason and van der Hilst, 2001) to mitigate effects of uneven sampling further and to reduce the size of the sensitivity matrix **G**. The data vector **d** represents the travel time residuals. The second and third terms are traditional Tikhonov regularizations. The second term favors a result that is close to the reference model and thus tends to minimize the

amplitude of the model; the third term reduces the difference between adjacent cells and thus produces smooth variations. **L** is a first order differential operator. λ_1 and λ_2 are the weights of Tikhonov regularization.

The last term in (1) is used to reduce the crustal anomaly smearing due to strong crustal heterogeneity along P-wave paths with small incidence angle (Li *et al.*, 2006), with **C** representing an *a priori*, high resolution local crustal model (Sun *et al.*, 2004; Xu *et al.,* 2007) that is embedded in the global crustal model (crust 5.1, Bassin *et al.*, 2000), and $\mathbf{m}_c$ is the crustal part in the model vector $\mathbf{m}$. We determine the weight λ_3 through synthetic tests (Li *et al.*, 2006)

4.4 Results

4.4.1 Checkerboard resolution test

We use checkerboard resolution tests to assess the ability of the data to resolve mantle beneath the Tibetan Plateau and surrounding regions. The input structure of ±1% velocity variation (Figures 4-4.0 and 4-5.0) was computed for each depth at a time. The synthetic travel times were created and inverted using the same inversion scheme and sampling (that is, sensitivity matrix) in the inversion. In Figures 4-4 and 4-5, we show the retrieved structure from the checkerboard resolution test at different depths for box sizes of $5^o \times 5^o$ and $2^o \times 2^o$, respectively.

In general, the $5^o \times 5^o$ input signals can be resolved at depths larger than 100 km (Figures 4-4.2~4.5). At 60 km depth, some of the input signals are smeared

beneath the Tarim basin, the northern Tibetan plateau, and the Indian Ocean (where there are no stations). The input signal in other parts, especially the eastern Tibetan plateau and Himalayas, is well recovered (Figure 4-4.1). For the $2^{o}\times2^{o}$ input pattern, some input anomalies are damped to near zero (indicating poor resolution) beneath Tarim basin, Indian plate, and South China sea at 60 km depth, but the recovery is good in the areas of our particular interest, such as the Himalayas, eastern Tibetan plateau, Sichuan Basin, and Burma (Figure 4-5.1). At larger depths, the $2^{o}\times2^{o}$ input patterns can be resolved very well in most of the area except under the Indian plate. Only ~30%-40% amplitude of the input signals has been resolved due to the regularization of the inversion. Therefore, the real velocity anomalies in the upper mantle may be about 2 or 3 times of the amplitude in the model.

4.4.2 Model improvement

Figure 4-6 shows the change in the model resulting from the crust correction and data addition. For illustration purposes, we only show the model update at 60 and 150 km depth. The addition of the data from the Tibetan arrays and the Chinese Seismograph Network (CSN) improve significantly the resolution in the crust and upper mantle beneath the plateau and surrounding regions. Indeed, the checkerboard resolution test at 100 km depth shows that the combined datasets can resolve velocity variations in more detail than the EHB dataset only (Figure 4-6A1, B1). For example, more input signals can be recovered beneath the eastern plateau and Red River fault area.

Only one station (LSA, Lhasa) on the Tibetan Plateau reports to the ISC/EHB data base. Consequently a low wavespeed "bulls-eye" is visible here, whereas the wavespeed variations are heavily damped elsewhere beneath the plateau (Figure 4-6A2). Since the reference Earth model has a crustal thickness of 35 km, a thick crust will appear as a very strong 'slow' anomaly. The thickness of the crust in most of the plateau exceeds 60 km. Without a crustal correction, we cannot prevent such low velocity anomalies of the Tibetan crust from causing artifacts to large depths in the mantle (Figure 4-6A3). With regularization to an *a priori* high resolution crustal model, we can recover strong low velocity anomalies (~10%) and confine it in the crust beneath the plateau (Figure 4-6B2, B3). Detailed description of the new model will be presented in section 4.4.3.

4.4.3 Structure of the upper mantle beneath Tibet and surrounding regions

In Figure 4-7 we present P-wave velocity variations beneath the Tibetan plateau and surrounding regions in map view. In Figure 4-8 we illustrate the structure associated with the Indian subduction through the Himalayas and Burma by means of vertical cross-sections. For presentation purposes, western and eastern Himalayas are defined to be separated by the 85°E meridian.

Pronounced high velocity anomalies prevail beneath the Himalayas and the western margin of Tibet down to 300 km depth (Figures 4-7.1~7.3). The high velocity anomalies become gradually weaken at large depths (Figures 4-7.4~7.6).

Indian subduction beneath western Himalayas: West of the Himalayas, that is, west of ~70°E, high velocity anomalies are detected beneath Pamirs, frontal

basin of the Indian plate and the southern Tibetan Plateau. High velocity anomalies beneath the Hindu Kush (between Pamirs and India) are visible in the mantle transition zone and appear to connect to high velocity anomalies beneath the Pamirs. Dense seismicity is located above the high velocity anomalies beneath the Hindu Kush and Pamirs in the upper mantle (Figures 4-8 A, B; Figures 4-7.1, 7.2).

Further east, near 75°E, a high velocity anomaly structure is detected beneath the entire Tibetan plateau and reaches as far north as the western margin of the Tarim basin. Earthquakes are mainly confined to shallow depth within the plateau and Tarim basin (Figures 4-8 C, D). Tests with synthetic data show that the resolution is rather poor in this region, but the fast structures beneath the plateau cannot be explained by lateral smearing of the strong anomalies beneath the Himalayas (Figure 4-9 D).

Further east (~80°E), a velocity anomaly with a steep dip angle is visible only beneath the Himalayan Block (Figure 4-8 G, H). Moderately high velocity anomalies are observable in the mantle transition zone and seem to connect the high velocity anomalies in the upper mantle beneath the plateau and in the lower mantle beneath the Indian plate (Figure 4-7.6; Figure 4-8 G, H). This connection is not yet well understood, but target resolution tests demonstrate that the fast structure in the mantle transition zone is not due to smearing between the high velocity anomalies in upper and lower mantle and that, with the limits of our

linearized inversions, resolution in the mantle transition zone is adequate (Figure 4-9 G).

Indian subduction beneath eastern Himalayas: In general, the high velocity anomaly beneath the eastern Himalayas is weaker than that beneath the western Himalayas. There are no significant fast structures in the upper mantle above 200 km under southern Tibet (Figures 4-7.1, 7.2).

At about 85°E, the high velocity anomaly dips from the foreland basin of Indian plate to a depth of 200-300 km beneath the Himalaya. Low velocity anomalies characterize the uppermost mantle beneath most of Tibetan plateau (Figures 4-8 I; Figure 4-7.1). A high velocity anomaly is still visible beneath the Himalayas in the lower mantle, but there is no evidence for a connection to shallow structure (Figures 4-8 I). Moderately high velocity anomalies are visible from 300 to 500 km depth beneath the Lhasa block of Tibet (around (90°E, 32°N), Figures 4-7.3~7.6; Figure 4-8 J). Resolution tests suggest that structures at shallow depth beneath the Lhasa block can be resolved by the data used and that the fast structures at larger depth are not due to smearing of anomalies at shallow depth (Figure 4-9 J).

Around ~90°E, the high velocity anomalies are confined to shallow depth beneath the foreland basin of the Indian plate and the Himalayas. At this longitude, there are almost no pronounced high velocity anomalies beneath the plateau. The fast structures in the upper mantle appear to be disconnected

completely from the high velocity anomalies in the lower mantle (Figures 4.7.1~7.6 and Figures 4.8 K, L).

Subduction beneath Burma: At depths larger than 200 km, the linear high velocity anomalies beneath Burma can be distinguished from the high velocities beneath the eastern Himalayas (Figure 4-7.2). With increasing depth, the fast structure is visible increasingly eastward, toward the Tengchong volcanic area and the Red River fault area (Figures 4-7.3~7.6). The dip angle of high velocity through the Eastern syntaxis is ~60°, which is much steeper than that beneath the Himalayas (Figure 4-8M). In map view, the fast structure is much narrower (Figures 4-7.2, 7.3).

Further south, the high velocity anomaly dips almost vertically into the mantle transition zone. To 150 km depth in the upper mantle, earthquakes occur near the top of dipping high wavespeed structure (Figures 4-8 O, P). The shallow upper mantle beneath the Tengchong volcanic region is marked by low velocity anomalies (Figure 4-7.1). Pronounced high velocity anomalies appear from 300 km depth beneath Xianshuihe-Xiaojiang Fault (in east of 100°E and south of 30°N, Figure 4-7.3). They trend NE-SW, extend to large depths, and merge with the fast velocity anomalies beneath Burma (Figures 4-7.4~7.6).

4.5 Discussion

4.5.1 Indian subduction

Subduction of Indian lithospheric mantle plays a key role in the evolution of

the Tibetan plateau. In the last decades, intensive geological, geomorphological, geochemistrical investigations on the plateau have advanced our understanding of the evolution of Tibet (e.g., Yin and Harrison, 2000; Tapponnier et al., 2001; Chung et al., 2005). However, these near-surface studies provide limited information about the deep structure, especially the present day subduction of the Indian plate beneath the plateau. Seismic imaging is a powerful tool to provide direct evidence for the subduction of the Indian lithospheric mantle (e.g., Van der Voo et al., 1999; Kosarev et al., 1999; Shapiro et al., 2002; Tilmann et al., 2003; Replumaz et al., 2004; Li et al., 2006). The seismic images in this study confirm our previous studies (Replumaz et al., 2004; Li et al., 2006) but provide a more detailed picture thanks to enhanced data coverage and resolution.

The subduction of Indian lithospheric mantle shows significant lateral variations along the Himalayas. West of 80°E, the Indian lithospheric mantle underthrusts the western plateau and extends about 400~500 km northeastward from Himalayan frontal thrust (Figure 4-8 C, D, E, and F). The Indian subducted lithosphere is confined to shallow depth (about 200 to 300 km depth, Figure 4-7.1~7.3) and does not appear connected with high velocity anomalies in the lower mantle. Between 80°E and 85°E, the dip of the Indian subducted lithosphere gradually steepens. High velocity anomalies associated with subduction of Indian lithospheric mantle connect locally to high wavespeed structures that have been interpreted as Tethys oceanic slabs (Van der Hilst et al., 1997; Grand et al., 1997; Van der Voo et al., 1999; Replumaz et al., 2004) (Figure 4-8 G, H, and I). East of

85°E, subducted Indian lithosphere is mostly confined to beneath the foreland basin and Himalayan Mountains. Although there is evidence for subduction of some Indian lithospheric mantle beneath the Lhasa block, perhaps down to 500 km depth, at shallow depth most of the Tibetan plateau seems underlain by low velocity anomalies (Figure 4-8 J). Close to the Eastern syntaxis, there is no evidence for Indian subducted mantle beneath Tibet. Indian subducted mantle at shallow depth has gradually disconnected from the Tethys oceanic slabs in the lower mantle.

The debate about the Indian subduction concerns two fundamental questions: (1) How far north has Indian lithospheric mantle subducted the plateau? (2) What is the relationship between the Indian subducted lithosphere in the upper mantle – if any - and the Mesozoic oceanic slabs in the lower mantle? The high resolution seismic images in this study provide more constraints on these two essential questions.

Our results strongly suggest that the shallow subduction of Indian lithospheric mantle beneath the Tibetan plateau only occurs in the western part of the collision zone. Further east, subduction is steeper, and beneath the Lhasa block (Figure 8J) most of the plateau is underlain by low velocity anomalies. These observations suggest that that most of the lithosphere beneath the central and eastern part of the plateau is of Asian origin (consistent with Tapponnier et al., 2001). Teleseismic imaging based on the data from the INDEPTH projects has generated an image that suggests that the Indian lithospheric mantle dips steeply into the mantle south

of Bangong-Nujiang suture zone (90°E, 31°N) (Tilmann et al., 2003, Figure 10a). In contrast, our imaging does not reveal any pronounced high velocity anomies at the shallower depths (Figure 4-7.1~7.3; Figure 4-10c), even if resolution tests demonstrate that such a structure should have been well resolved by the dense data coverage used in our study (Figure 4-9 J). The images reveal a fast structure at 400-500 km beneath the Bangong-Nujiang suture zone, which we interpret to be the result of subduction of Indian lithosphere from the Zangbo suture (trend depicted by black lines in Figure 4-10c). This interpretation is consistent with Kosarev et al. (1999, Figure 4-10b) and argues against the suggestion of the significant underthrusting of the Indian lithospheric mantle the Tibetan plateau (e.g., Zhou and Murphy, 2005).

It is difficult to reconcile our observations with a scenario such as that of Tilmann et al. (2003), where the Indian lithosphere sinks steeply soon after its horizontal underthrusting to south of the Bangong-Nujiang suture. It could be that the high velocity anomalies that they see at shallow depth are due to smearing of high velocity anomalies at large depth as a consequence of the spatial limit of the array data (red question mark in Figure 4-10a).

The nature of the connection between structures related to the subduction of the Indian lithosphere in the shallow mantle and structures in the lower mantle is not clear, but it seems to vary along the collision zone. Resolution tests show that the fast structure in the mantle transition zone beneath the central Himalayas is not a smearing artifact (Figure 4-9 G). However, there are no fast structures in the

transition zone beneath the western and eastern Himalayas (Figure 4-8 C, D, K, and L). Based on a global P-wave tomographic study, Van der Voo et al. (1999) suggested that the Indian lithosphere had been dragging down into the mantle directly beneath the Yarlung Tsangpo suture zone by Tethys oceanic lithosphere that is now in the lower mantle. Our results suggest that only beneath the central Himalayas the lower mantle slabs are still connected to the Indian subducted lithosphere, which may suggest that the present-day structures represent a late stage of the part of continental collision driven by slab pull. Although it leaves some room for alternate interpretations, the steeper dip angle in the central part of the Indian subduct may be related to the pull by the Tethys oceanic lithosphere in the lower mantle (Figure 4-8 G, H, I, and J). In contrast, beneath western and eastern Himalayas, absent of fast structures in the mantle transition zone suggests that the pull by the Tethys oceanic slabs no longer affects this part of the Indian subduction (Figure 4-8 C, D, E, K and L). By implication, the ongoing collision between the Indian and Eurasian plates may be driven by the pushing force from the far field spreading at the Indian Ridge and the subduction of the Indian plate elsewhere (e.g., Indonesia). Seismic images of this study reveal the complicated spatial-temporal evolution of the Indian subduction.

Lateral variation of Indian subduction along the Himalayas presented here, if confirmed by the later studies, has important implications for our understanding of the evolution of the Tibetan plateau. For example, a number of mechanisms have been proposed for the formation of late Cenozoic north-south rifts in central Tibet,

such as, gravitational collapse of the plateau (e.g., Dewey, 1988), convective removal of the lower mantle lithosphere (e.g., England and Houseman, 1989), and oblique convergence between India and Asia (e.g., Seeber and Pecher, 1998). However, the role of the Indian subducted lithosphere in these models is largely unknown. Our results show that the location of rifts in central Tibet (from ~80°E to ~90°E) coincides with where the change in the dip angle of the Indian subducted lithosphere occurs (Figure 4-7.1~7.4 and Figure 4-8 F~G). This suggests that the increase in the dip angle of the Indian subducted lithosphere from west to east may be one of sources to form rifts in central Tibet.

4.5.2 The Tibetan plateau

The crust under the Tibetan plateau has been generally well imaged and its thickness is about double that of the normal crust (e.g., Kind *et al.*, 2002; Li *et al.*, 2006). In contrast, the upper mantle structure beneath the plateau is only known with low resolution from surface wave dispersion studies (e.g., Romanowicz, 1982; Rapine et al., 2003; Friederich, 2003) and large scale P-wave travel time tomography (Bijwaard *et al.*, 1998; Li *et al.*, 2006; Huang and Zhao, 2006). The seismic images presented here provide more constrains on the deep structure beneath the plateau. Although the southwestern plateau is marked by pronounced high velocity anomalies, most of the plateau is underlain by low velocity anomalies, especially under the eastern part of the plateau (Figure 4-7.1, 7.2).

In Figure 4-11, we compare our model with the global P-wave model from the finite frequency travel time data (Montelli *et al.*, 2004) and the shear wave model

from the surface wave dispersion study (Lebedev and van der Hilst, 2007) around the Tibetan plateau. Since our model is at much higher spatial resolution than either of these models, in order to compare with these large scale seismic images, we apply low-frequency filter to P-wave perturbations in our model (Figure 4-11A1, A2). At this low resolution, the basic features of two P-wave models is similar: high velocity anomalies are situated beneath the Himalayas, Ordos block and Sichuan Basin; low velocity anomalies prevail beneath the central and eastern plateau and along a broad zone following the Red River fault (Figure 5-11 A1, A2, B1, and B2). The shear wave model also show high velocity anomalies beneath Pamirs, Himalayas, Ordos block and Sichuan Basin and low velocity anomalies under Red River fault range. The most conspicuous differences between the P-wave models and shear wave model are beneath the central and eastern plateau. At 200 km depth, the surface wave model shows pronounced high velocity anomalies, however the P-wave models show low velocity anomalies (Figure 4-11 A2, B2 and C2).

The checkerboard tests show that the resolution at 200 km depth beneath the central and eastern Tibetan plateau is adequately good (Figure 4-5.3) and crust correction used in the inversion has prevented smearing of the thick crust into the upper mantle (Li et al., 2006). In order to further assess our resolution we performed the following test. For test purposes, we infer the P wave model by assuming that the P wave perturbation is half of the shear wave perturbation (Masters et al., 2000) (Figure 4-12a). We use this inferred P wave model as a

priori information in the penalty function (e.g., as $\mathbf{m}_c$ in equation (1)). The results will be close this inferred P wave model if the constraint by data is weak. In contrast, if the constraint by data is strong, the results will depart from this a priori information. This test shows that low velocity anomalies are dominant beneath the central and eastern plateau (Figure 4-12b) and that results depart from the input P-wave model. This demonstrates that the constraint by P-wave travel time data is strong beneath the central and eastern plateau and that low P-wave speeds are required to fit the data.

The reason for the controversy between shear wave model and P-wave model is not yet clear. The lateral resolution of the shear wave model is ~500 km (Lebedev, personal communication). Without further resolution tests, it is hard to evaluate the lateral smearing in the shear wave model under the plateau. This is, however, beyond the scope of this study. Although the seismic images in this study could not provide precise thickness of the lithosphere beneath the plateau, the low velocity anomalies beneath the central and eastern plateau suggest that the Tibetan lithosphere is of Asian origin. Our results are consistent with expectation from models of convective removal of the thickened Asian lithosphere under Tibet (e.g., Houseman *et al.*, 1981) and with the suggestion by Romanowicz (1982) that little mantle lithosphere remains beneath Tibet.

4.5.3 The Burma subduction

At the corner between the Sumatra-Andaman and the Indian subduction zones,

the Indo-Burma ranges are structurally complex and seismically active (Ni *et al.*, 1989). The Indian plate is subducting northward whereas the Burma microplate descends eastward beneath the Eurasian plate (Satyabala, 1998). Seismic tomography also reveals the east-dipping high velocity anomaly along the Burma arc (Li *et al.*, 2006; Huang and Zhao, 2006). However, resolution in these studies is insufficient for the investigation of the spatial extent of subduction beneath Burma and its relationship with the Indian subduction across the eastern Himalayan syntaxis.

The subduction through Burma is well resolved by the data used in our study. Close to the Eastern syntaxis, the Burma subduction is confined to the upper mantle with a gentle dip angle of ~ 60^{o} (Figure 4-8 M, N). Further south, eastward Burma subduction is accompanied by seismicity at shallow depth and the subducted plate sinks to the mantle transition zone with a steep dip angle (Figure 4-8 O, P). While a number of studies have shown the presence of an eastward dipping Indian lithosphere, the issue of whether the subduction is still active has been debated (Ni *et al.*, 1989; Satyabala, 1998; Rao and Kumar, 1999; Guzman-Speziale and Ni, 2000; Satyabala, 2000). The observation that the compressional principal axes of main large earthquakes are nearly parallel to the trend of the thrust and fold belts of the region has lead to a consensus that the subduction is no longer active (e.g., Guzman-Speziale and Ni, 1996; Rao and Kumar, 1999). However, from analysis of tensional stress regime within the subducting slab, Satyabala (1998) inferred active eastward subduction of Burmese microplate. The

continuity of subducted plate beneath the Burmese arc in the upper mantle (e.g., Figure 4-8P) may be evidence in support of active subduction under the Indo-Burma region.

Another interesting question about subduction in the Indo-Burma region is its continuity across the Eastern syntaxis with the subduction beneath the Himalayas. Our results show that fast structure under the east of the Eastern syntaxis is disconnected from the Indian subduction beneath the Himalayas at depths larger than ~200 km depth (Figure 4-7.2). This suggests that the eastward Burmese subduction has been separated from the northward Indian subduction and become an independent part during the western retreat of the Burmese arc over the Miocene.

Tengchong is an active volcanic and geothermal area east of the Indo-Burma arc (Figure 4-1, around (98°E, 25°N)). Its most recent eruption occurred in 1609 (Qin *et al.*, 1996). Negative gravity anomaly, high electrical resistivity, and high heat flow indicate presence of the magma chamber in the crust beneath Tengchong (Sun *et al.*, 1989; Kan *et al.*, 1996). A number of Cenozoic strike-slip faults are located in the Tengchong area (Figure 4-1). However, the deeper seismic structure beneath Tengchong has not been very clear, in part because of poor resolution in previous studies (Huang *et al.*, 2002). Our regional array data reveals that pronounced low velocity anomaly is dominant in the shallow upper mantle beneath the Tengchong area (Figure 4-7.1, Figure 4-8 M, N). The slow structure is confined to ~150 km depth (Figure 4-8 M, N). At large depth, high velocity

anomaly subducted from the Burmese arc underlies the Tengchong area (Figure 4-7.3~7.5). The volcanic activity in the Tengchong area is more likely related to the subducted slabs from the Burmese arc.

4.5.4 Transition of tectonic regime in the Sichuan-Yunnan region

An intriguing high velocity anomaly between Sichuan and the Eastern syntaxis separates the low velocity anomalies beneath the Songpan-Ganze of eastern Tibetan plateau from those along Red River fault region in the shallow mantle (Figure 4-13). Resolution tests show that this anomaly is not a smearing artifact from nearby fast structures beneath Sichuan and Burma (Figure 4-14). Geodetic measurements suggest that near-surface deformation is part of a clockwise rotation around the eastern Himalayan syntaxis (King, *et al.*, 1997; Chen *et al.*, 2000; Figure 4-1). Shear wave splitting measurements show east-west fast direction in central and southern Tibet, which is consistent with near-surface deformation (Sol *et al.*, 2007; Huang *et al.*, 2000). In the Sichuan-Yunnan region, Lev et al. (2006) found a profound transition of fast polarization directions from primarily north-south in the north to mostly east-west orientation in the south (Figure 4-13). Coexistence of a complex pattern of fast polarization direction and high velocity anomalies under the middle of the Xianshuihe-Xiaojiang fault system suggests a fundamental transition in the deformation regime in the upper mantle (Figure 4-13). This may be a boundary marking a transition in tectonic regime from deformation due to continental collision in the NW and deformation due to subduction (from Burma and the Pacific) in the SE. The low velocity anomalies

beneath the Red River fault in the upper mantle (Figure 4-13) may be related to upper mantle processes beneath the South China Sea.

Our results also reveal high velocity anomalies beneath the Precambrian crust of Ordos and Sichuan basins to 250-300 km depth. Resolution tests show that the data can resolve the shallow structure and that the high velocity beneath the Sichuan basin is not a smearing artifact (Figure 4-15). These observations are consistent with previous studies of Li *et al.* (2006) and Lebedev *et al.* (2003). These high velocity anomalies imply a stable continental root beneath the Ordos block and Sichuan Basin. This stable continental root may block the eastward extrusion of crust and/or upper mantle of the eastern Tibetan plateau driven by the continent collision. This also suggests that the tectonic processes east of Ordos and Sichuan are more likely related to the ocean subduction system of western Pacific and Phillipine Sea to the northeast rather than the continental collision in the southwest (Zhang *et al.*, 2003).

4.6 Conclusions

P-wave velocity variations in the upper mantle beneath the Tibetan plateau and surrounding regions have been investigated using a combination of data from Tibetan arrays, CSN, and EHB. The results lead us to the following conclusions:

a) The subduction of the Indian lithospheric mantle varies considerably from west to east.

b) Although part of the Indian subducted lithosphere extends to the central Tibetan plateau beyond the eastern Himalayas and has reached to ~400 km depth, it does not extend north of the Bangong-Nujiang Suture (~33°N) and the main Indian subducted lithosphere is situated beneath the western plateau to 300 km depth. By implication, most of the Tibetan lithosphere is of the Asian origin.

c) Some high velocity materials are detected in the transition zone in the central Himalayas (~85°E), which appear to connect with the Indian subducted lithosphere in the upper mantle with the Mesozoic oceanic slabs in the lower mantle. In the eastern and western Himalayas we do not detect such connections.

d) At depth larger than 200 km, the subduction under Burma seems to be separated from Indian subduction through the eastern Himalayas. Volcanic activity in the Tengchong area is more likely related to the Burma subduction than to other deep mantle processes.

e) Coexistence of a complex pattern of fast polarization direction high velocity anomalies under the middle of the Xianshuihe-Xiaojiang fault system suggests that upper mantle heterogeneity may be a cause for the observed complex anisotropy pattern.

f) Continental roots (marked by high velocity anomalies) beneath the Precambrian Ordos Block and Sichuan basin extend to 250-300 km depth. Together high velocity anomalies from Burma, these continental roots may form a transition between the collision controlled tectonic regime in the NW and subduction controlled regime to the SE.

Acknowledgements

We thank to Prof. Chen and the staff at Chengdu Institute of Geology and Mineral Resources for their support and help. We thank Dr. Aldersons to make the automatic picking software available to us. We thank Einat Lev for her shear wave splitting results. We appreciate for the constructive discussion with Prof. Burchfiel and Prof. Royden at MIT. This work was funded by NSF grant 6892042 of Collaborative Research in Eastern Tibet.

References

Abers, G.A., and Roecker S.W., 1991. Deep-structure of an arc-continent collision: Earthquake relocation and inversion for upper mantle P and S wave velocities beneath Papua New Guinea. *J. Geophys. Res.*, 96, 6379-6401.

Acton, G.D., 1999. Apparent polar wander of India since the Cretaceous with implications for regional tectonics and true polar wander. In: Radhakrishna, T., Piper, J.D.A. (Eds.), The Indian Subcontinent and Gondwana: A Palaeomagnetic and Rock Magnetic Perspective, Mem. Geol. Soc. India, vol. 44, pp. 129– 175.

Aldersons, F., Ben-Avraham Z., Hofstetter, A., Kissling, E., and Al-Yazjeen, T., 2003. Lower crustal strength under the Dead Sea basin from local earthquake data and rheological modeling. *Earth Planet. Sci. Lett.*, 214, 129-142.

Argand, E., 1924. La tectonique de l' Asie. Proc. 13th Int. Geol. Cong., vol. 7, pp. 171– 372.

Baer, M., and Kradolfer, U. 1987. An automatic phase picker for local and teleseismic events. *Bull. Seism. Soc. Am.*, 77, 1437-1445.

Bassin, C., Laske, G., and Masters, G., 2000. The Current Limits of Resolution for Surface Wave Tomography in North America. *EOS Trans AGU* 81, F897.

Besse, J., and Courtillot, V., 1988. Paleogeographic maps of the continents bordering the Indian Ocean since the early Jurassic. *J. Geophys. Res.* 93B, 1791– 1808.

Bijwaard, H., Spakman, W, and Engdahl, E.R., 1998. Closing the gap between regional and global travel time tomography. *J. Geophys. Res.*, 103, 30055-30078.

Chen Z., B.C. Burchfiel, Y. Liu, R.W. King, L.H. Royden, W.Tang, E. Wang, J. Zhao, and X. Zhang, 2000. Global Positioning System measurements from eastern Tibet and their implications for India/Eurasia intercontinental deformation, *J. Geophys. Res.* 105 16215–16228.

Chung, S.-L., et al. 2005, Tibetan tectonic evolution inferred from spatial and temporal variations in post-collisional magmatism, *Earth Sci. Rev.*, 68, 173–196.

Coward M.P., Kidd W.S., Shackleton R.M., and Zhang H., 1988, The structure of the Tibet Geotraverse, Lhasa to Golmud; in Chang C., Shackleton R.M., Dewey J.F. and Yin J., (eds) The Geological Evolution of Tibet: Phil. Trans. R. Soc. London, A 327, 207-336.

Dewey J., Shackleton R.M., Chang C., and Sun, Y., 1988. The tectonic evolution of the Tibetan Plateau; In Chang C., Shackleton R.M., Dewey J.F. and Yin J.,

(eds) The Geological Evolution of Tibet: Phil. Trans. R. Soc. London, A 327, 379-413.

Dewey, J.F., 1988. Extensional collapse of orogens, *Tectonics*, 7, 1123-1140.

DeMets, C., Gordon, R.G., Angus, D.F., and Stein, S., 1990. Current plate motions. *Geophys. J. Int.*, 101, 425-478.

England, P., and Houseman, G., 1986. Finite strain calculations of continental deformation: 2. Comparison with the India –Asia collision zone. *J. Geophys. Res.* 91, 3664– 3676

England, P., and Houseman, G., 1989. Extension during continental convergence, with application to the Tibetan plateau. *J. Geophys. Res.*, 94, 17561-17579.

Engdahl, E.R., van der Hilst, R.D., and Buland, R., 1998. Global teleseismic earthquake relocation with improved travel times and procedures for depth determination. *Bull. Seism. Soc. Am.*, 88, 722-743.

Friederich, W., 2003. The s-velocity structure of the East Asian mantle from inversion of shear and surface waveforms. *Geophys. J. Int.*, 153, 88– 102.

Holmes, A., 1965. Principles of Physical Geology, Second edition The Ronald Press Company, New York. 1128 pp.

Grand, S.P., van der Hilst, R.D., and Widiyantoro, S. 1997. Global seismic tomography: A snapshot of convection in the earth, *GSA Today*, 7, 1-7.

Guzman-Speziale, M. and J. F. Ni, 1996. Seismicity and Active Tectonics of the Western Sunda Arc, in The Tectonic Evolution of Asia, edited by An Yin and T. Mark Harrison, pp 63-84, Cambridge University Press, New York, 1996.

Guzman-Speziale, M. and J. F. Ni., 2000. Comment on "Subduction in the Indo-Burma region: Is it still active" by S. P. Satyabala, *Geophys. Res. Lett.* 27, 10654066

Houseman, G. A., D. P. McKenzie, and P. Molnar, 1981. Convective instability of a thickened boundary layer and its relevance for thermal evolution of continental convergent belts, *J. Geophys. Res.*, 86, 6115–6132.

Holmes, A., 1965. Principles of Physical Geology, Second edition, The Ronald Press Company, New York. 1128 pp.

Huang, J., Zhao, D., and Zheng, S., 2002. Lithospheric structure and its relationship to seismic and volcanic activity in southwest China. *J. Geophys. Res.* 107 (B10), 2055.

Huang, J., and D. Zhao, 2006. High-resolution mantle tomography of China and surrounding regions, J. Geophys. Res. ,111, B09305, doi:10.1029/2005JB0040 66.

Huang W., J.F. Ni, F. Tilmann, D. Nelson, J. Guo, W. Zhao, J., Mechie, R. Kind, J. Saul, R. Rapine, and T.M. Hearn, 2000. Seismic polarization anisotropy beneath the central Tibetan Plateau, *J. Geophys. Res.* 105 27979 - 27990.

Kan, R., J. Zhao, and D. Kan, 1996. The tectonic evolution and volcanic eruption in Tengchong volcanic and geothermal region (in Chinese), *Seismol.Geomagn. Obs. Res.*, 17, 28– 33.

Kárason, H., and van der Hilst, R.D., 2001. Tomographic imaging of the lowermost mantle with differential times of refracted and diffracted core phases (*PKP*, *Pdiff*). *J. Geophys. Res.*, 106, 6569-6587.

Kárason, H., and Van der Hilst, RD, 2000. Constraints on mantle convection from seismic tomography. In M.A. Richards, R. Gordon and R.D. van der Hilst (Editors). History and Dynamics of Plate Motion. *Am. Geophys. Union, Geophys. Monogr. Ser.*, 121, 277-288.

Kárason H., 2002. Constrains on mantle convection from seismic tomography and flow modeling, Ph.D. thesis, 228 pp., M. I. T., Cambridge, MA, USA.

Kennett, B.L.N., Engdahl, E.R., and Buland, R., 1995. Constrains on seismic velocities in the Earth from travel times. *Geophys. J. Int.*, 122, 108-124.

Kind, R., Yuan, X., Saul, J., Nelson, D., Sobolev, S.V., Mechie, J., Zhao, W., Kosarev, G., Ni, J., Achauer, U., and Jiang, M., 2002. Seismic images of crust and upper mantle beneath Tibet: evidence for Eurasian plate subduction. *Science* 298, 1219– 1221.

King R. W., F. Shen, B.C. Burchfiel, L.H. Royden, E. Wang, Z. Chen, Y. Liu, X. Zhang, J. Zhao, and Y. Li, 1997. Geodetic measurement of Crustal Motion in Southwest China, *Geology* 25 179–182.

Kosarev, G., Kind, R., Sobolev, S.V., Yuan, X., Hanka, W., and Oreshin, S., 1999. Seismic evidence for detached Indian lithospheric mantle beneath central Tibet. *Science* 283, 1306– 1308.

Lee, T.Y., and Lawver, L.A., 1995. Cenozoic plate reconstruction of Southeast Asia. *Tectonophysics* 251, 85– 138.

Lebedev, S., and Nolet, G., 2003. Upper mantle beneath Southeast Asia from S velocity tomography. *J. Geophys. Res.* 108, 2048–2074.

Lebedev, S., and Van der Hilst, R.D., 2007. Global upper-mantle tomography with the automated multi-mode surface and S waveforms, *Geophys. J. Int.* (under review).

Lev, E., Long, M., and van der Hilst, R.D., 2006. Seismic Anisotropy in Eastern Tibet from Shear-Wave Splitting Reveals Changes in Lithosphere Deformation. *Earth Planet. Sci. Lett.*, 251, 293-304.

Li, C., van der Hilst, R.D., and Toksöz, M.N., 2006. Constraining spatial variations in P-wave velocity in the upper mantle beneath SE Asia, *Phys. Earth Planet. Inter.*, 154, 180-195.

Li S.L, Mooney W.D., and Fan J.C. 2006. Crustal structure of mainland China from deep seismic sounding data, *Tectonophysics* 420, 239–252

Li, Z.X., 1998. Tectonic history of the major East Asian lithosphere blocks since the mid-Proterozoic. In Flower M. et al. (Editors). Mantle Dynamics and Plate Interactions in East Asia, Geodyn. Ser., 27, 211-243.

Masters G., Laske, G., Bolton, H., and Dziewonski A.M., 2000. The relative behavior of shear velocity, bulk sound speed, and compressional velocity in the mantle: Implications for Chemical and thermal structure. In Earth's Deep Interior, edited by S. Karato, A. M. Forte, R. C. Liebermann, G. Masters, and L. Stixrude, pp. 63-87. Washington, D.C.: Amer. Geophys. Union.

Molnar P. and Tapponnier P., 1975. Cenozoic tectonics of Asia: Effects of a continental collision. *Science*, 189, 419-426

McNamara, D. E., T. J. Owens, and W. R. Walter, 1995. Observations of regional phase propagation across the Tibetan Plateau, *J. Geophys. Res.*,100, 22,215–22,229.

McNamara, D. E., W. R. Walter, T. J. Owens, and C. J. Ammon, 1997, Upper mantle velocity structure beneath Tibet Plateau from Pn travel time tomography, *J. Geophys. Res.*, 102, 493– 505.

Montelli, R., Nolet, G., Dahlen, F.A., Masters G., Engdahl E.R., and Hung S.H., 2004. Finite-frequency tomography reveals a variety of plumes in the mantle. *Science*, 303, 338-343.

Nelson, K.D., et al., 1996. An INDEPTH view of the structure of the lithosphere beneath Tibet. *Science* 274, 1684– 1688.

Ni, J. F., M. Guzman-Speziale, M. Bevis, W. E. Holt, T. C. Wallace, and W. Seager, 1989. Accretionary tectonics of Burma and the three-dimensional geometry of the Burma subduction zone, *Geology* 17, 68-71.

Owens, T.J., and Zandt, G., 1997. Implications of crustal property variations for models of Tibetan plateau evolution. *Nature* 387, 37– 43.

Patriat, P., and Achache, J., 1984. India–Eurasia collision chronology has implications for crustal shortening and driving mechanism of plates. *Nature* 311, 615– 621.

Paige, C.C., and Saunders, M.A., 1982. LSQR: an algorithm for sparse linear equations and sparse least squares. *ACM Trans. Math. Soft.* 8, 43-71.

Powell, C. McA., 1986. Continental underplating model for the rise of the Tibetan Plateau. *Earth Planet. Sci. Lett.* 81, 79–94.

Qin, J., X. Qian, and G. Huangpu, 1996. The seismicity feature of the volcanic area in Tengchong (in Chinese), *Seismol. Geomagn. Obs. Res.*, 17, 19–27.

Rao, N. P. and Kumar R., M. 1999, Evidences for Cessation of Indian Plate Subduction in the Burmese Arc Region, *Geophys. Res. Lett.* 26(20), 3149–3152.

Rapine, R., F. Tilmann, M. West, J. Ni, and A. Rodgers, 2003. Crustal structure of northern and southern Tibet from surface wave dispersion analysis, *J. Geophys. Res.*, 108(B2), 2120, doi:10.1029/2001JB000445.

Replumaz, A., and P. Tapponnier, 2003. Reconstruction of the deformed collision zone Between India and Asia by backward motion of lithospheric blocks, *J. Geophys. Res.*, 108(B6), 2285, doi:10.1029/2001JB000661.

Replumaz, A., Kárason, H., van der Hilst, R.D., Besse, J., and Tapponnier, P., 2004. 4-D evolution of SE Asia's mantle from geological reconstructions and seismic tomography. *Earth Planet. Sc. Lett.*, 211, 103-115.

Romanowicz, B. A., 1982. Constraints on the structure of the Tibet Plateau from pure path phase velocities of Love and Rayleigh waves, *J. Geophys. Res.*, 87, 6865– 6883.

Roger, F., Tapponnier, P., Arnaud, N., Scharer, U., Brunel, M., Xu, Z., and Yang, J., 2000. An Eocene magmatic belt across central Tibet: mantle subduction triggered by the Indian collision? *Terra Nova* 12, 102– 108.

Satyabala, S.P., 1998. Subduction in the Indo-Burma Region: Is it Still Active?, *Geophys. Res. Lett.* 25(16), 3189–3192.

Satyabala, S. P., 2000. Reply to comment on ''Subduction in the Indo-Burma region: Is It Still Active?'', *Geophys. Res. Lett.* 27(7), 1067–1068.

Seeber, L. and A., Pecher, 1998. Strain partitioning along the Himalayan arc and the Nanga parbat antiform, *Geology*, 26, 791-794.

Shapiro, N.M., and Ritzwoller, M.H., 2002. Monte-Carlo inversion for a global shear-velocity model of the crust and upper mantle. *Geophys.J. Int.* 151, 1–18.

Sol, S., Meltzer, A., Burgmann, R., Van der Hilst, R.D., King, R., Chen, Z., Koons, P., Lev, E., Liu, Y.P., Zeitler, P.K., Zhang, X., Zhang, J., and Zurek, B., 2007. Geodynamics of southeastern Tibet from seismic anisotropy and geodesy, *Geology*, in press.

Sun, J., C. Xu, and Z. Jiang, 1989. The electric structure of the crust and upper mantle under western Yunnan and its relationship to crustal tectonics (in Chinese), *Seismol. Geol.*, 11, 35– 45, 1989.

Tapponnier, P., Peltzer, G., Armijo, R., Le Dain, A., and Cobbold, P., 1982. Propagating extrusion tectonics in Asia: new insights from simple experiments with plasticine. *Geology* 10, 611– 616.

Tapponnier, P., Zhiqin, X., Roger, F., Meyer, B., Arnaud, N., Wittlinger, G., and Jingsui, Y., 2001. Oblique stepwise rise and growth of the Tibet Plateau. *Science*, 294, 1671-1677

Tilmann, F., Ni, J., and INDEPTH seismic team, 2003. Seismic imaging of the downwelling Indian lithosphere beneath central Tibet. *Science* 300, 1424–1427.

Van der Hilst, R.D., Widiyantoro, S., and Engdahl, E.R, 1997. Evidence for deep mantle circulation from global tomography. *Nature*, 386, 578-584.

Van der Voo, R., Spakman, W., and Bijwaard, H., 1999. Tethyan subducted slabs under India, *Earth Planet. Sci. Lett.*, 171, 7-20.

Willett, S.D., and Beaumont, C., 1994. Subduction of Asian lithospheric mantle beneath Tibet inferred from models of continental collision. *Nature* 369, 642–645.

Xu, L., Rondenay, S., and Van der Hilst, R.D., Velocity Structure beneath Southeastern Tibet from Teleseismic Receiver Functions, *Phys. Earth Planet. Inter.*, (under review).

Yao, H., van der Hilst, R.D., and De Hoop, M.V., 2006. Surface-wave array tomography in SE Tibet from ambient seismic noise and two-station analysis: I - Phase velocity maps, *Geophys. J. Int.*, 166, 732-744, doi: 10.1111/j.1365-246X.2006.03028.x.

Yin, A., and T. M. Harrison, 2000. Geologic evolution of the Himalayan-Tibetan orogen, *Annu. Rev. Earth Planet. Sci.*, 28, 211– 280.

Zhou, H.W., and Murphy, M.A., 2005. Tomographic evidence for wholesale underthrusting of India beneath the entire Tibetan plateau. *J. Asian Earth Sci.* 25, 445–457.

Zhang P.Z., Z. Shen, M. Wang, G.W., R. Burgmann, P. Molnar, Z. Niu, J. Sun, J.Wu, H. Sun, and X. You, 2004. Continuous deformation of the Tibetan Plateau from global positioning data, *Geology* 32 809–812.

Zhang, Y., Ma, Y., Yang, N., Shi, W. & Dong, S. 2003. Cenozoic extensional stress evolution in North China. Journal of Geodynamics, 36, 591–613.

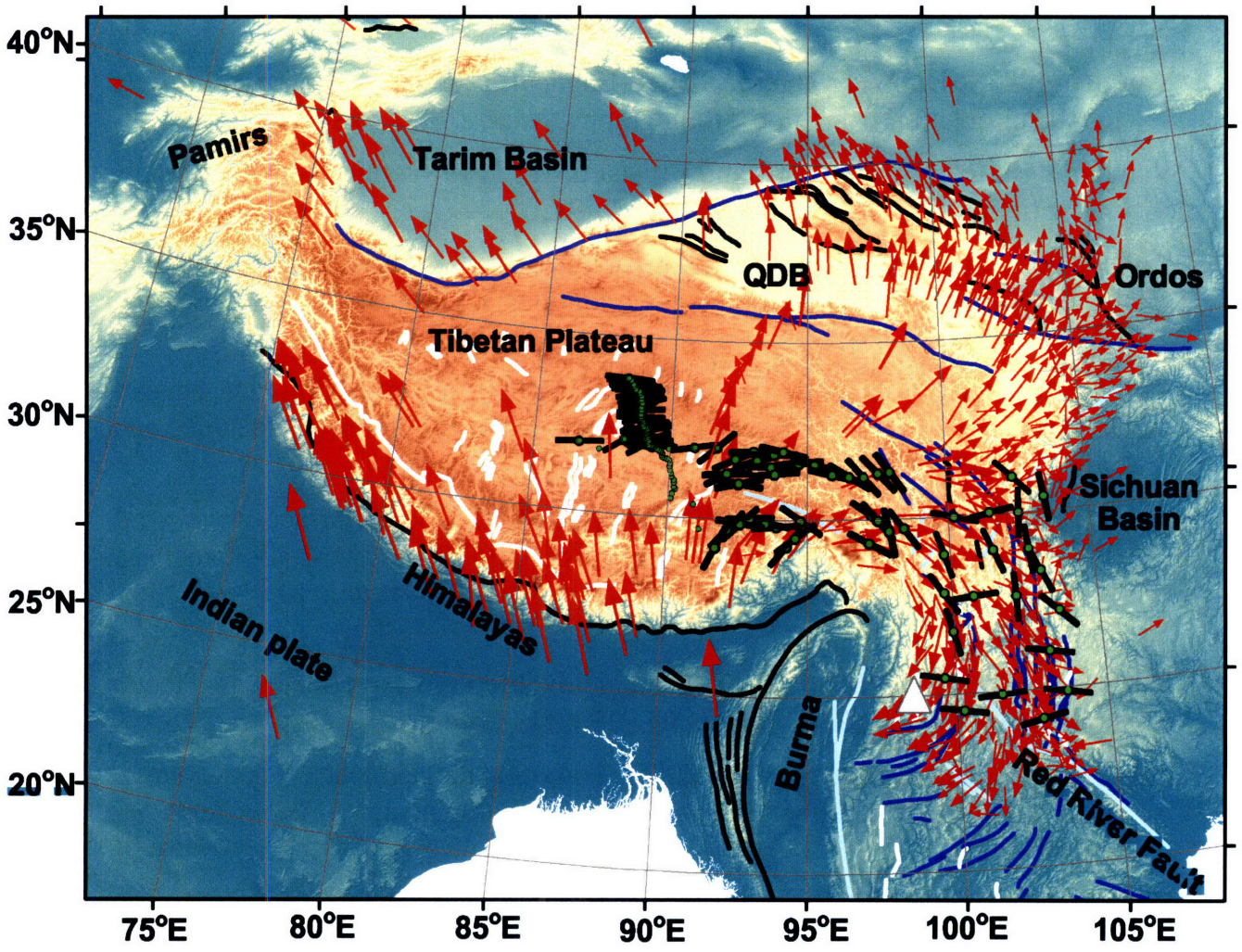

Figure 4-1. Red arrows denote geodetically measured surface velocities relative to the south China block (Chen *et al.*, 2000; Zhang *et al.*, 2004). Black lines with green dots show shear fast polarization direction estimated from waves splitting studies (Huang *et al.*, 2000; Sol *et al.*, 2007; Lev *et al.*, 2006). The background shows the topography of East Asia and active faults around Tibet (blue: left-lateral strike-slip faults; light blue: right-lateral strike-slip faults; black: thrust faults; white: normal faults). The white triangle is the location of the Tengchong volcano.

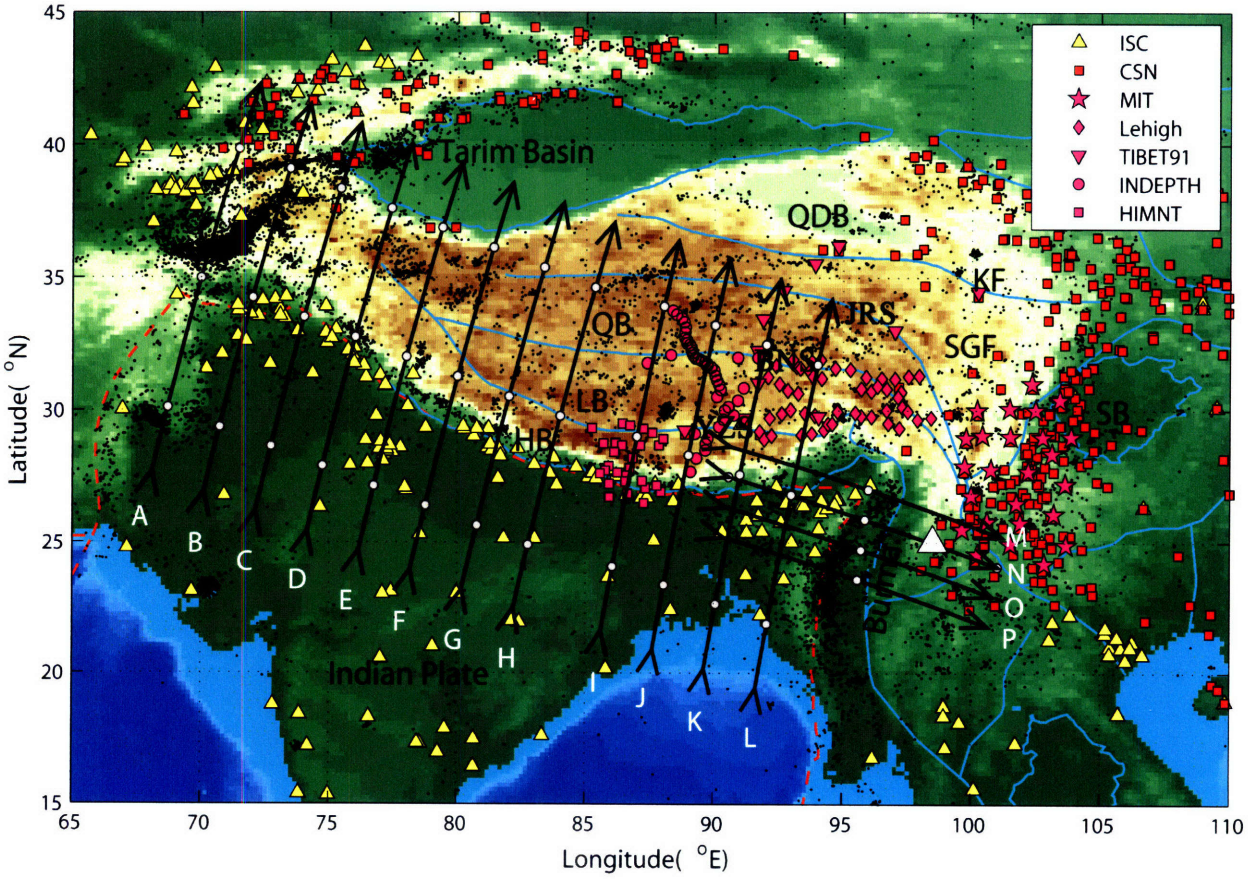

Figure 4-2. The distribution of stations and events in the Tibetan Plateau and surrounding regions. The black dots represent earthquakes during 1964~2006 from the EHB. The white triangle is the location of the Tengchong volcano. Dashed red lines are the plate boundaries, according to NUVEL-1 (DeMets *et al.*, 1990). The blue lines mark the boundaries beneath the main tectonic blocks in the region, where QDB-Qaidam Basin, KF-Kunlun Fault, SB-Sichuan Basin, SGF-Songpan Ganzi Foldbelt, QB-Qiangtang Block, LB-Lhasa Block, HB-Himalayan Block, YZS-Yarlung-Zangbo' suture, BNS-Bangong-Nujiang suture, JRS-Jinsha River suture (modified from Li, 1998 and Tapponnier *et al.*, 2001). The black arrows, labeled as A, B …, show the location of sixteen cross sections through the Himalayas and Burma shown in Figure 4-8.

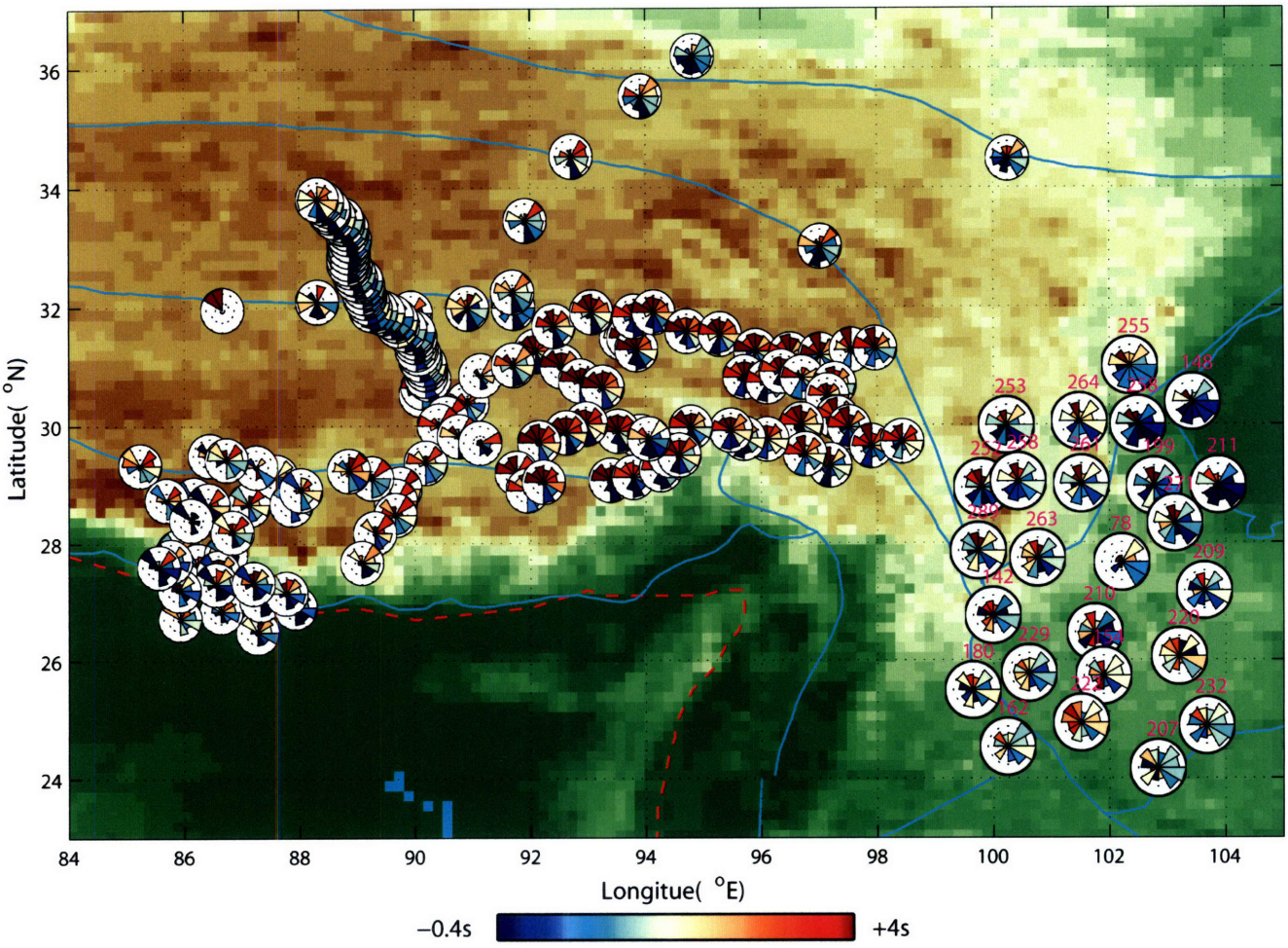

Figure 4-3. The rose histogram shows the direction distribution of travel time residuals of the Tibetan arrays after elevation correction. There are ~170 seismometers and 35,000 pickings in total. The residuals are calculated based on 1-D reference model *ak135* (Kennett *et al.*, 1995). The numbers next to MIT-CIGMR station denote the total number of picks for each station. Residuals of arrivals from the direction of the Tibetan Plateau are quite large, mainly due to the thick Tibetan crust and relatively low velocity perturbations in the upper mantle beneath the plateau.

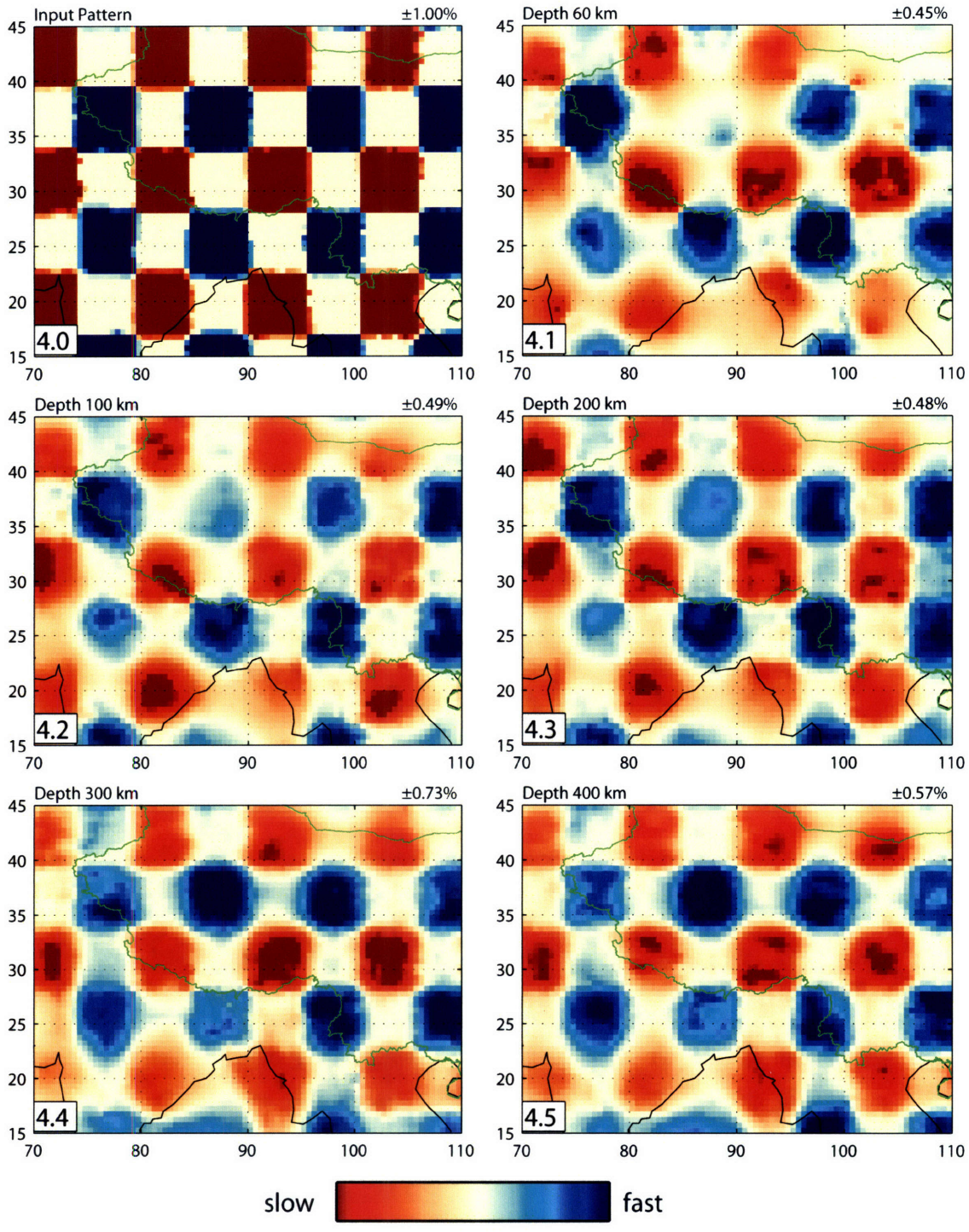

Figure 4-4. Checkerboard resolution test for target anomalies at different depths as indicated in left up corner in each subplot. The color scale is shown in the righ up corner in each subplot. Input pattern ($5^{o}\times5^{o}$) is shown in 4.0. The green line is Chinese border and the black line shows the coast line.

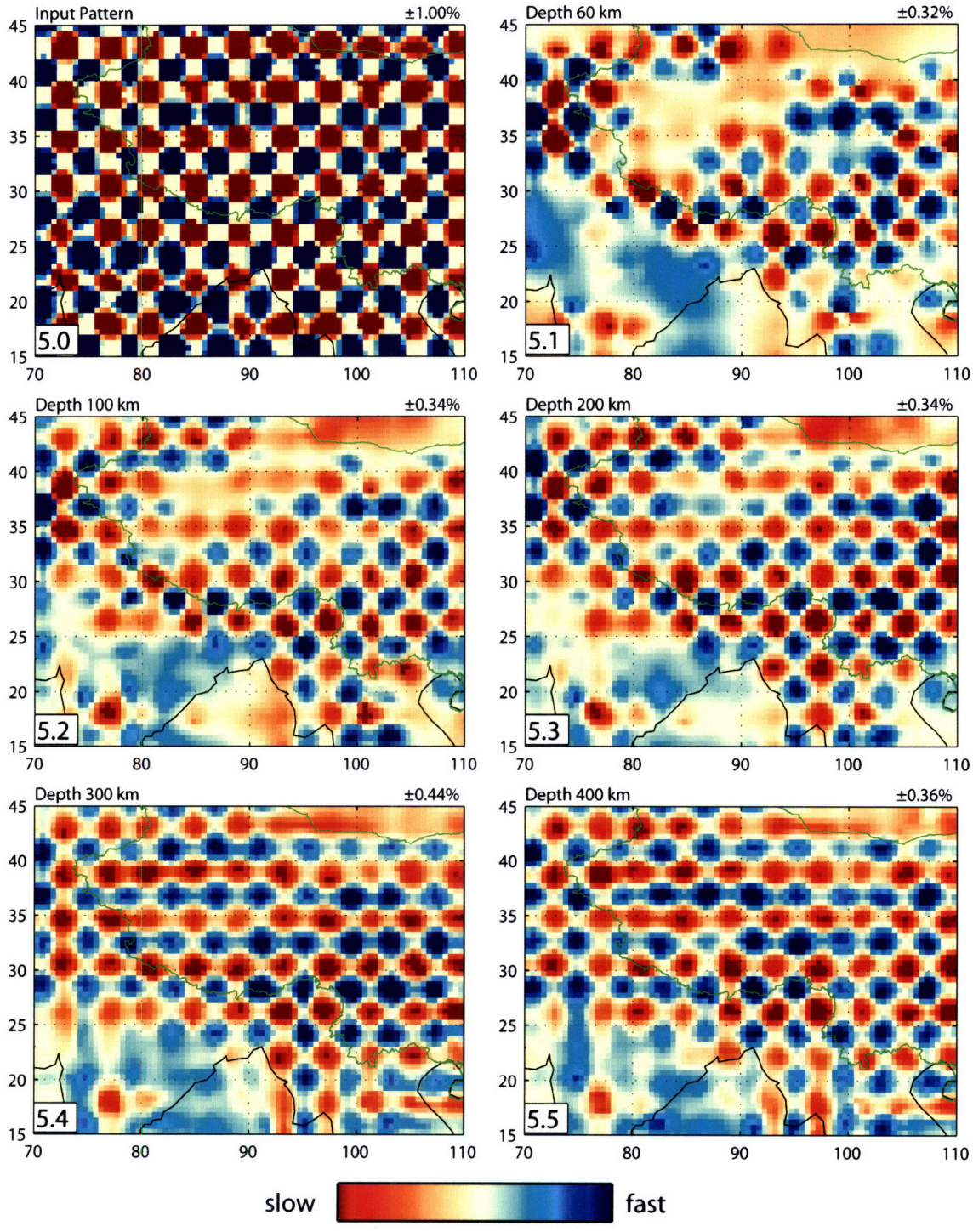

Figure 4-5. Same as Figure 4-4 except the input pattern is 2°×2°.

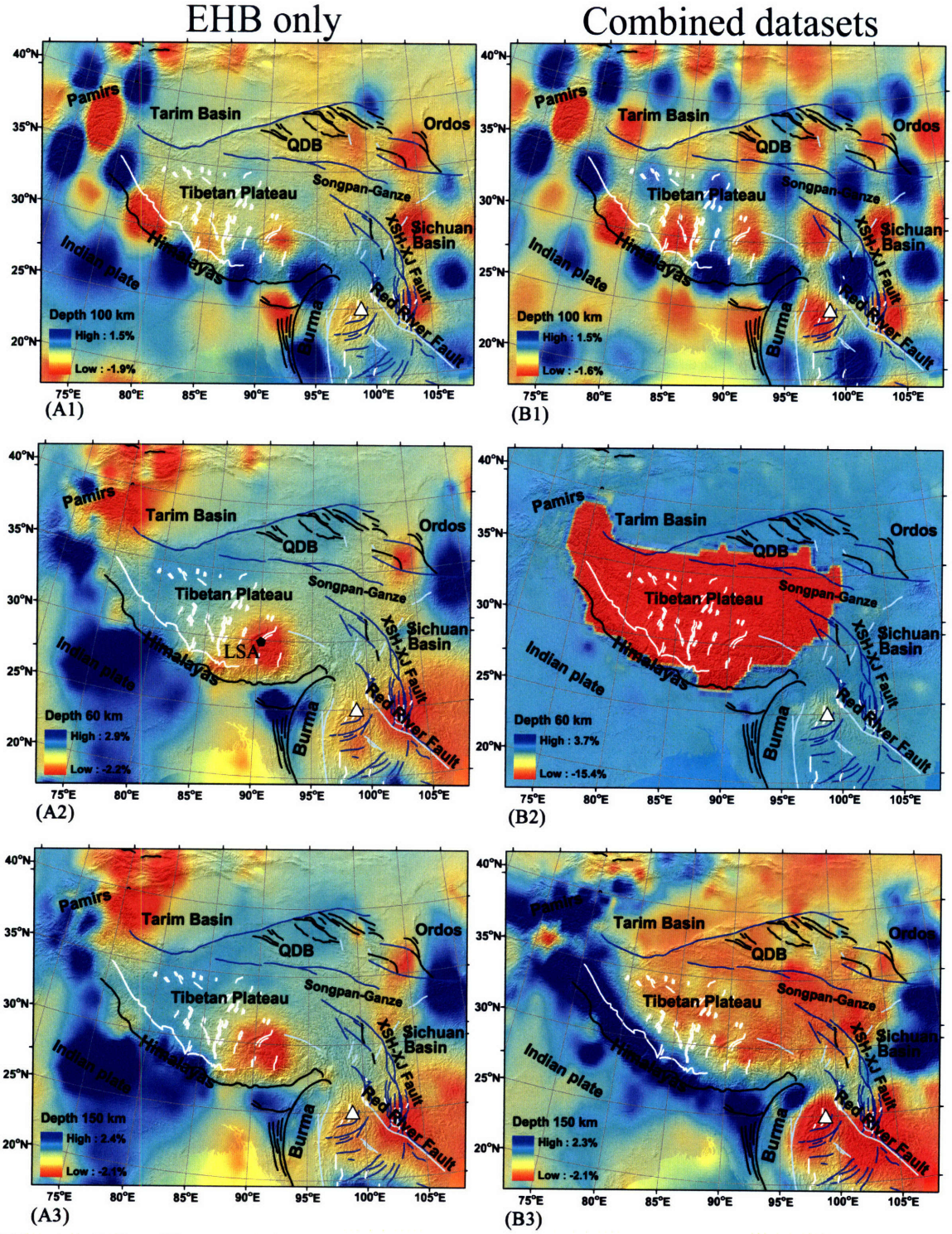

Figure 4-6. Effects of data addition and crust correction at 60 km and 150 km and resolution improvement at 100km. (A1) and (B1) depict the checkerboard resolution test before and after adding data from CSN and Tibetan arrays. (A2) and (A3) Model with only EHB data and without crustal correction. (B2) and (B3) Model with data incorporated from EHB, Tibetan arrays, and CSN, and with a crustal correction.

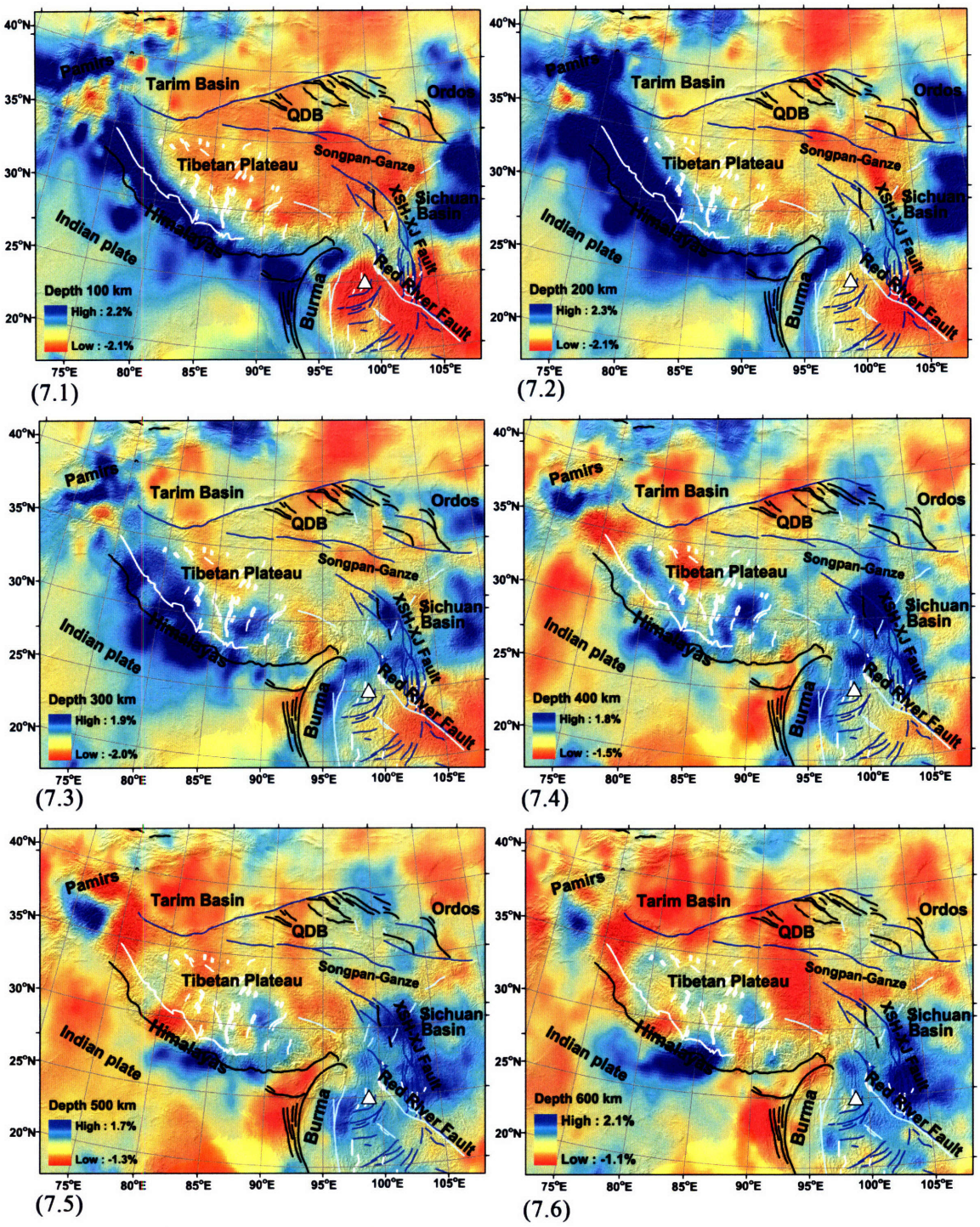

Figure 4-7. P-wave anomalies beneath Tibet and surrounding areas at different depths as indicated on the left lower corner in each subplot. The blue and red represent high and low velocity anomalies respectively. The white triangle is the location of the Tengchong volcano. The lines show active faults around Tibet (blue – left-lateral strike-slip faults; light blue – right-lateral strike-slip faults; black – thrust faults; white – normal faults). QDB: Qaidam basin; XSH-XJ: Xianshuihe-Xiaojiang.

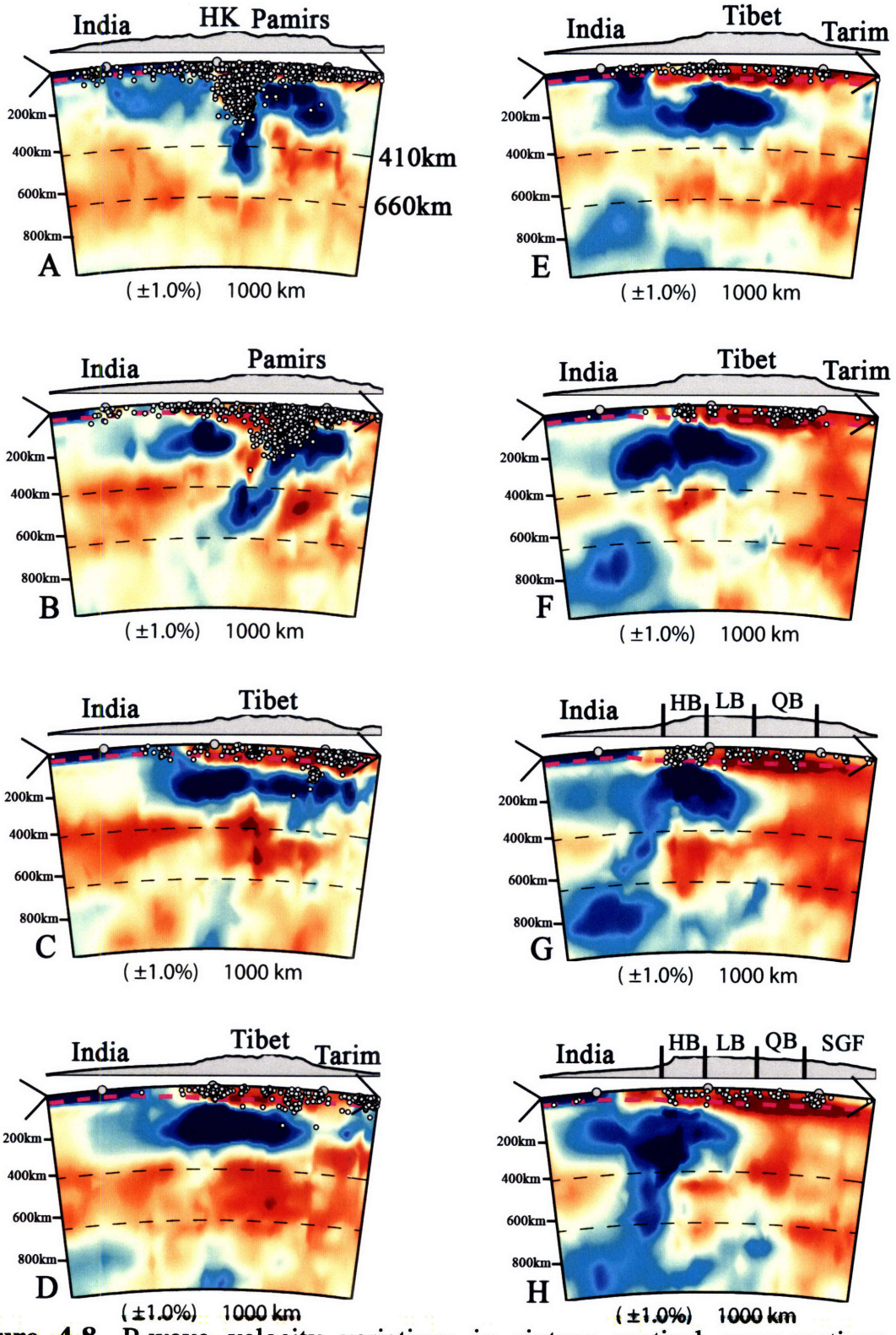

Figure 4-8. P-wave velocity variations in sixteen vertical cross-sections of through the Himalayas and Burma shown in Figure 4-2. The gray circles are earthquakes and magenta dash lines display the Moho. Gray shadow on the top of each subplot is the topography, where HK-Hindu Kush; HB-Himalayan block; LB-Lhasa Block; QB-Qiangtang block; Tch V.-Tengchong Volcano.

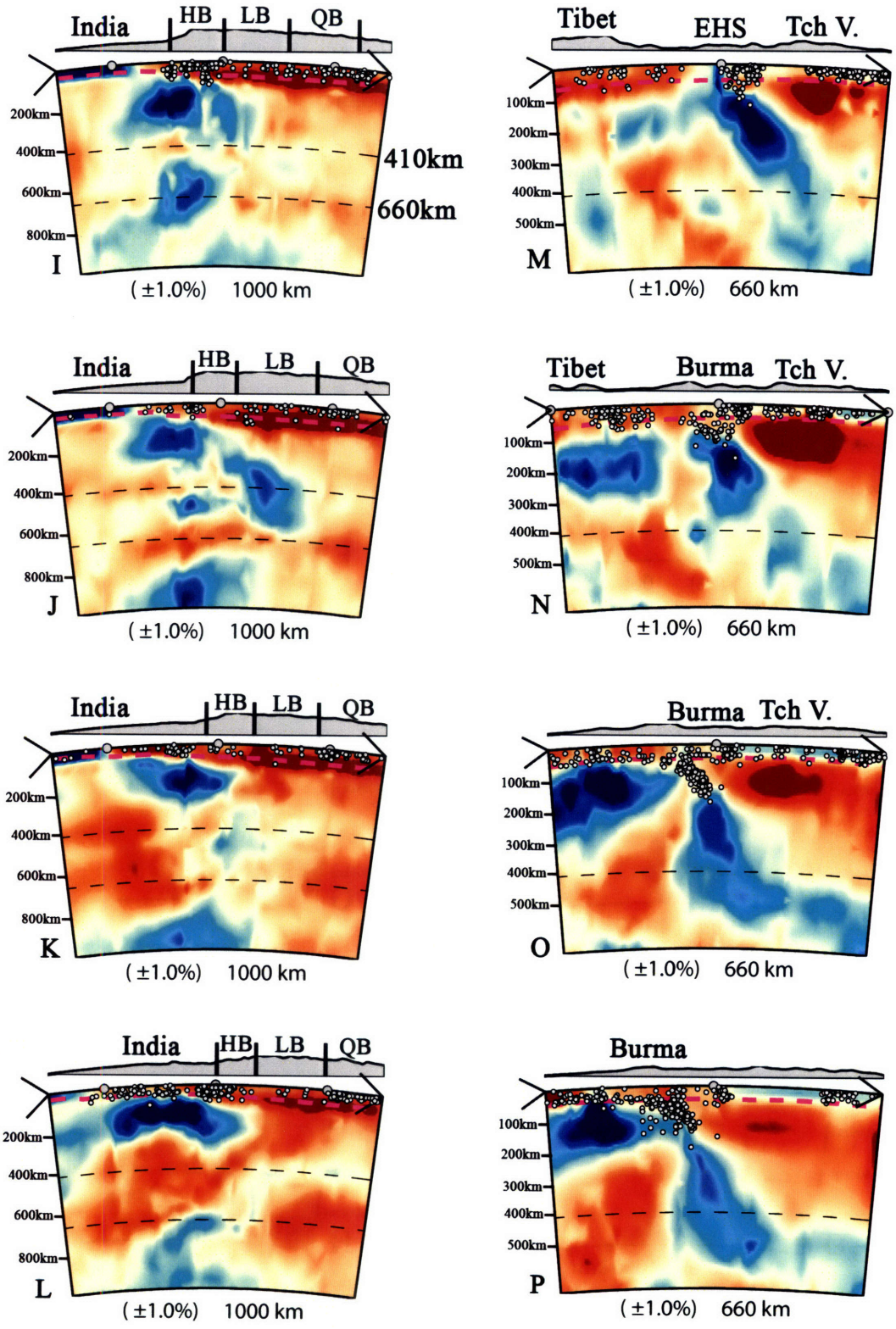

Figure 4-8. Continued.

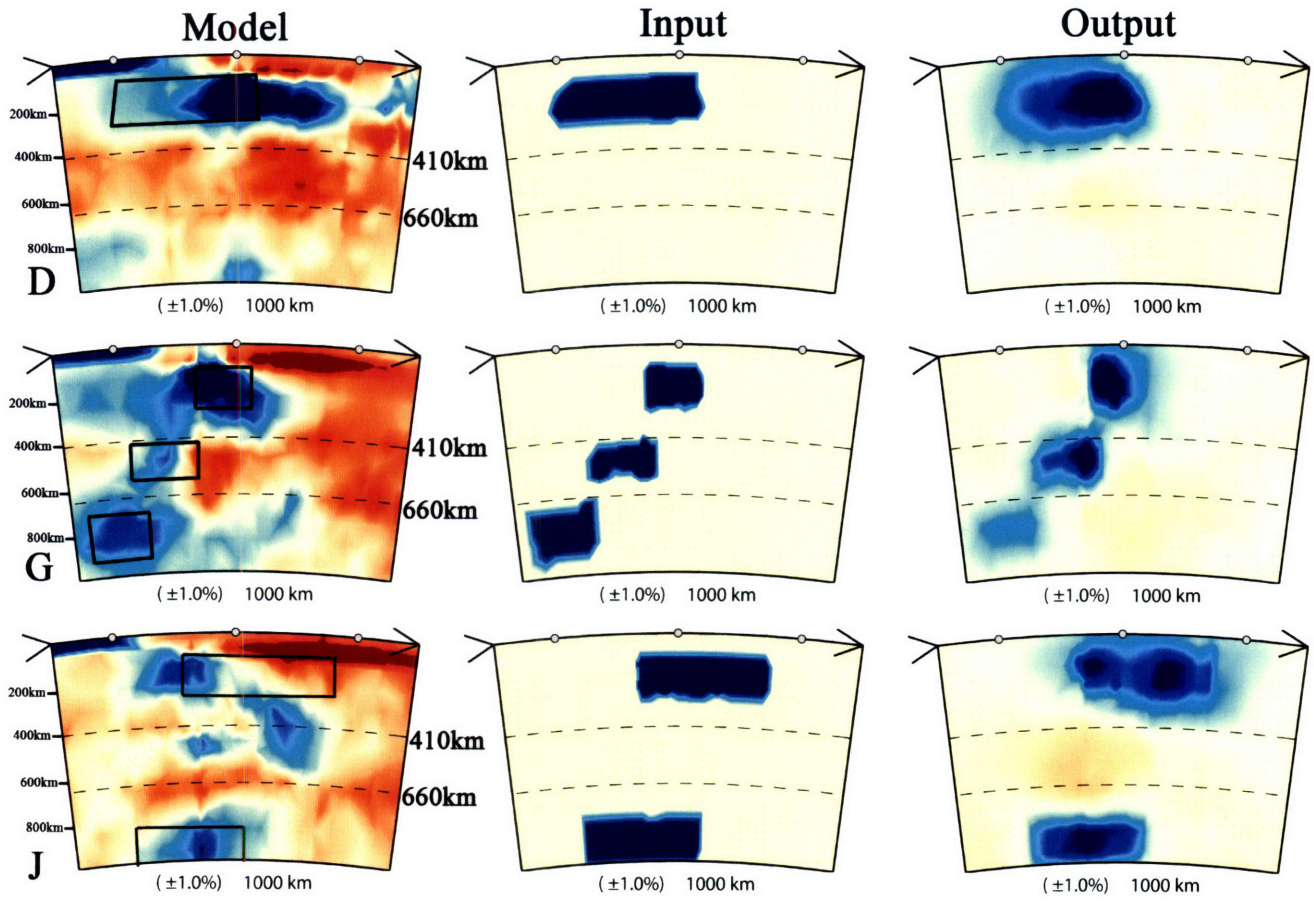

Figure 4-9. Target resolution tests for the Indian subduction along the Himalayas (The location of cross-sections D, G and J is shown in Figure 4-2). The left column is the tomographic image (Figure 4-8) and black boxes depict the range of input signal; the middle column is the test input signal; the right column is the recovery. In cross-section D, input signals beneath Himalayas can be recovered and there is no smearing beneath western Tibet. Image recovery is poor beneath the Indian plate. In cross-section G, the high velocity in the upper mantle and the mantle transition zone can be resolved. The resolution in the lower mantle beneath the Indian plate along cross-section G is not good. The cross-section J suggests that if high velocity lithosphere were present beneath eastern Tibet our data coverage would be sufficient to detect it. The high velocity anomalies beneath Lhasa block at ~400 km depth are not smearing effects from the structure at shallow depth.

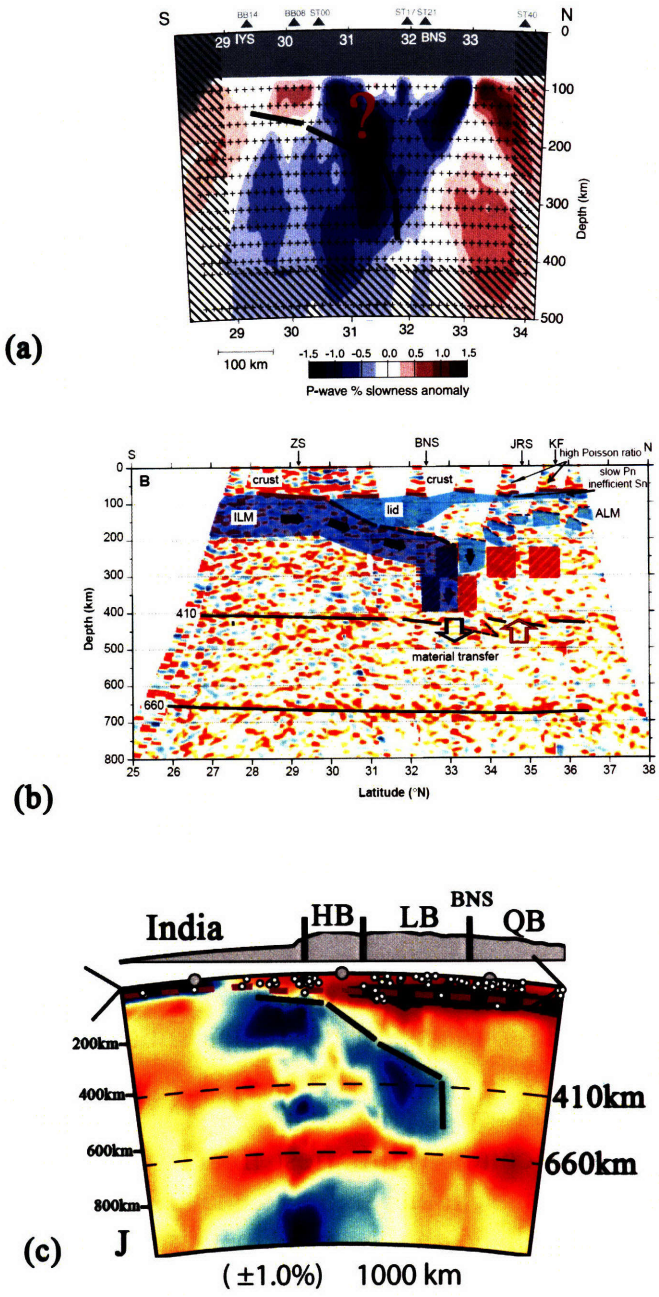

Figure 4-10. Comparison with seismic imaging studies from INDEPTH projects beneath central Tibet (around in rang of [86°E, 90°E] and [27°N, 35°N]). (a) Teleseismic tomography based on the INDEPTH II and III data (Tilmann *et al.*, 2003); (b) Teleseismic receiver function image from the INDEPTH II and Sino-American PASSCAL experiments (Kosarev *et al.*, 1999); (c) this study.

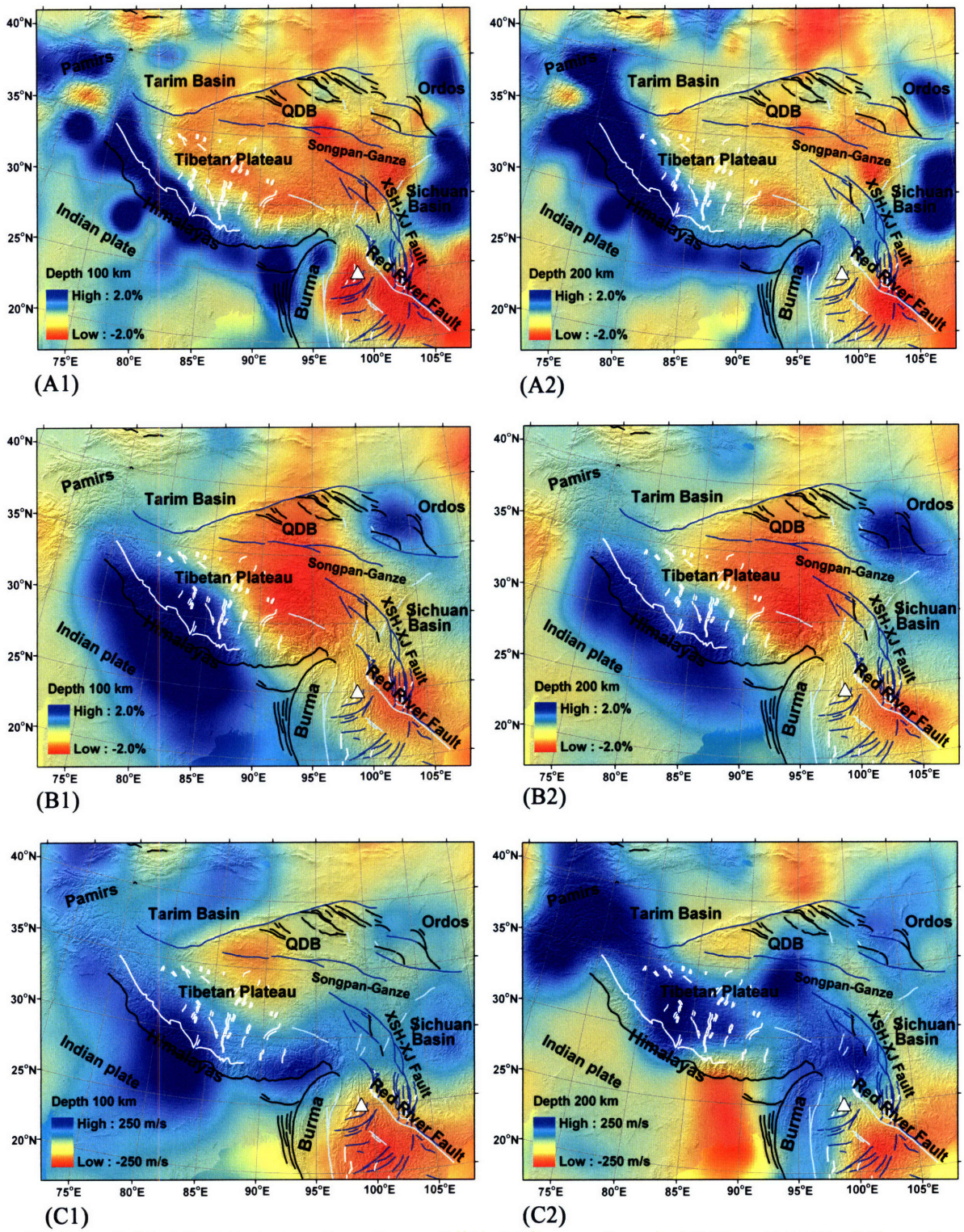

Figure 4-11. Model comparison beneath the Tibetan plateau. (A1) and (A2): this study; (B1) and (B2): P wavespeeds perturbation of model updated from Montelli *et al.*, (2004) at 100 km and 200 km depths. (C1) and (C2) Shear wave speeds perturbation of model from Lebedev *et al.*, (2006).

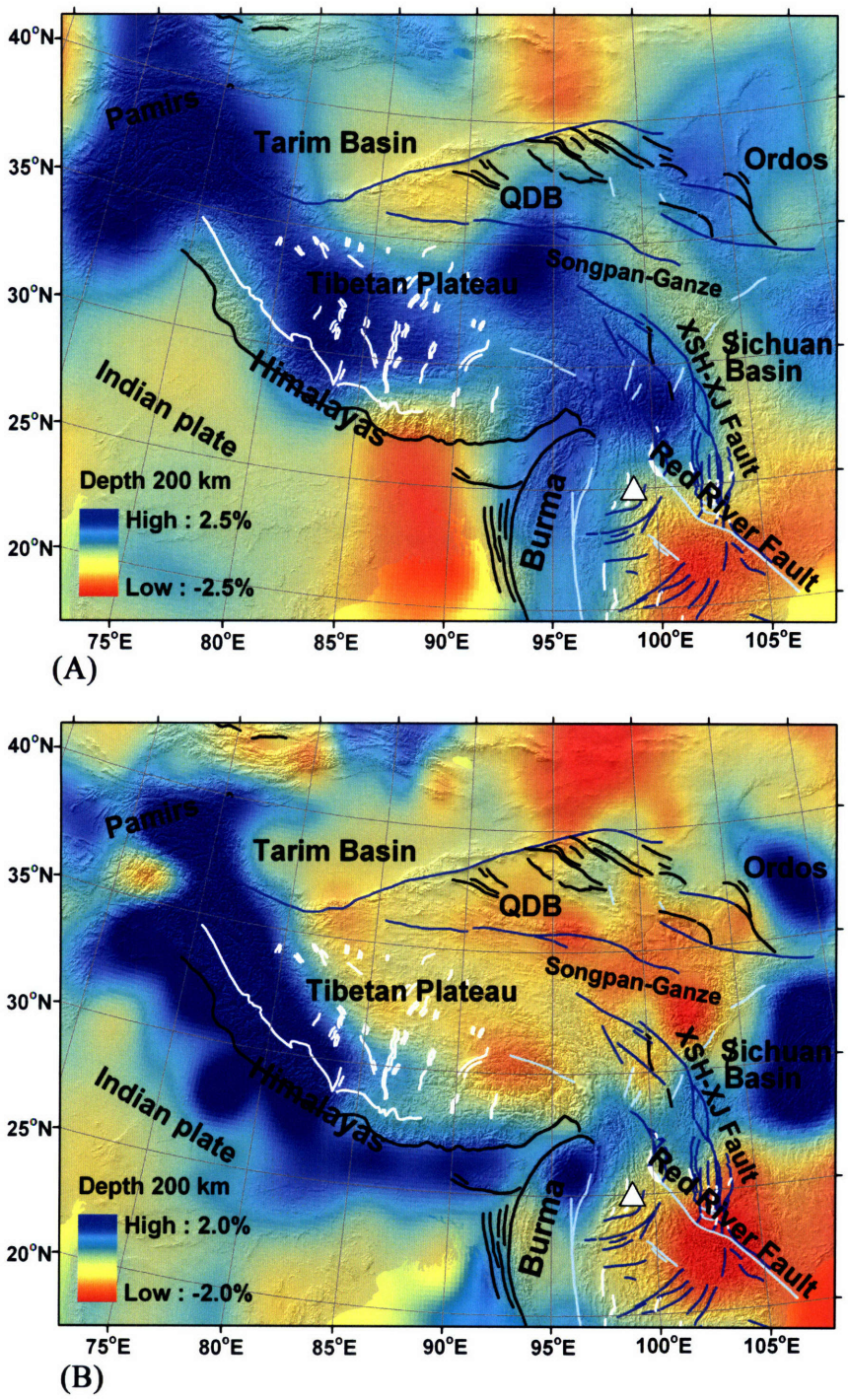

Figure 4-12. (A) Constraint model inferred from the surface wave model at 200 km depth (Lebedev *et al.*, 2007). We assume P-wave perturbation is half of shear wave perturbation. (B) Inversion results with the constraint model in the penalty function. The results are closely similar to the model (Figure 5-8A2). This test indicates that the constraint by the data around Tibet is strong.

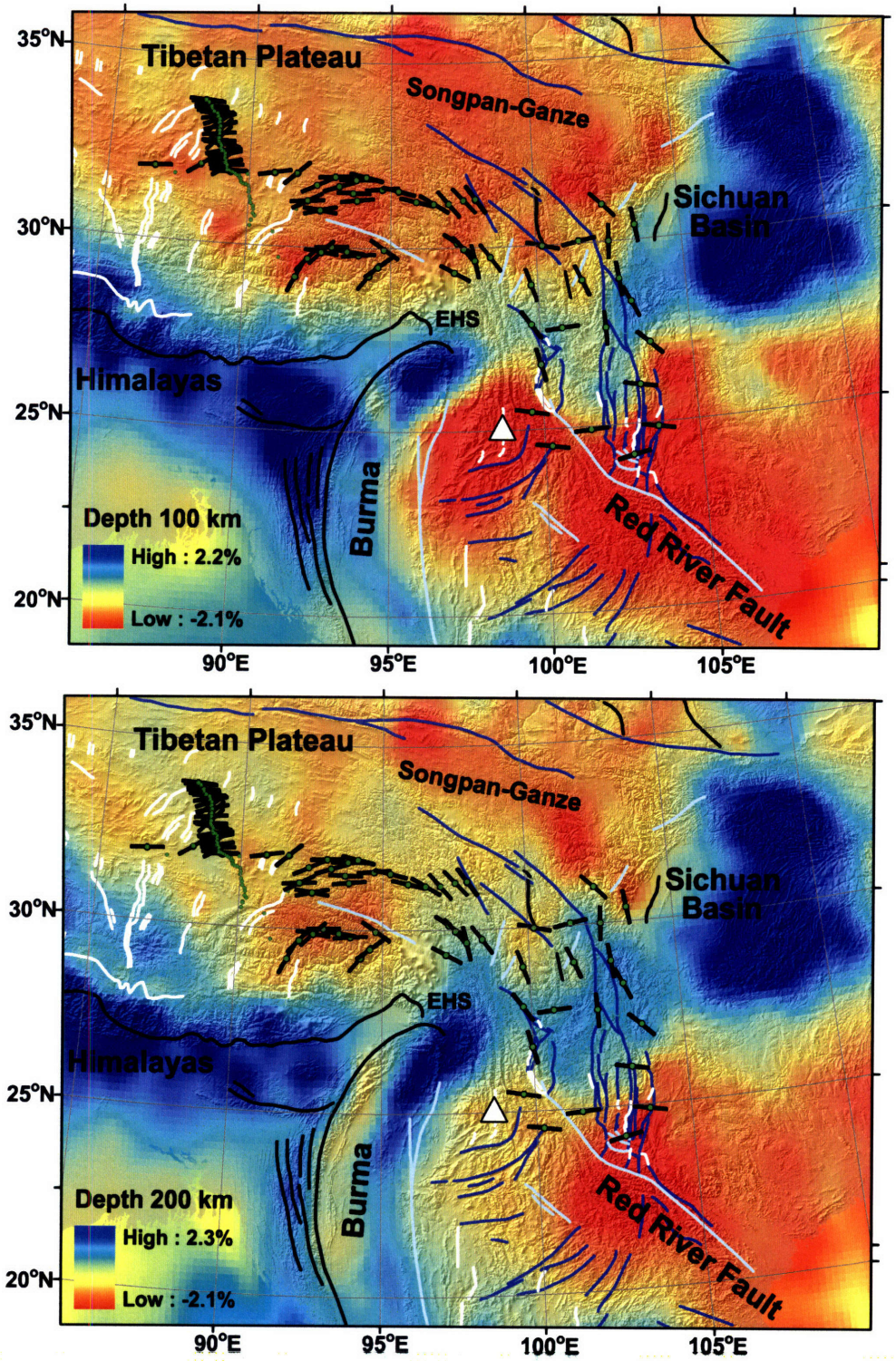

Figure 4-13. P-wave velocity perturbations (as shown on the left corner) at 100 and 200 km depths with the background of shear wave splitting results and active faults (Figure 4-1).

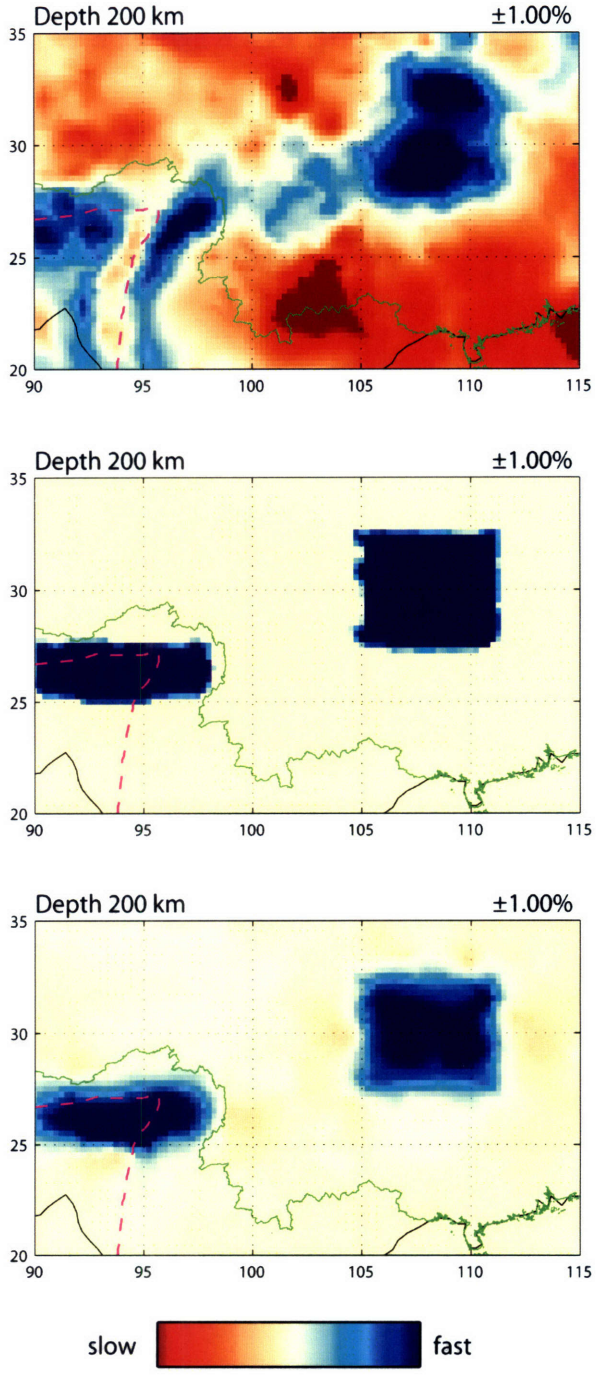

Figure 4-14. The target resolution tests for the high velocity beneath the Eastern syntaxis and the Sichuan basin. +1.5% velocity anomalies were generated beneath the Eastern syntaxis and Sichuan basin from 150 km to 250 km depth. The figure shows the map view at 200 km depth. Input signals can be well resolved and there are no smearing effects between them, thus demonstrate that the high velocities between Sichuan and the Eastern syntaxis are not artifacts.

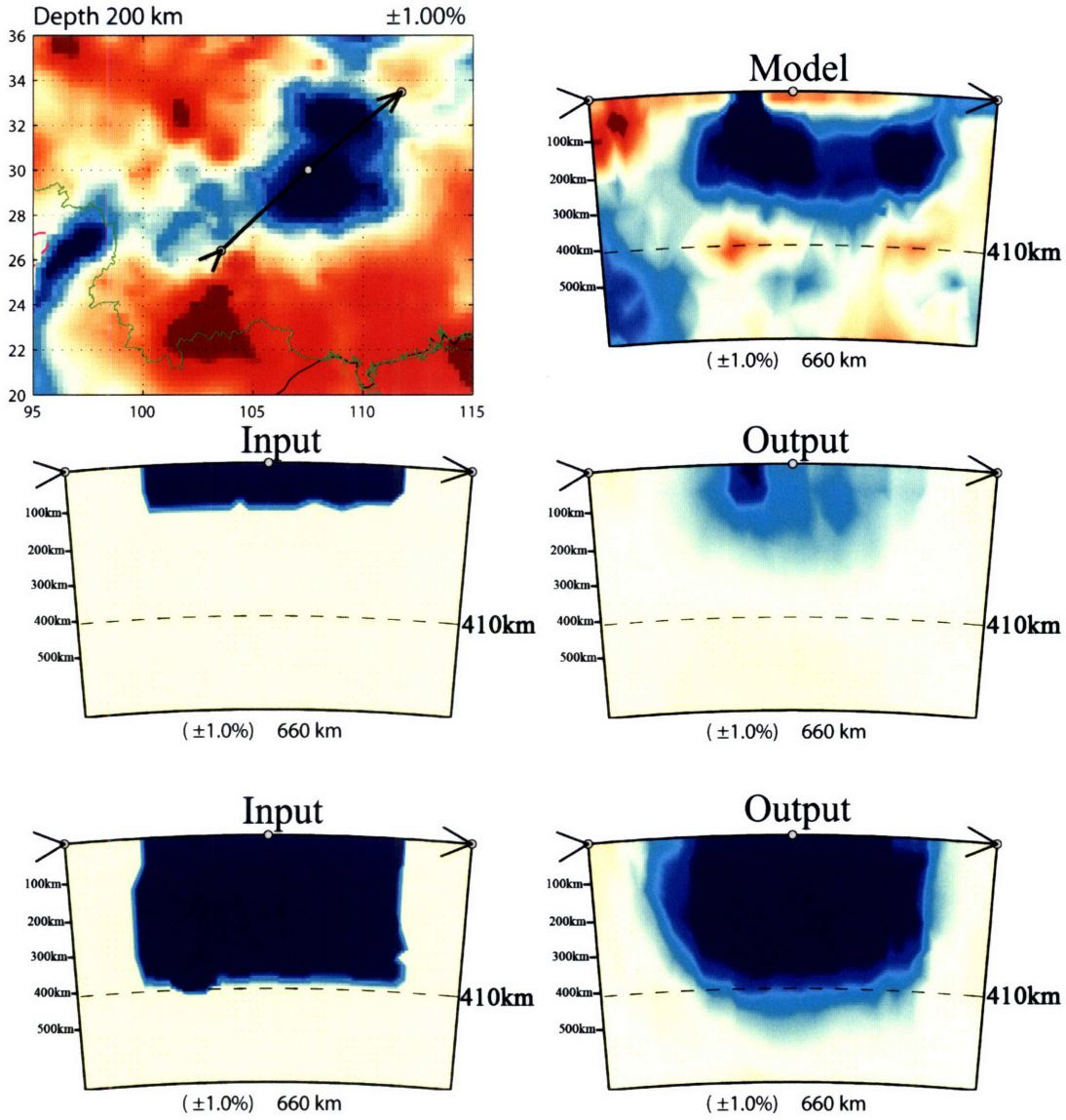

Figure 4-15. Target test for fast structures beneath the Sichuan basin. The first row is the model at 200 km depth and cross-section along profile as indicated. The second row is recovery test for the high velocity from surface to 100 km depth. The Third row is the recovery test for 400 km thick high velocity.

Chapter 5

Constraints on the evolution of East Asia's mantle from P-wave travel time tomography[4]

Abstract

High resolution tomographic images of the mantle structure beneath East Asia have been obtained through inversion of travel time data from global and regional seismograph stations and regional (temporary) arrays. These data resolve three-dimensional (3-D) upper mantle heterogeneity in unprecedented detail. In the west, high velocity anomalies are dominant beneath the Himalayas and the western portion of the Tibetan plateau to 300 km depth, which represent the northeastward subducting Indian lithospheric mantle. In the east, western Pacific slabs subducting from the Japan and Izu-Bonin trenches are deflected in the mantle transition zone beneath the Japan Sea and East China. These stagnant slabs likely influence upper mantle circulation beneath East Asia and might be related to volcanism in Korea and northeast China (such as the Changbai volcanic area). Low wavespeed structures in the shallow mantle beneath the Red River fault region connect to deep, slow anomalies beneath the South China Foldbelt. Tomographic imaging also reveals high wavespeed continental roots of the Precambrian Ordos block and Sichuan Basin (to 250-300 km depth) and strong heterogeneity between the latter and the Burma ranges further to the west. Together these structures may mark a transition in tectonic regime from the continental collision control in the west to control by subduction of Pacific, Philippine Sea and Indonesia plates to the east and the southeast.

---

[4] Li C., Sun R., van der Hilst R.D., Burchfiel B.C., and Royden L.H.. Constraints on the evolution of East Asia's mantle from P-wave travel time tomography, in preparation for submission to *J. Geophys. Res.*

5.1 Introduction

East Asia is a tectonically diverse and active area. In the southwest, the continental collision and post-collisional convergence between the Indian and Eurasian plates have raised the Tibetan Plateau and have produced the Himalaya, Pamirs and the Hindu-Kush mountains (Molnar and Tapponnier, 1975; Tapponnier *et al.*, 2001). The retreating western Pacific and Philippine Sea slabs in the east have generated island arcs, marginal seas, and a number of continental rifts and extension zones in northeast China (Northrup *et al.*, 1995; Zhang *et al.*, 2003; Schellart and Lister, 2005). These two geodynamic systems form a large-scale dynamic clockwise rotation in East Asia, which dominates the tectonic evolution of East Asia (Black arrows in Figure 5-1). There is controversy, however, about their relative importance for the tectonic evolution of East Asia. One group of researchers emphasized that the eastward extrusion of large-scale lithospheric blocks resulting from the India-Eurasia collision has controlled the widespread deformation in East Asia (Molnar and Tapponnier, 1975; Tapponnier and Molnar, 1977; Tapponnier *et al.*, 1982; Replumaz and Tapponnier, 2003). Recent studies suggest, however, that the slab rollback promoted by a reduction in velocity of the subducting Pacific and Philippine plates produced a number of Cenozoic back-arc or marginal basins along the East Asian margin (e.g., Northrup *et al.*, 1995; Schellart *et al.*, 2003) and the rollback of the Java-Sumatra slab may have aided southward motion of Indochina (Widiyantoro and Van der Hilst, 1996).

It has been suggested that the back-arc deformation caused by this slab roll-back can occur as far west as the Baikal rift zone, located some 3300 km from the subduction zone (Schellart and Lister, 2005; Lebedev and van der Hilst, 2007) and that subduction-induced mantle upwelling led to widespread uplift, volcanism and extension of East China (Tatsumi *et al.*, 1990; Tian *et al.*, 1992; Yin, 2000). It can be expected that the complex tectonics in East Asia have produced strong heterogeneity in the upper mantle. Alternatively, 3-D crust and upper mantle heterogeneity can provide crucial insight into the interaction of the continental collision and slab rollback and advance our understanding for the tectonic evolution of East Asia.

Seismic tomography has been used to study the heterogeneous crust and upper mantle of East Asia for at least two decades. Surface wave tomography can constrain crust and the shallow upper mantle when station distribution is relatively sparse. For instance, Lebedev and Nolet (2003) have shown that Precambrian continental roots with ~300 km thickness exist beneath Sichuan Basin by inversion of fundamental Rayleigh mode and S and multiple S waves. The inversion of shear and surface waveforms has also revealed a seismically fast Indian lithosphere under southwestern Tibet to ~250 km depth (Friederich, 2003). Multimode surface waveform tomography provided 3-D shear wave speed and thermal lithospheric thickness in East Asia (Priestley *et al.*, 2006). However, the horizontal resolution of surface wave tomography is, typically, several hundred kilometers due to the

relatively low frequency data and the sparse distribution of stations used. Moreover, surface wave tomography gradually loses resolution with increasing depth.

In regions with good data coverage, short-period travel time tomography can provide higher resolution than surface wave tomography. A number of P-wave travel time tomographic studies have focused on imaging subducting oceanic lithospheric slabs of western Pacific and Philippine Sea plates and have found that slabs subducted from the Japan trench have been stagnant beneath Japan Sea and East China in the mantle transition zone due to the east-direction rollback (e.g., van der Hilst *et al.*, 1991; Fukao *et al.*, 1992; Fukao *et al.*, 2001). Liu *et al.* (1990) provided 3-D velocity images of the upper mantle beneath the Chinese continent and adjacent regions with a block size of 2-5° by using the regional and teleseismic data from Chinese stations. Since then, many tomographic studies have focused on detailed crust and upper mantle structure beneath selected regions of China using the travel time data from regional stations (e.g., Sun and Liu, 1995; Liu *et al.*, 2000; Huang *et al.*, 2002; Xu *et al.*, 2002). The data from temporary seismic arrays have provided better constraints on crust and upper mantle beneath the Tibetan Plateau (e.g., Kind *et al.*, 1996; Kosarev *et al.*, 1999; Kind *et al.*, 2002; Tilmann *et al.*, 2003; Yao *et al.*, 2006).

With the data from the Chinese network becoming more openly available, seismologists have begun to combine the data from global and Chinese stations to

provide the large scale crust and upper mantle structure of East Asia with higher resolution than before (Li *et al.*, 2006; Huang and Zhao, 2006). However, the resolution of these studies is still insufficient for detailed investigations of upper mantle structures, which hinders our understanding of the tectonic evolution of East Asia.

In this paper we present a new high resolution P-wave tomographic model and investigate the relationship between heterogeneous structures in the upper mantle and the complex tectonic history of East Asia. We augmented the data set used in Chapter 3 (that is, *Li et al.* (2006)) with data from ~1200 Chinese regional seismic stations and ~170 Tibetan seismic array stations (Figure 5-2). The combined datasets provide unprecedented resolution of the upper mantle structure beneath East Asia, especially beneath the Tibetan plateau. Our results reveal that the northeastward subducting Indian lithospheric mantle underlies only the western portion of the Tibetan plateau, which implies that most of the Tibetan lithosphere is of Asian origin (see Chapter 4 for a more detailed discussion). The oceanic lithospheric slabs of the western Pacific Ocean and the Philippine Sea are very well resolved, as is the "stagnant" slab in the mantle transition zone beneath the Japan Sea, East China, and Yangtze Craton. In between these dynamics systems, Precambrian continental roots beneath Ordos block and Sichuan Basin stand out by higher than average P wavespeed to 250-300 km depth. These stable

continental roots may form a transition in tectonic regime from subduction control in the east and southeast to (continental) collision control in the west.

5.2 Data and Method

We combined the travel time data from the International Seismological Centre (reprocessed by Engdahl, van der Hilst and Buland, 1998, hereinafter referred to as EHB), the Chinese Seismic Network (CSN), and seismic arrays on the Tibetan plateau. The station distribution of each dataset is shown in Figure 5-2. In addition, we used the differential times of *PP-P* (Woodward and Master, 1991) to add, globally, more constraints on upper mantle structure. We implemented an adaptive parameterization, a crust correction, and 3-D sensitivity kernels to analyze our travel time data. See Chapter 2 for a more detailed description of data and methods.

5.3 Results

5.3.1 Checkerboard resolution tests

In order to assess the general resolution of our results, we performed checkerboard tests at different depths for box sizes of $3^{\circ}\times3^{\circ}$ and compared them to the previous resolution tests. The input structure of ±1.5% velocity variation checkerboard (Figure 5-3.0) was used to compute synthetic travel times for each depth at a time. These synthetic travel times were inverted using the same inversion scheme and sampling as used in building the model from earthquake

data. As expected, the full dataset resolves the input structure better than our previous set of the Annual Bulletin Chinese Earthquakes (ABCE) and EHB datasets (Figure 3-6). In particular in the shallow mantle, the input pattern is resolved better under the mainland of China, especially around the Tibetan plateau (Figure 5-3.1, 3.2; Figure 3-6.1, 6.2). This improvement comes mainly from the dense data coverage provided by the Chinese Seismography Network (CSN) and the Tibetan arrays (Figure 5-2). For larger depths, the input patterns are adequately recovered under our regions of interest, such as the Tibetan plateau, the Himalayas, East China, and the eastern margin of Eurasia plate (Figure 5-3.4~3.9).

5.3.2 Upper mantle structure beneath East Asia

We present the P-wave velocity variations by means of map views (Figure 5-4) and vertical cross sections (Figure 5-5). The main faults, topographic relief, tectonic units and major volcanic centers are shown for geological reference. The major features of the model are described below.

The eastern margin of Eurasia: The most significant features along the eastern margin of Eurasia are the high velocity anomalies associated with the subducting Western Pacific and Philippine Sea slabs and the low velocity anomalies beneath the associated back arc regions. From 100 km to 400 km in the upper mantle, narrow fast structures along the Japan and Izu-Bonin trenches are clearly visible (Figure 5-4(a)~(e); Figure 5-6(a)~(e), (l)~(n)). Another narrow fast structure, which parallels the Ryukyu trench, is detected beneath the East China Sea. (Figure 5-6(d)~(f), (i)~(k)). These structures are associated with the

subduction of the western Pacific plate at the Japan and Izu-Bonin trenches and the subduction of the Philippine plate from the Ryukyu trench, respectively. The top of these fast structures are seismically active (Figure 5-6(a)~(f), (i)~(m)). In map view, these fast structures are located further west with increasing depth and extend to the mantle transition zone beneath the Japan Sea and East China Sea (Structures TZ1 and TZ2 in Figure 5-4(f) and Figure 5-6(b)~(e), (j)~(l)). Structures TZ1 and TZ2 in the mantle transition, interpreted as the stagnant slabs due to the east-directed retreat of the Pacific and Philippine plates (e.g., Van der Hilst *et al.*, 1991; Fukao *et al.*, 1992; Fukao *et al.*, 2001), are visible as far west as ~120°E longitude (Figure 5-5(f); Figure 5-6(b), (c)). Low velocity anomalies are dominant beneath the Japan Sea, East China and the northern corner of the Philippine Sea in 100~400 km depth (structure S4 in Figure 5-4(b)~(d) and Figure 5-6(a)~(e), (l)). These slow structures are located just west of the west-dipping fast velocity anomalies beneath the Japan, Izu-Bonin, and Ryukyu trenches (Figure 5-4(b)~(d); Figure 5-6(b)~(e)).

TZ beneath Yangtze Craton: A large fast velocity area with a NE-SW trend is dominant in the mantle transition zone beneath the Yangtze Craton (structure TZ3 in Figure 5-4(f), (g); Figure 5-6(d)~(f), (g), (i)). This fast structure is detected as the two separated parts below 600 km depth in the mantle transition zone (Structure TZ3A and TZ3B in Figure 5-4(g), (h); Figure 5-6(e)). Structure TZ3B extends as far west as ~100°E and connects with the fast structures in the lower mantle beneath the Indo-China block (Figure 5-6(f)).

Continental roots below Basins: The model reveals fast velocities beneath some basins in East Asia, such as the Songliao, Huabei, Khorat, Ordos and Sichuan basins (Figure 5-4(b)~(d)). Fast structure characterizes the western part of the Songliao basin in northeast China, which is consistent with our previous study (Li *et al.*, 2006). Fast structure beneath the Huabei basin in East China becomes gradually weaker with increasing depth (Figure 5-4(b)~(c)). Fast structures beneath the Ordos block and the Sichuan Basin are pronounced down to 250-300 km depth (Figure 5-4(b)~(d); Figure 5-6(b)~(e); Figure 5-10). Pn wave studies of the Ordos block and the Sichuan Basin show that the seismic velocity is high in the uppermost mantle with little seismic anisotropy (Hearn *et al.*, 2004; Liang *et al.*, 2004). The seismicity is very low and there are only a few large earthquakes. These results suggest that the Ordos block and the Sichuan Basin are relatively rigid and tectonically stable units.

Southwest China: The upper mantle beneath southwest China is characterized by large low velocity anomalies. A pronounced slow structure is situated 100 km depth beneath the Tengchong volcanic area (Structure S1 in Figure 5-4(b) and Figure 5-6(f)). Further southeast, another larger slow structure characterizes the upper mantle to 300 km depth beneath region along the Red River fault (Structure S2 in Figure 5-4(b)~(d) and Figure 5-6(g)). Beneath the South China Foldbelt, slow velocity anomalies are visible from 200 km to 500 km depth (Structure S3 in Figure 5-4(c)~(f) and Figure 5-6(e), (f), (h), (i)). High velocity anomalies dip from

Burma to the east reach to the Tengchong volcanic area at depth larger 300 km (Figure 5-4(c)~(e)).

The Tibetan plateau: At 60 km depth, P wavespeed is anomalously low compared to global reference values because of the thick crust of the Tibetan Plateau (Figure 5-4a). Low velocities are detected well below the crust, however, and extend to at least 200 km depth beneath the plateau (Figure 5-4(b), (c)). In contrast, wavespeed is high beneath the Himalayas and the western portion of the plateau (Figure 5-4(b)~(d)). The latter was interpreted as the (sub-horizontal) northward subduction of the Indian lithospheric mantle. The northern edge of this fast velocity does not seem to extend to the Bangong-Nujiang suture zone (~33°N), which places important constraints on how far north the Indian plate has subducted beneath Tibet (see Chapter 4 for a more detailed discussion).

5.3.3 Resolution tests for stagnant slabs in the mantle transition zone

We have implemented resolution tests for the stagnant slabs in the mantle transition zone. Here, we show two examples through the cross-section (b) and (e) (upper parts in Figure 5-7 and Figure 5-8).

In Figure 5-7, the input pattern consists of 1.5% high velocity anomalies confined to the range of the TZ1 structure in cross section (b). This test is designed to evaluate the resolution in the TZ1 structure and if the TZ2 structure is a smearing artifact. The synthetic data were calculated from the input model, and the recovery model is shown in the lower part in Figure 5-7. Although some signals in the western part are missed, the data can resolve most of the input pattern.

Smearing across the box boundaries is small. This demonstrates that the TZ2 structure is not an artifact due to the high velocities of the TZ1.

In Figure 5-8, the input signal comprises the mantle transition zone over almost the entire width of the cross section (e). This test is designed to evaluate whether the separated fast structures in the mantle transition zone (structures TZ1, TZ2, and TZ3) result from incomplete sampling of a single TZ structure. The test shows that the input pattern of a large fast structure can be well resolved and there are no separated parts in the recovery model. Thus, the fast structures TZ1, TZ2, TZ3A and TZ3B do not come from a single large fast structure due to poor resolution of a larger, laterally contiguous structure.

5.4 Discussion

5.4.1 Stagnant slabs in the mantle transition zone

Along the eastern margin of Eurasia, the Pacific and Philippine Sea plates are subducting beneath East Asia, creating one of the largest trench-arc-back arc systems on Earth (Figure 5-1). Many regional and global tomographic studies have focused on the 3-D mantle structure of the western Pacific subduction zone and have revealed the basic structure of the subducting slabs (e.g., van der Hilst *et al.*, 1991; Fukao *et al.*, 1992; Zhao *et al.*, 1994; Fukao *et al.*, 2001). Compared to any previous study, we have used denser data coverage and obtained clearer images of the subducted slabs, especially beneath China.

As in many previous studies, this study suggests that the subducted slabs of Pacific and Phillipine sea plates are stagnant in the mantle transition zone beneath Japan Sea, East China Sea and East China (e.g., van der Hilst *et al.*, 1991; Fukao *et al.*, 1992), and perhaps over a larger region of the mantle transition zone than previously thought. Only some sections (e.g., Figure 5-6 (l)) suggest a possible connection with structure deeper in the lower mantle. Our model reveals several separated parts of the stagnant slabs in the mantle transition (TZ1, TZ2, and TZ3 in Figure 5-4(f)). The TZ1 is located beneath the Japan Sea and is parallel to the Japan and Izu-Bonin trenches. The TZ2 is located beneath the Bohai and the Yellow Sea and is west of the TZ1. The TZ3 is located beneath the Yangtze Craton and could be separated into western and eastern parts (TZ3A and TZ3B in Figure 5-4(g)). Resolution tests show that the separation of stagnant slabs in the mantle transition zone is not due to the poor resolution (Figure 5-8).

The (lateral) discontinuous nature of slab fragments stagnant in the mantle transition zone indicates that they might result from different periods of subduction of the Pacific plate. In Figure 5-9, we show the reconstruction of arcs in Southeast Asia since the Late Cretaceous by Honza and Fujioka (2004). The Japan Trench retreated eastward over ~3000 km since the Late Cretaceous (~85Ma). The South China Trench gradually disappeared after the Earliest Oligocene (~35Ma). Figure 5-10 illustrates the relationship between tomography images at 500 km and 600 km depths and the South China Trench and Japan Trench in the Late Cretaceous (~85Ma) and Earliest Eocene (~52Ma). These

reconstructions suggest that structure TZ3B resulted from subduction at the South China Trench in the Late Cretaceous (Figure 5-10(A)). In contrast, the TZ3A and TZ2 may be related to the Japan Trench in the Earliest Eocene (Figure 5-10(B)). These relationships suggest that the fast structures in the mantle transition zone might have resulted from Eocene subduction at the South China and Japan trenches, respectively. There are many uncertainties in plate reconstructions in Southeast Asia. For example, results by Replumaz and Tapponnier (2003) suggest little movement of the South China coast line over the Cenozoic. Therefore, further investigation of the images of subducted slabs, such as quantification of slab accumulation and slab sinking rate, would provide more constraints on the evolution of arcs in East Asia. This is a topic of future research.

5.4.2 Slow structures in the upper mantle

This study reveals widespread low velocity anomalies in the upper mantle beneath East Asia (Structure S1, S3, S3 and S4 in Figure 5-4(b)-(e)). Structure S1 is located at the uppermost mantle beneath the Tengchong Volcano and is, most likely, related to subduction below the Burmese arc (Chapter 4). Structure S2 is situated beneath an area along the Red River Fault zone down to 200 km depth. Structure S3 is beneath the South China Foldbelt from 200 km to 500 km depths. Structure S4 is beneath Japan Sea, southern Japan, and the northern Philippine Sea and is parallel to the Pacific subduction from the Japan Trench and Izu-Bonin Trench.

The widespread slow structures may be important for our understanding of the tectonic evolution of East Asia. For example, they may be related to the thinning of the lithosphere under East China (Deng *et al.*, 2000), Cenozoic extension in North China (Zhang *et al.*, 2003), active intraplate volcanism (such as Changbai, Qiongbei and Datong volcanoes in Figure 5-4(c)), and high heat flow (Zang *et al.*, 2003). Although the mechanism of these slow structures is largely unknown, they are more likely related to the subduction of the Pacific, Philippine Sea, and Indo-Australia plates. One possible reason is the dehydration from stagnant slabs in the mantle transition zone (Huang and Zhao, 2006). Another alternative is the upwelling of hot mantle materials induced by the eastward rollback of Pacific and Philippine Sea slabs. Further detailed investigation of these low velocity anomalies would advance our understanding of the evolution of East Asia.

5.4.3 Stable units in the central East Asia: Sichuan and Ordos

In central East Asia, two regions are tectonically stable compared with the surrounding areas: the Ordos block and the Sichuan Basin. The Ordos block is the major Precambrian continental nucleus of the Sino-Korean Craton (Figure 5-1) and it is surrounded by intensive intracontinental rifting and extension from the Cenozoic. Changes in the direction of extensional stress around the Ordos block show that the early Tertiary rifting phase east of the Ordos block was initiated by westward subduction of the Pacific plate and that the Pliocene deformation in the southwest of the Ordos block is mainly the consequence of late-stage India-Eurasia convergence (Zhang *et al.*, 2003). In the south, the Sichuan Basin is the

Precambrian nucleus of the Yangtze Craton (Figure 5-1). The left-lateral strike-slip Xianshuihe-Xiaojiang fault system is located in the southwest of the Sichuan basin. Numerical modeling shows that the steep topography in the western boundary of the Sichuan Basin has been generated due to the strong crust and mantle of the Sichuan Basin during the eastward ductile flow of the lower crust in the eastern Tibetan plateau (Clark and Royden, 2000). The Ordos block and the Sichuan Basin are geographically located in East Asia between the subduction of the western Pacific plate in the east and the Eurasia-India collision in the southwest. Their geotectonic setting suggests that these ancient blocks play an important role in the interaction between these two large-scale dynamics systems.

In our tomographic images, the Ordos block is characterized by fast velocity anomalies in the upper mantle to 300 km depth (Figure 5-10(a)). Pronounced high velocity anomalies are situated beneath the eastern part of Sichuan Basin down to 250-300 km depth (Figure 5-10(c)). This fast structure extends beyond the eastern boundary of the Sichuan Basin and extends to the middle of Yangtze Craton (~111°E, Figure 5-7(b)). Low velocity anomalies are situated beneath the Qinling-Dabie orogen between Ordos block and Yangtze Craton (Figure 5-7(d) and (e)). The resolution test demonstrates that the fast structure beneath the Sichuan Basin is not an artifact (Chapter 4, Figure 4-13). The two stable blocks may be composed of rigid rock and thus have been less deformed under the compressional stress regime caused by the India-Asia collision from the southwest. The seismicity west of Ordos block and Sichuan Basin is very dense, whereas there are only a few

earthquakes in the large area east of Ordos block and Sichuan Basin (Figure 3-2). Therefore Ordos and Sichuan Basin could form a transitional boundary for the tectonic regimes of these two dynamics systems. There are several interesting questions about these stable blocks, such as how long do they remain stable? How are they influenced by the India-Eurasia collision and the Pacific subduction? These questions will be addressed in further studies.

5.5 Conclusions

East Asia is a tectonically diverse and active region. High resolution P-wave tomography has revealed significant heterogeneity in the upper mantle under East Asia. The main results of this study are:

a) The eastward retreating slabs of western Pacific and Phillipine plates are deflected in the transition zone beneath Korea, the Japan Sea, and East China. Some of Mesozoic subducted slabs have reached as far west as 110°E longitude under the Yangtze Craton. Cenozoic extension, volcanic activity and high heat flow in the eastern margin of Eurasia might be related to the upwelling mantle materials induced by the eastward slab rollback and stagnant slabs in the mantle transition zone.

b) Precambrian continental roots under Ordos block and Sichuan Basin, which extend to about 300 km depth, may construct a boundary of transition in tectonic regimes from the India-Eurasia collision controlling the southwest to Pacific, Philippine Sea, and Java-Sumatra subductions controlling the east and southeast.

Effect of the India-Eurasia collision on the tectonic evolution of East Asia might be only confined to the Tibetan plateau and surrounding regions.

Acknowledgements:

This work was fund by NSF grant 6892042 of Collaborative Research in Eastern Tibet.

Reference:

Clark, M.K., and Royden, L.H., 2000. Topographic ooze: Building the eastern margin of Tibet by lower crustal flow. Geology, 28, 703-706.

Deng, Q., X. Feng, and P. Zhang, 2000, Active Tectonics of the Chinese Tianshan Mountains (in Chinese), 399 pp., Seismol. Press, Beijing.

Engdahl, E.R., van der Hilst, R.D., and Buland, R., 1998. Global teleseismic earthquake relocation with improved travel times and procedures for depth determination. Bull. Seism. Soc. Am., 88, 722-743.

Friederich, W., 2003. The S-velocity structure of the East Asian mantle from inversion of shear and surface waveforms. Geophys. J. Int., 153, 88–102.

Fukao, Y., Obayashi, M., Inoue, H., and Nenbai, M., 1992. Subduction slabs stagnant in the mantle transition zone. J. Geophys. Res. 97, 4809–4822.

Fukao, Y., S. Widiyantoro, and M. Obayashi, 2001. Stagnant slabs in the upper and lower mantle transition region, Rev. Geophys., 39, 291– 323.

Hearn, T. M., S.Wang, J. Ni, Z. Xu, Y. Yu, and X. Zhang, 2004. Uppermost mantle velocities beneath China and surrounding regions, J. Geophys. Res., 109, B11301. doi:10.1029/2003JB002874.

Honza, E., and Fujioka, K., 2004. Formation of arcs and backarc basins inferred from the tectonic evolution of Southeast Asia since the Late Cretaceous. Tectonophysics, 384, 23-53.

Huang, J., Zhao, D., Zheng, S., 2002. Lithospheric structure and its relationship to seismic and volcanic activity in southwest China. J. Geophys. Res. 107 (B10), 2055.

Huang, J. and D. Zhao, 2006. High-resolution mantle tomography of China and surrounding regions, J.G.R., 111, B09305, doi:10.1029/2005JB004066.

Kind, R., Ni, J., Zhao, W., Wu, J., Yuan, X., Zhao, L., Sandvol, E., Reese, C., Nabelek, J., Hearn, T., 1996. Mid-crust lowvelocity zone beneath the southern Lhasa block: Results from the INDEPTH-II earthquake recording program. Science 274, 1692–1694.

Kind, R., Yuan, X., Saul, J., Nelson, D., Sobolev, S.V., Mechie, J., Zhao, W., Kosarev, G., Ni, J., Achauer, U., Jiang, M., 2002. Seismic Images of crust and upper mantle beneath Tibet: evidence for Eurasian plate subduction. Science 298, 1219–1221.

Kosarev, G., Kind, R., Sobolev, S.V., Yuan, X., Hanka,W., Oreshin, S., 1999. Seismic evidence for a detached Indian lithospheric mantle beneath Tibet. Science 283, 1306–1309.

Lebedev, S., Nolet, G., 2003. Upper mantle beneath Southeast Asia from S velocity tomography. J. Geophys. Res. 108, 2048–2074.

Lebedev, S. and Van der Hilst, R.D., 2007. Global upper-mantle tomography with the automated multi-mode surface and S waveforms, Geophysical Journal International (under review).

Liang, C., X. Song, and J. Huang, 2004. Tomographic inversion of Pn travel times in China, J. Geophys. Res., 109, B11304, doi:10.1029/2003JB002789.

Liu, F., H. Wu, J. Liu, G. Hu, Q. Li, and K. Qu, 1990. 3-D velocity image beneath the Chinese continent and adjacent regions, Geophys. J. Int., 101, 379–394.

Liu, F., J. Liu, D. Zhong, J. He, and Q. You, 2000. The subducted slab of Yangtze continental block beneath the Tethyan orogen on western Yunnan, Chin. Sci. Bull., 45, 466– 471.

Li, C., R.D. van der Hilst, M.N. Toksöz, 2006. Constraining P-wave velocity variations in the upper mantle beneath Southeast Asia, Phys. Earth Planet. Inter. 154, 180–195.

Li S.L, Mooney W.D., Fan J.C. 2006. Crustal structure of mainland China from deep seismic sounding data, Tectonophysics 420, 239–252

Molnar, P. & Tapponnier, P., 1975. Cenozoic tectonics of Asia: effects of a continental collision. Science, 189, 419–426.

Montelli, R., Nolet, G., Dahlen, F.A., Masters G., Engdahl E.R., and Hung S.H., 2004. Finite-frequency tomography reveals a variety of plumes in the mantle. Science, 303, 338-343.

Northrup, C.J., Royden, L.H. & Burchfiel, B.C. 1995. Motion of the Pacific Plate relative to Eurasia and its potential relation to Cenozoic extension along the eastern margin of Eurasia. Geology, 23, 719–722.

Priestley, K., E. Debayle, D. McKenzie, and S. Pilidou, 2006. Upper mantle structure of eastern Asia from multimode surface waveform tomography, J. Geophys. Res., 111, B10304, doi:10.1029/2005JB004082.

Romanowicz, B. A., 1982. Constraints on the structure of the Tibet Plateau from pure path phase velocities of Love and Rayleigh waves, J. Geophys. Res., 87, 6865– 6883.

Rapine, R., F. Tilmann, M. West, J. Ni, and A. Rodgers, 2003. Crustal structure of northern and southern Tibet from surface wave dispersion analysis, J. Geophys. Res., 108(B2), 2120, doi:10.1029/2001JB000445.

Replumaz, A., and P. Tapponnier, 2003. Reconstruction of the deformed collision zone Between India and Asia by backward motion of lithospheric blocks, *J. Geophys. Res.*, 108(B6), 2285, doi:10.1029/2001JB000661.

Schellart, W.P., Jessell, M.W. and Lister, G.S. 2003. Asymmetric deformation in the backarc region of the Kuril arc, northwest Pacific: New insights from analogue modeling. Tectonics, 22(1047), doi:10.1029/2002TC001473.

Schellart, W.P., Lister, G.S., 2005. The role of the East Asian active margin in widespread extensional and strike-slip deformation in East Asia. Journal of the Geological Society, London 162, 959–972.

Sun, R., and F. Liu, 1995. Crust structure and strong earthquakes in Beijing, Tianjin and Tangshan area. I. P wave velocity structure, Chin. J. Geophys., 38, 599–607.

Tapponnier, P. and Molnar, P., 1977. Active faulting and tectonics in China. J. Geophys. Res. 82, 2905–2930.

Tapponnier, P., Zhiqin, X., Roger, F.,Meyer, B., Arnaud, N.,Wittlinger, G., Jingsui, Y., 2001. Oblique stepwise rise and growth of the Tibet Plateau. Science 294, 1671–1677.

Tatsumi, Y., S. Maruyama, and S. Nohda, 1990. Mechanism of backarc opening in the Japan Sea: Role of asthenospheric injection, Tectonophysics, 181, 299–306.

Tian, Z.-Y., Han, P. & Xu, K.-D. 1992. The Mesozoic–Cenozoic East China rift system. Tectonophysics, 208, 341–363.

Tilmann, F., Ni, J. and INDEPTH III Seismic Team, 2003. Seismic imaging of the downwelling Indian lithosphere beneath central Tibet. Science 300, 1424–1427.

van der Hilst, R.D., Engdahl, E.R., Spakman, W., Nolet, G., 1991. Tomographic imaging of subducted lithosphere below northwest Pacific island arcs. Nature 353, 37–43.

Widiyantoro, S., and Van der Hilst, R.D., 1996. Structure and evolution of subducted lithosphere beneath the Sunda arc, Indonesia, Science, v. 271, p. 1566-1570.

Woodward R.L., Masters G., 1991. Global upper mantle structure from long-period differential travel-times. J. Geophys. Res., 96 (B4): 6351-6377

Xu, Y., F. Liu, J. Liu, and H. Chen, 2002. Crust and upper mantle structure beneath western China from P wave travel time tomography, J. Geophys. Res., 107(B10), 2220, doi:10.1029/2001JB000402.

Yin, A. 2000. Mode of Cenozoic east–west extension in Tibet suggesting a common origin of rifts in Asia during the Indo-Asian collision. Journal of Geophysical Research, 105, 21745–21760.

Yao H, R.D. van der Hilst and M.V. de Hoop, 2006. Surface-wave array tomography in SE Tibet from ambient seismic noise and two station analysis: I– phase velocity maps, Geophys. J. Int. 166, 732–744.

Zang, S.X., Li, C., Ning, J.Y., Wei, R.Q., 2003. A preliminary model for 3-D rheological structure of the lithosphere in North China. Sci.China, Ser. D 46 (5), 461–473.

Zhang, Y., Ma, Y., Yang, N., Shi, W. & Dong, S. 2003. Cenozoic extensional stress evolution in North China. Journal of Geodynamics, 36, 591–613.

Zhao, D., A. Hasegawa, and H. Kanamori 1994. Deep structure of Japan subduction zone as derived from local, regional and teleseismic events, J. Geophys. Res., 99, 22,313–22,329.

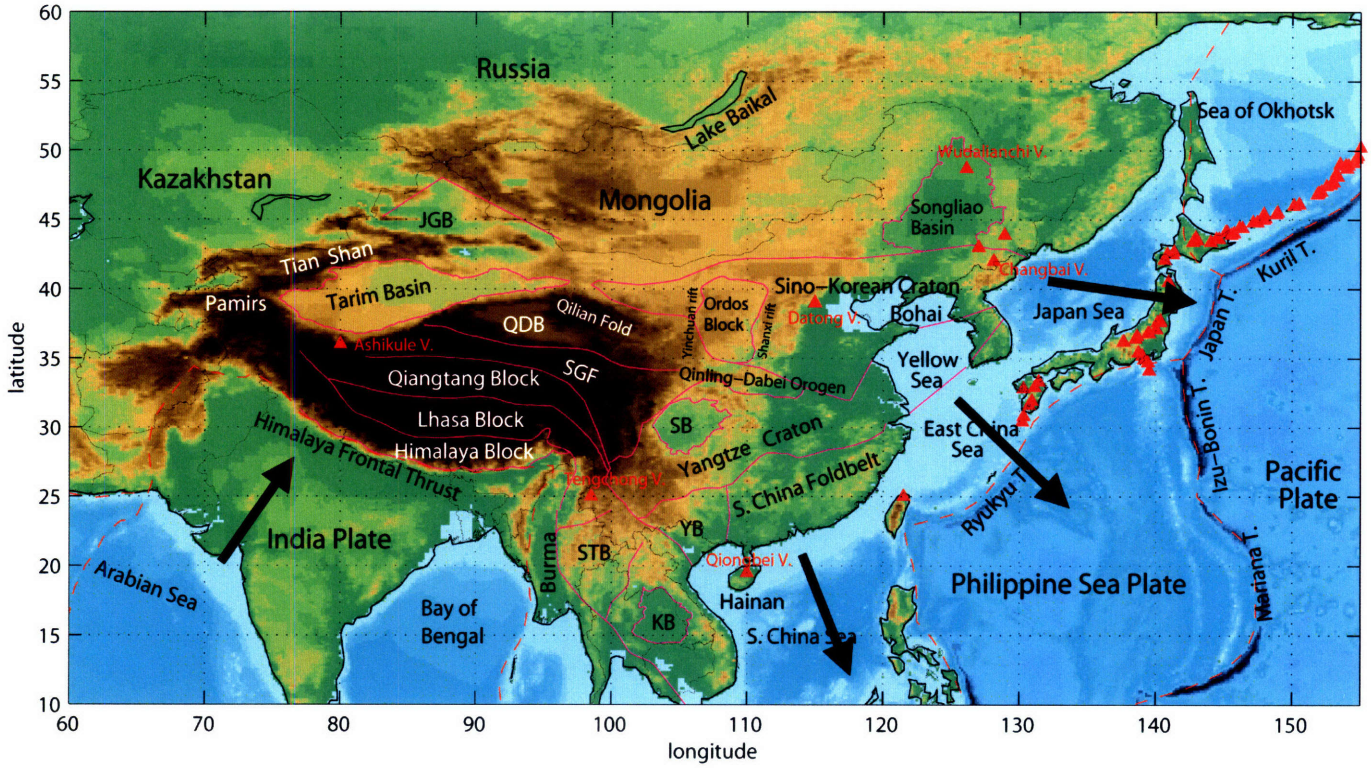

Figure 5-1. The main tectonic elements in East Asia. The dashed red lines are plate boundaries, according to NUVEL-1 (DeMets et al., 1990). The thick purple lines denote main tectonic structures, where SB-Sichuan Basin, KB-Khorat Basin, STB-Shan Thai Block, YB-Youjiang Block, JGB-Junggar Basin, SGF-Songpan Ganzi Foldbelt (modified from Li, 1998 and Tapponnier et al., 2001). The red triangles represent volcanoes. Black arrows depict the continent collision in the west and slab rollback in the east and the southeast form a large scale clockwise rotation in East Asia.

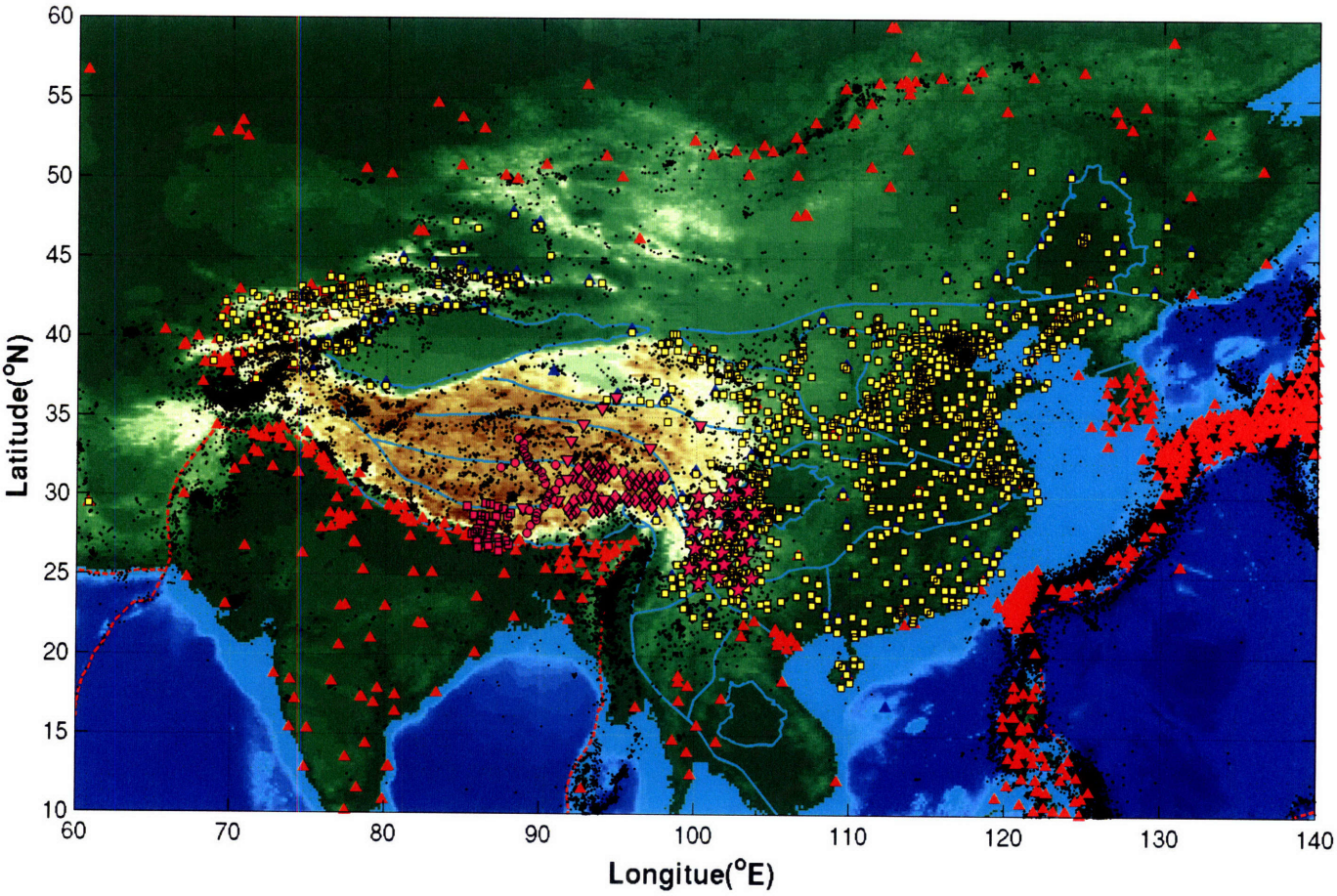

Figure 5-2. Distribution of stations and earthquakes (black dots) in East Asia. Red triangles depict the 1223 stations of the EHB in East Asia, of which about 20 stations are located in the mainland of China. Blue triangles represent about 100 stations of Annual Bulletin of Chinese Earthquakes (ABCE). Yellow squares are about 1200 stations from Chinese Seismic Network (CSN). Magenta samples represent stations from seismic arrays in the Tibetan plateau. From east to west, starts - MIT-CIGMR array (2003-2004); diamond - Lehigh-CIGMR array (2003-2004); inverse triangle - Sino-American array (1991-1993); dots - INDPEHT-II (1994) and INDEPHT-III (1998-1999); squares - Himalayan Nepal Tibet array (2001-2003).

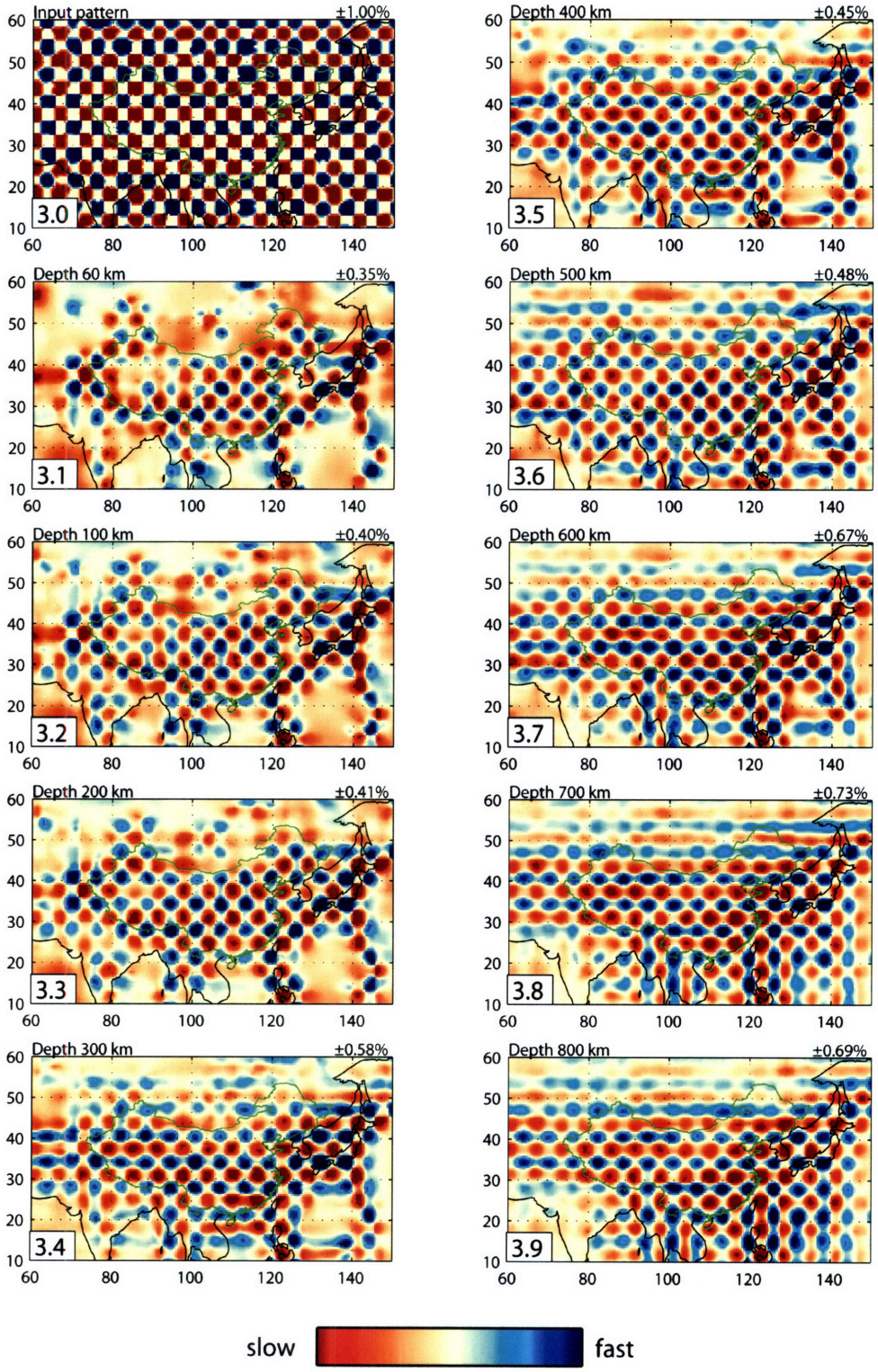

Figure 5-3. Checkerboard resolution test for target anomalies at different depths as indicated in left up corner in each subplot. The color scale is shown in the righ up corner. Input pattern ($3^{o}\times3^{o}$) is shown in 3.0. The green line is the boundary of China and black line represents coast line.

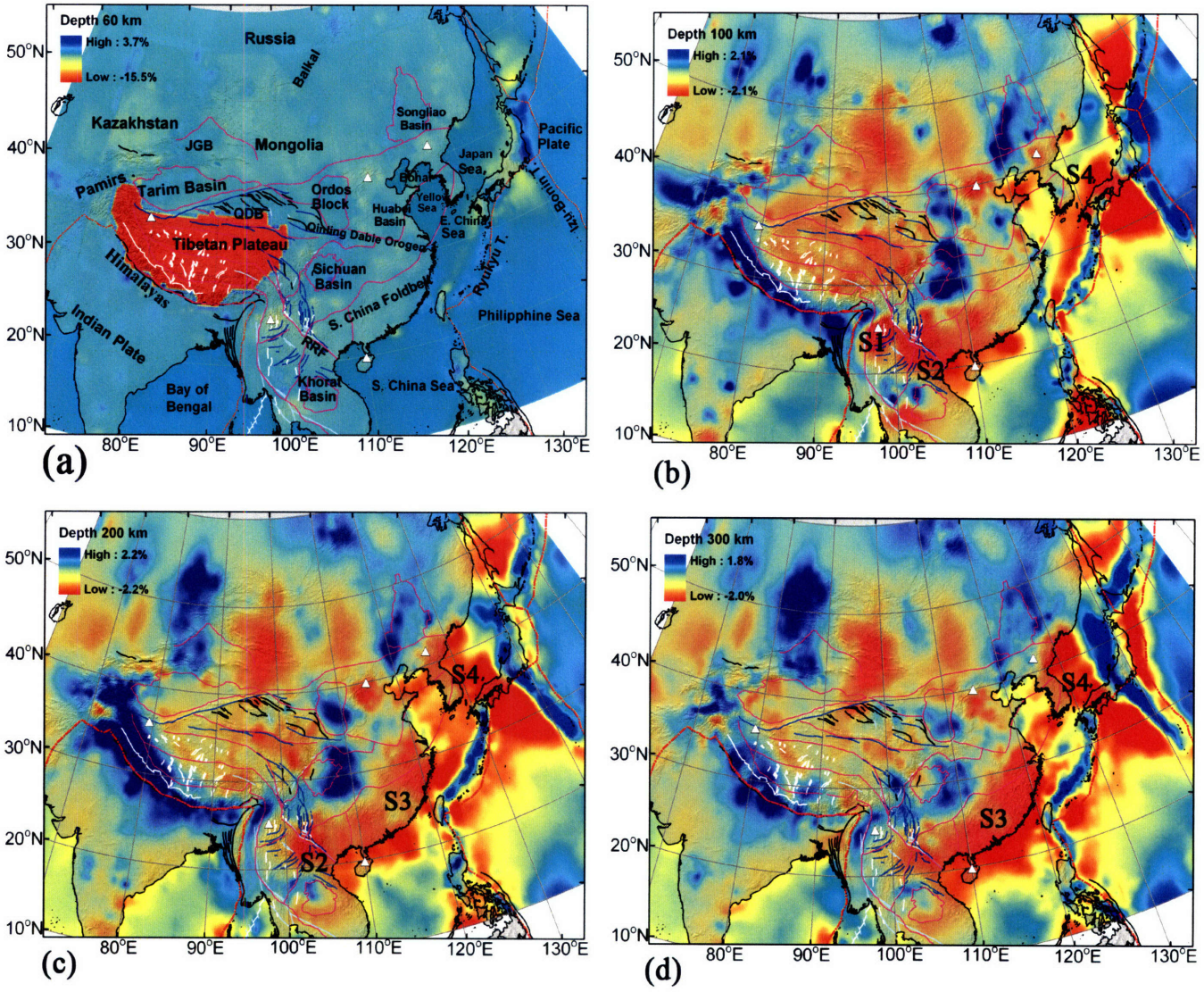

Figure 5-4. Lateral *P* wavespeeds perturbation at each depth layer (relative to the average velocity). The blue and red represent fast and slow perturbation. The depth of each layer and the perturbation scale are shown on the left corner in each subplot. White triangles represent the volcanoes in mainland of China (see Figure 5-1).

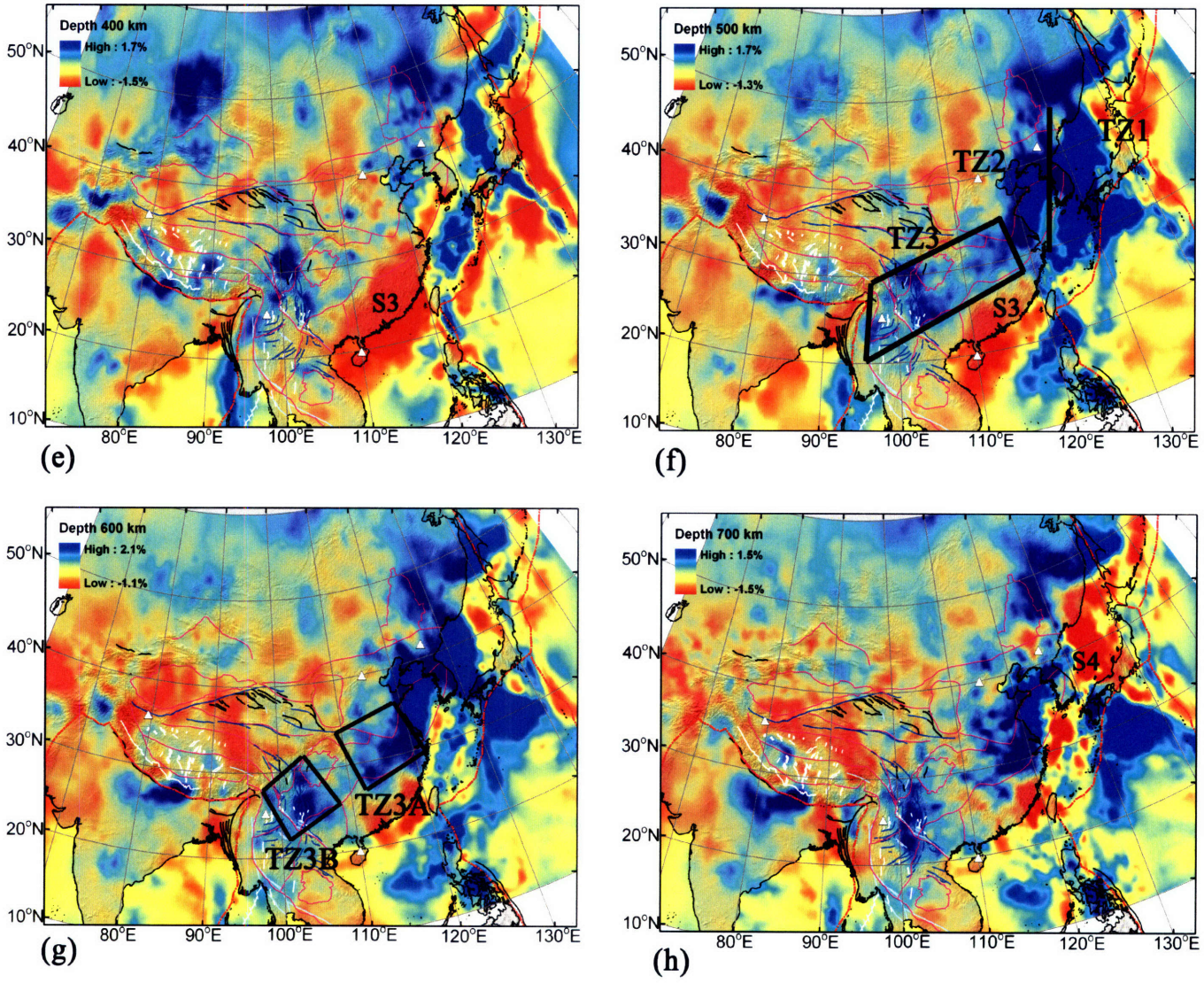

Figure 5-4. (continued)

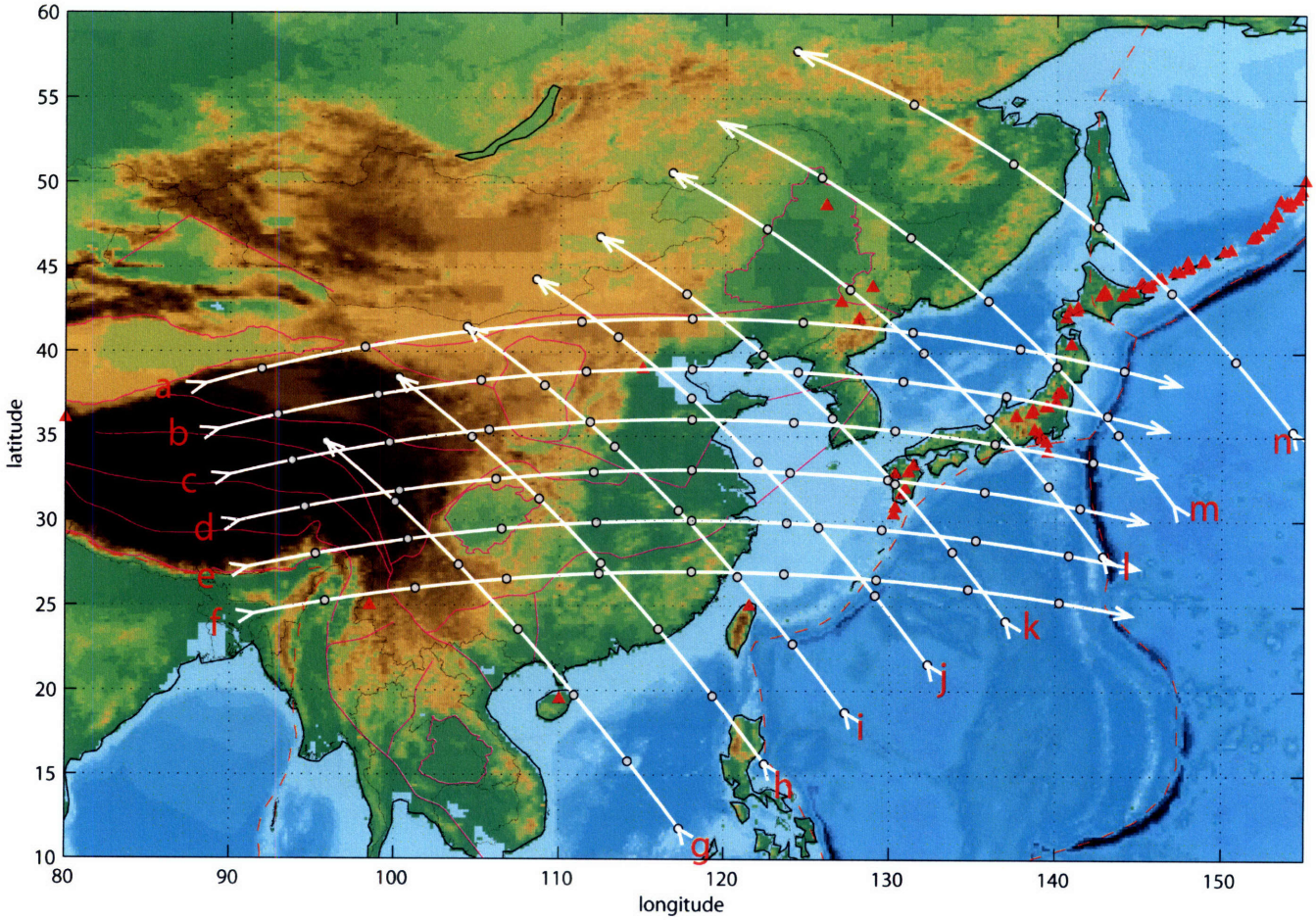

Figure 5-5. The location o vertical cross sections shown in Figure 5-6.

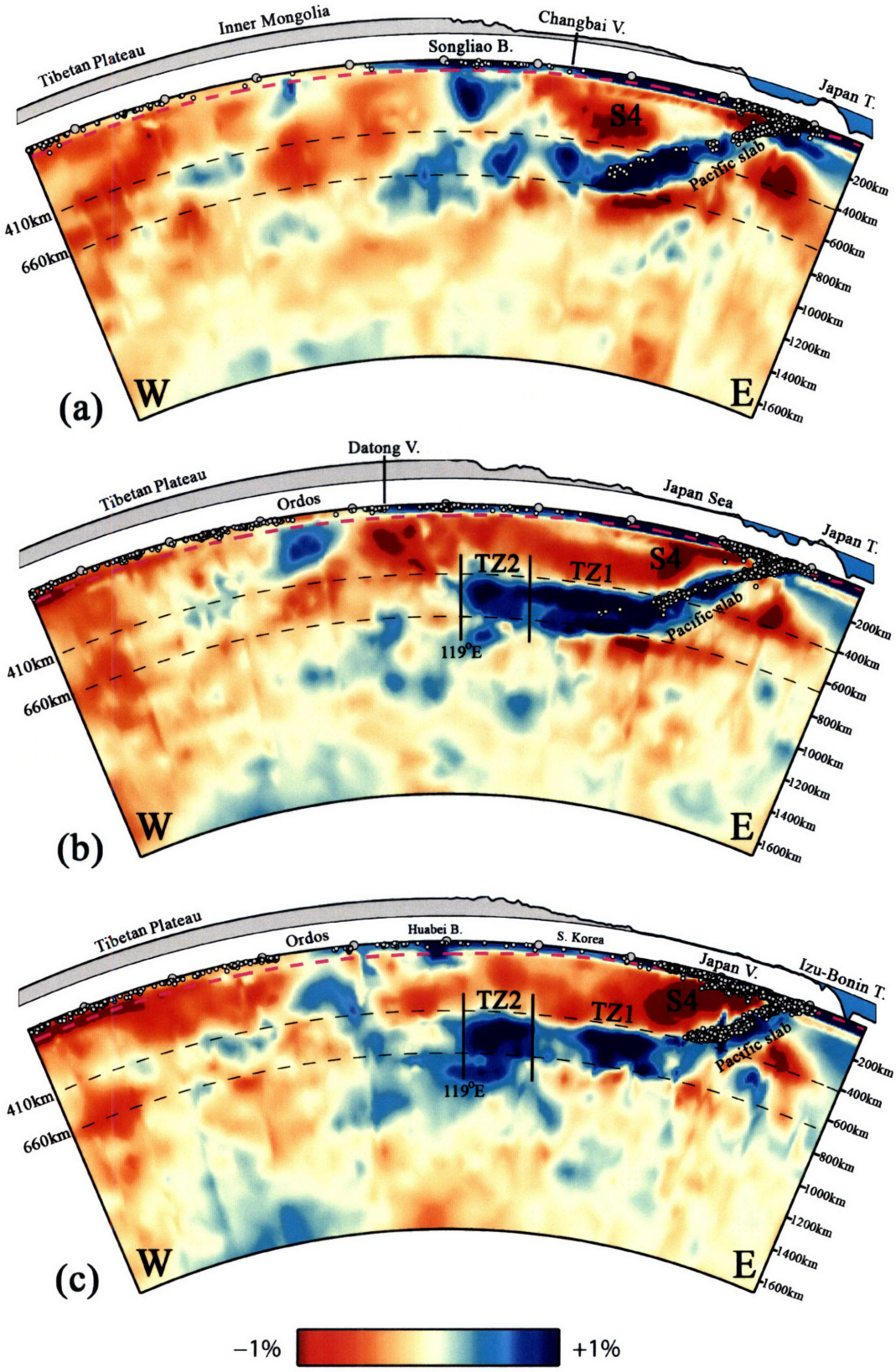

Figure 5-6. The vertical cross sections from the Tibetan plateau to the Pacific Ocean.

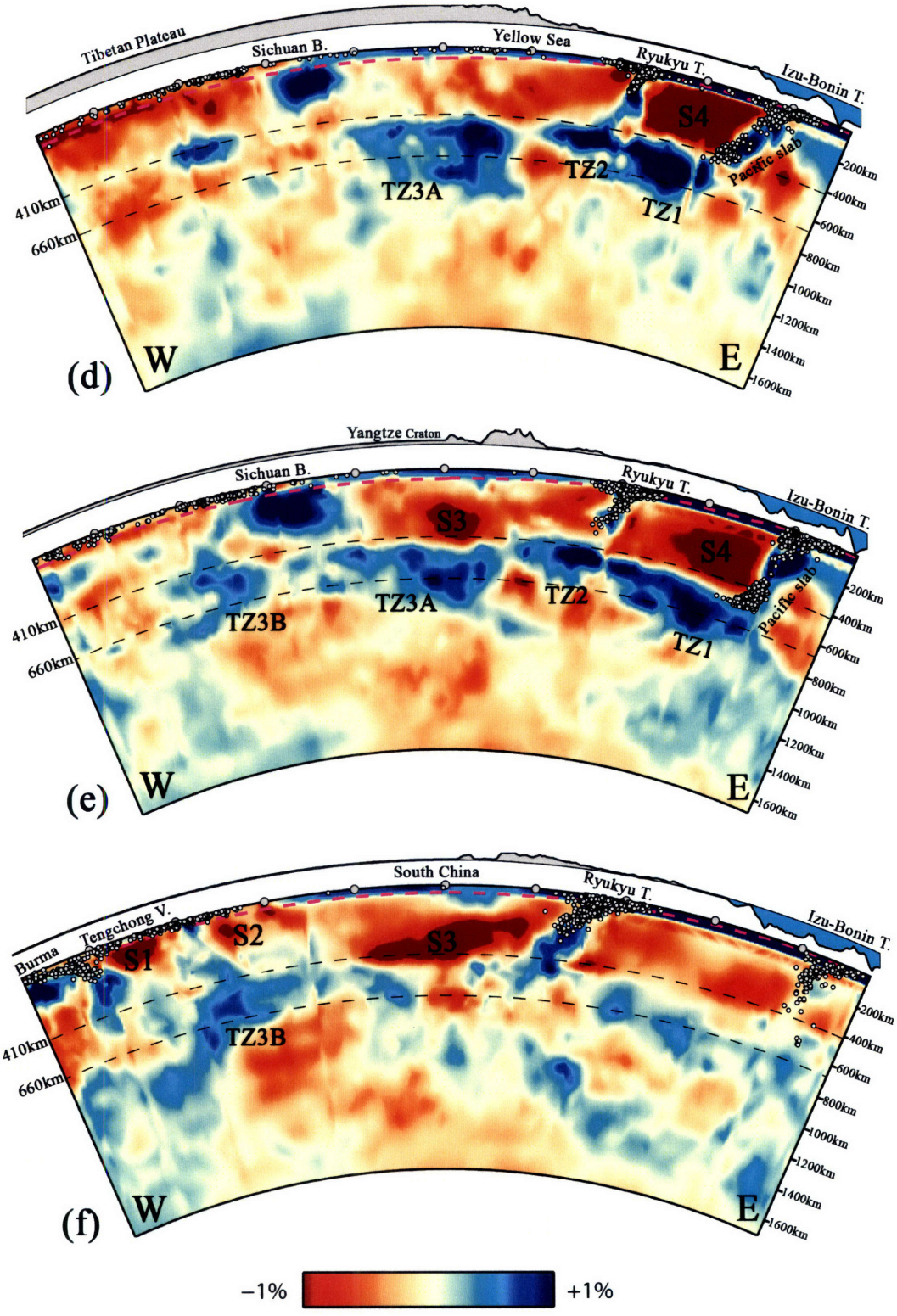

Figure 5-6. (Continued)

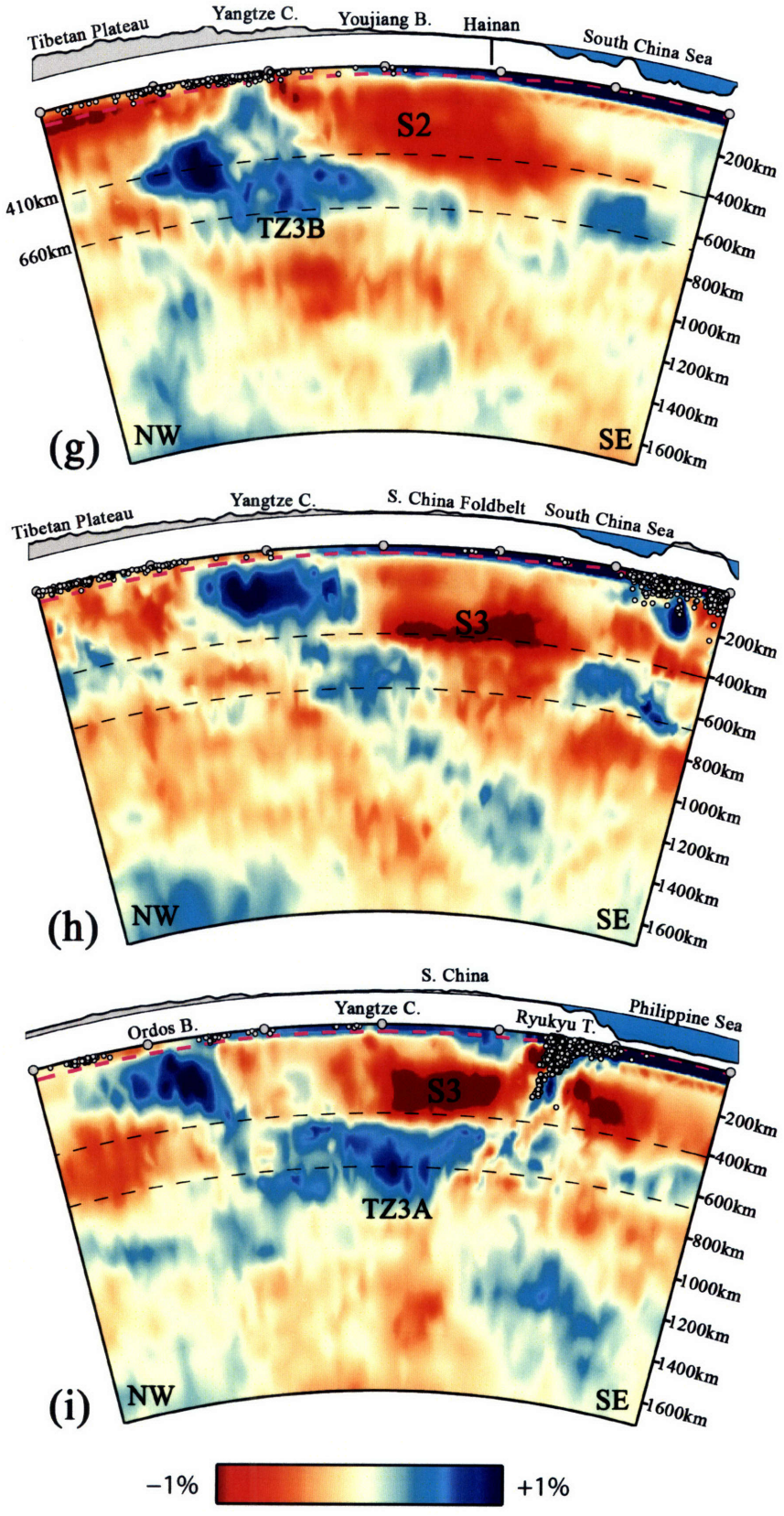

Figure 5-6. (Continued)

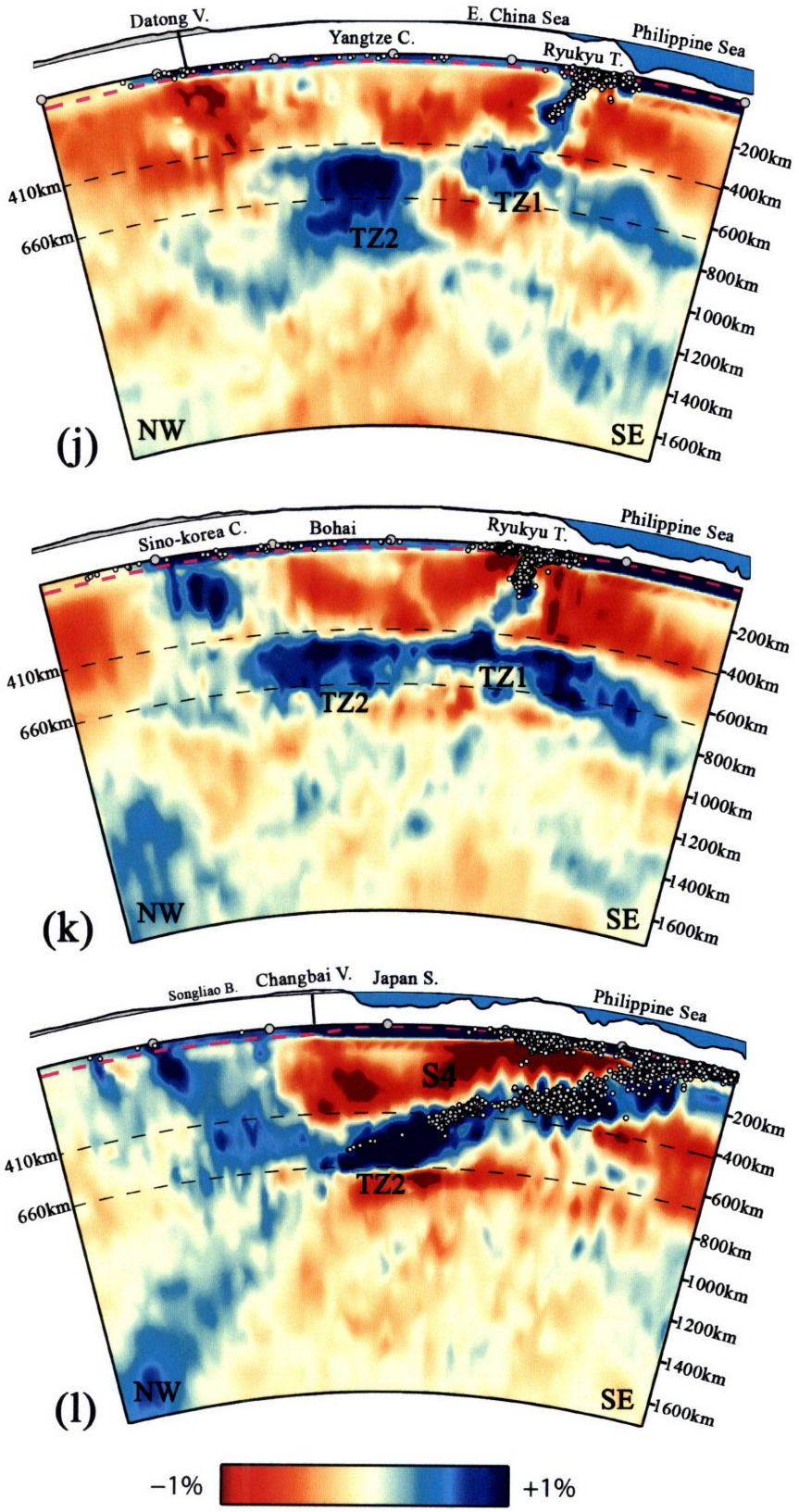

Figure 5-6. (Continued)

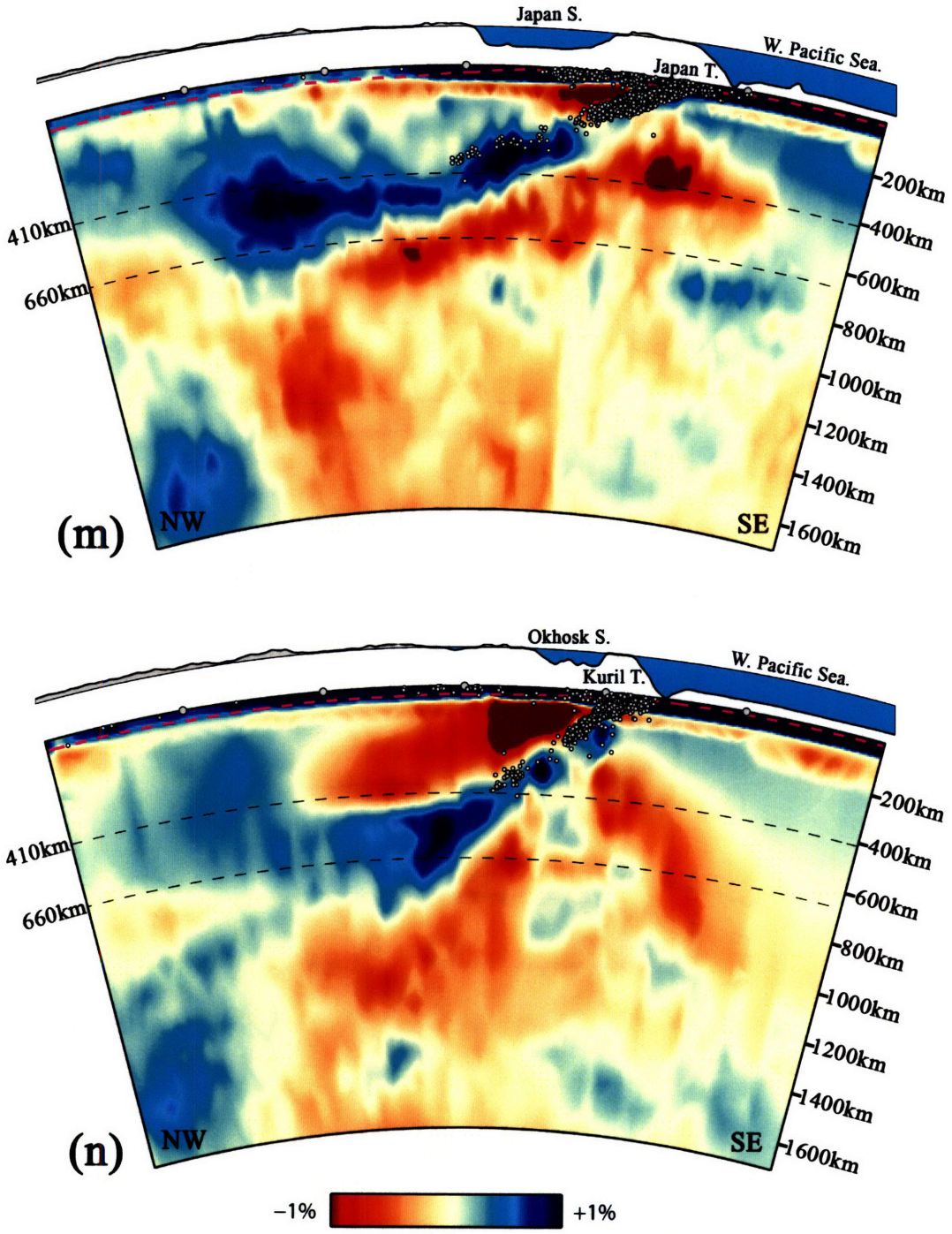

Figure 5-6. (Continued)

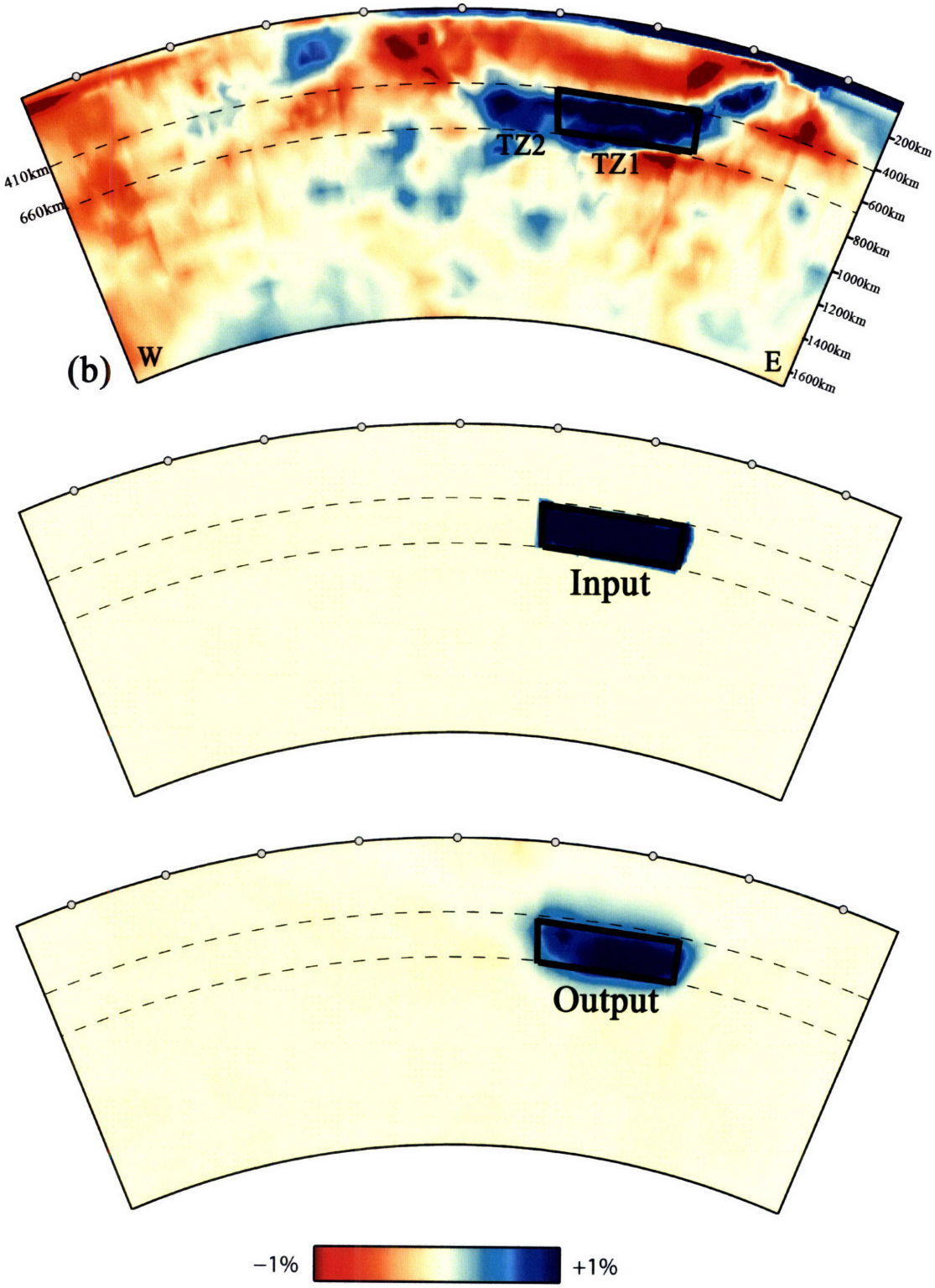

Figure 5-7. Recovery test for the Pacific slab beneath East China in the transition zone.

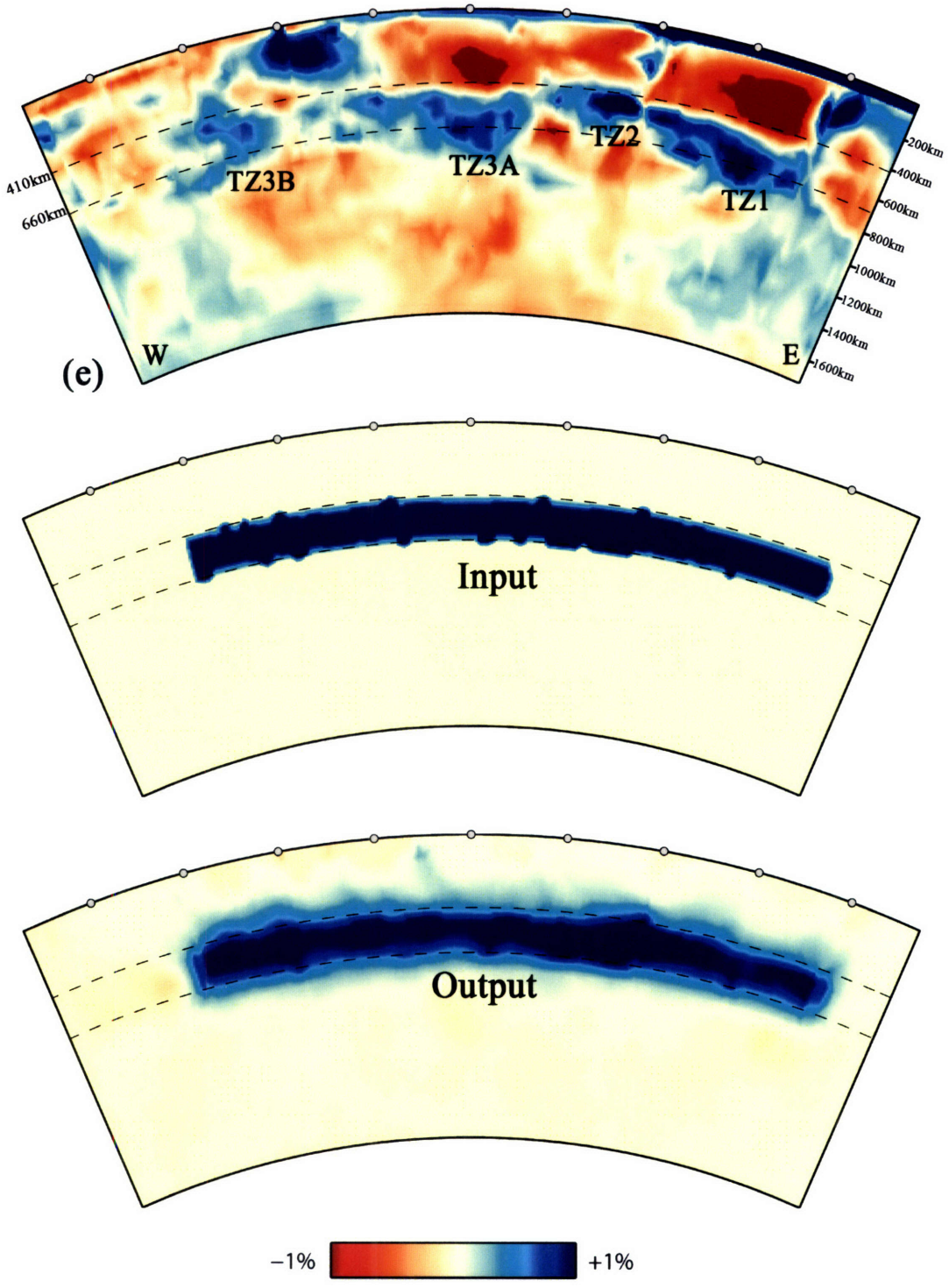

Figure 5-8. Recovery test for the Pacific slab beneath East China in the transition zone.

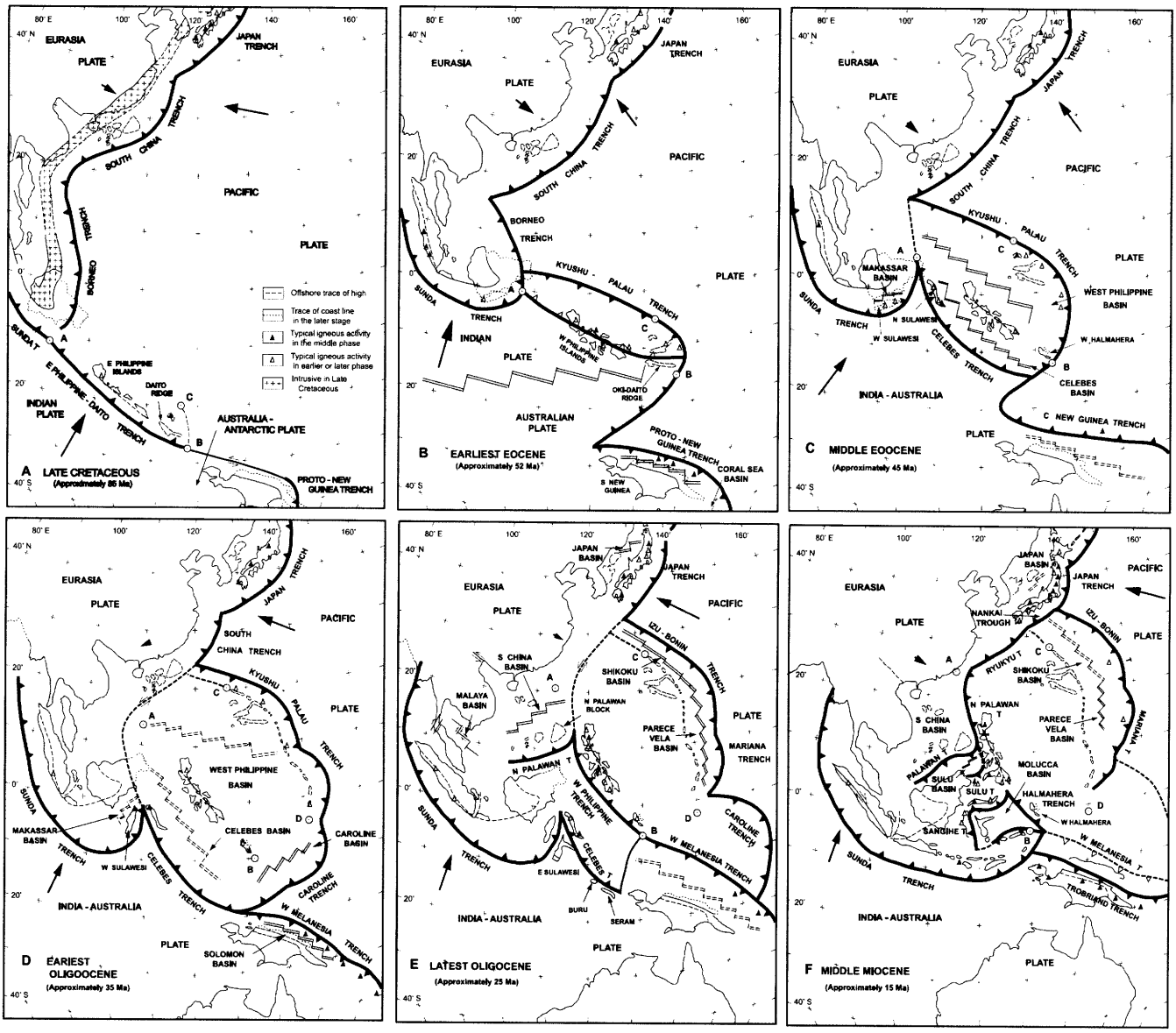

Figure 5-9. Reconstruction of Southeast Asia since the Late Cretaceous (Honza and Fujioka, 2004).

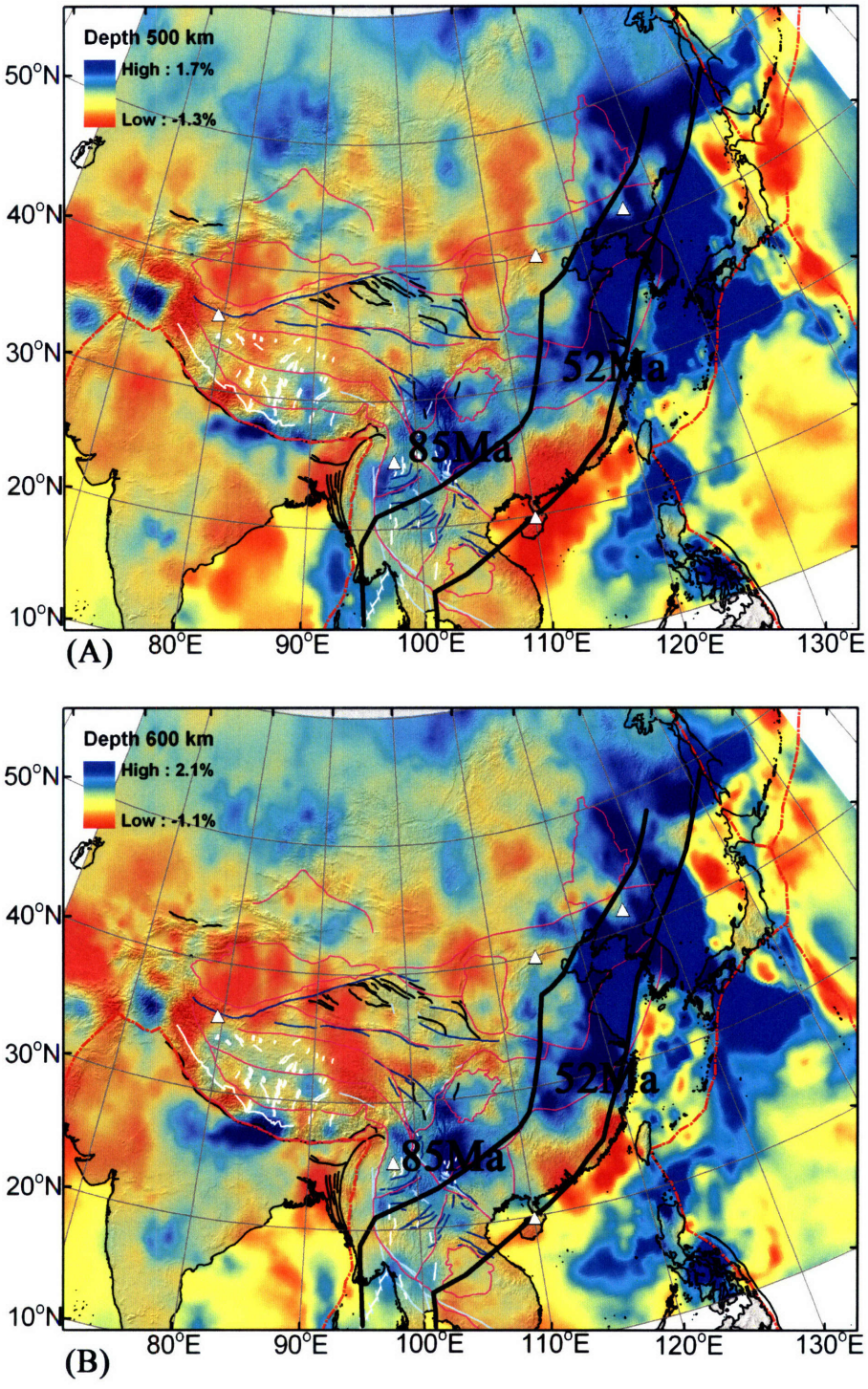

Figure 5-10. The South China Trench and Japan Trench in the Late Cretaceous (~85Ma) and Earliest Eocene (~52Ma) with P-wave velocity perturbations at 500 km depth (A) and 600 km depth (B).

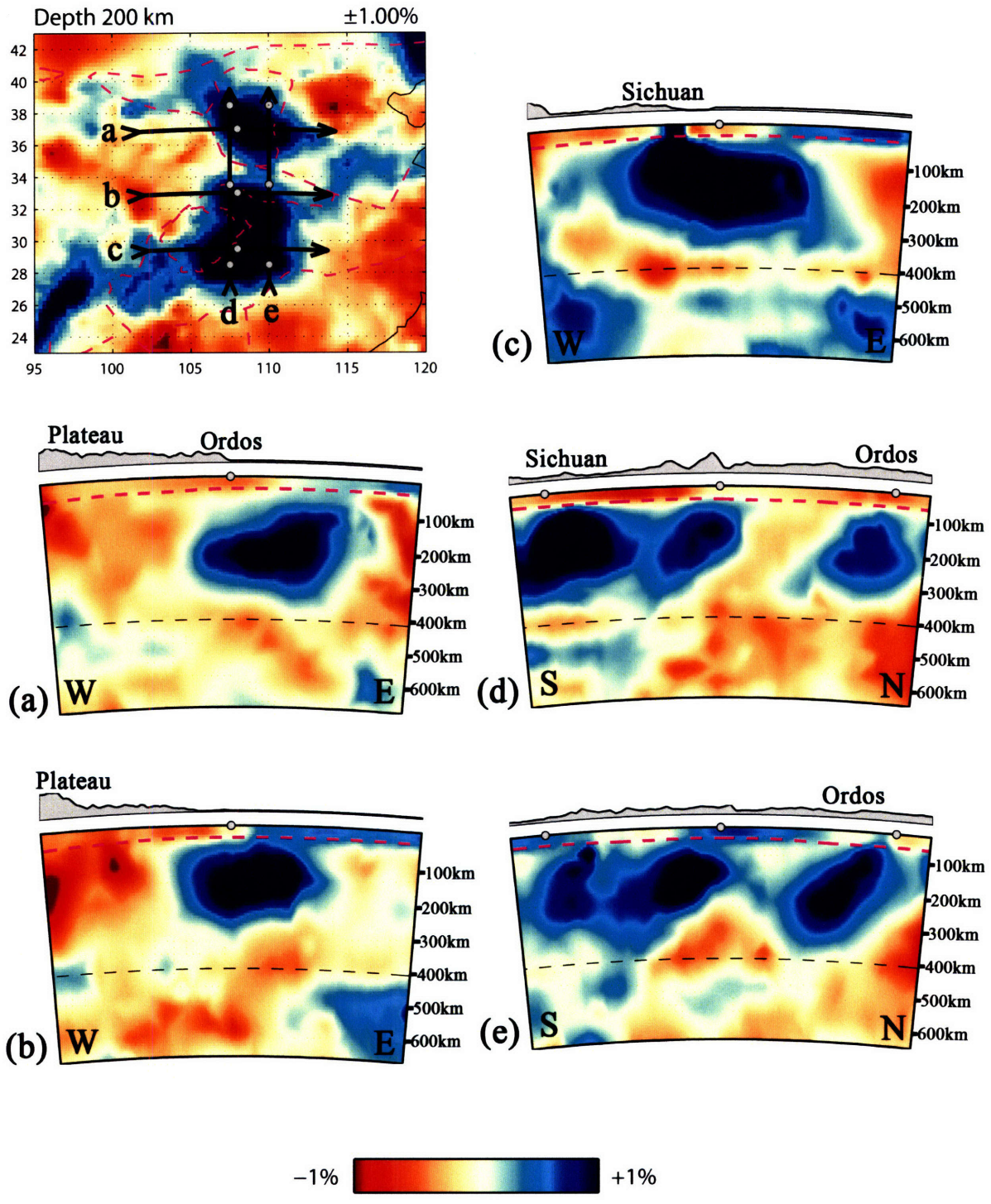

Figure 5-11. High velocity anomalies under the Ordos block and Sichuan Basin.

Chapter 6

Concluding remarks

6.1 Summary

The main objectives of the research presented in this thesis are twofold. The first goal was to develop an approach toward multi-scale (travel time) tomographic imaging of the lithosphere an underlying upper mantle that makes better use of *a priori* information (such as crust structure), that can exploit new, unique data sets, and that is flexible (with regard to addition of such data sets and the availability of new crust models). The second goal was to use this improved capability to construct high resolution 3-D models of mantle structure beneath East Asia and, in particular, Tibet and surrounding regions.

Our approach to high resolution tomography is based on (i) the combined use of a large range of different types of seismic data, both from global catalogs as well as from provincial or temporary seismic networks, (ii) the use of approximate finite frequency sensitivity kernels to account for differences in frequency content and in measurement technique, (iii) the use of an irregular grid with cell-size adapted to sampling density, and (iv) the use of *a priori* information, e.g., on crustal structure from receiver function analysis.

Tomographic imaging of the upper mantle beneath the Tibetan Plateau and East Asia at large has long been hindered by lack of data from seismograph stations in the region. Therefore, an important motivation was to improve image resolution by augmenting existing data sets with data that have hitherto been unavailable for such research. For this effort I have used several unique data sets. First, with automated procedures I picked the arrival time from temporary seismic arrays on or near the Tibetan Plateau. Furthermore, through collaborating with Chinese scientists, I have gained access to a wealth of teleseimic and regional data recorded (since 1967) at ~1200 stations of the Chinese Seismography Network (CSN). With these unique data sets I have obtained a higher resolution model than was previously available.

The large scale geological features and upper mantle structure of East Asia are influenced by two large scale geodynamic systems: the eastward rollback of the subducted slabs beneath the western Pacific and Philippine arcs in the east and the India-Eurasia collision in the west. By delineating upper mantle structures and in combination with results from other lines of research, our tomographic models have provided key constraints on effects and relative roles of these geodynamic systems. The major findings of this research are:

(1) Mantle structure associated with the Indian subduction varies considerably along the strike of the collision zone. From west to east, the dip angle of Indian subduction increases and the distance over which the plate underthrusts the

Tibetan Plateau decreases. In the west, the Indian lithosphere subducts sub-horizontally under the entire western plateau, to as far North as the western margins of the Tarim Basin. In the east, the Indian plate underthrusts the Himalayas and the Plateau as far North as the Bangong-Nujiang Suture (near ~33°N) and subducts steeper into the mantle to at least 400 km depth beneath the plateau. Oblique subduction and changes of dip angle in the central part of the collision zone may cause and determine the location of the north-south trending normal faults in central Tibet.

(2) That – from west to east – the Indian plate underthrusts a smaller fraction of the Tibetan Plateau implies that the lithosphere underlying the central and eastern part of the Tibetan Plateau is of the Asian origin.

(3) Some high velocity materials are detected in the transition zone in the central Himalayas (~85°E), which appear to connect with the Indian subducted lithosphere in the upper mantle with the Mesozoic oceanic slabs in the lower mantle. In the eastern and western Himalayas we do not detect such connections.

(4) At depth larger than 200 km, the subduction under Burma can be distinguished from Indian subduction beneath the eastern Himalayas. A well resolved low wavespeed anomaly beneath the Tengchong area suggests that volcanic activity here is related to back arc processes associated with the Burma subduction and not due to deep mantle processes. In contrast, the anomalously low wavespeeds beneath the Red River Fault system extend much deeper into the

upper mantle and seem more continuous with the slow mantle regions beneath southeastern China and the South China Sea (including the Hainan island).

(5) The variability of the fast polarization directions across the Xianshuihe-Xiaojiang fault system (XXFS), as inferred from shear wave splitting (Lev et al., 2006), occurs above a mantle region with pronounced high velocity anomalies. This suggest that upper mantle heterogeneity between the Sichuan Basin and the Burma ranges causes (or, at least, contributes to) the observed complex anisotropy pattern.

(6) The eastward retreating slabs of western Pacific and Phillipine plates are deflected in the transition zone beneath the Korea, Japan Sea, and East China. Some of Mesozoic subducted slabs have reached as far west as 110°E longitude under the Yangtze Craton, which might have resulted from the Eocene subduction at the South China and Japan trenches. Cenozoic extension, volcanic activity, as well as high heat flow in East China might be related to the widespread low velocity anomalies in the upper mantle induced by the eastward slab rollback of Pacific and Philippine plates and the southward slab rollback of Indo-Australia plate.

(7) Precambrian continental roots under Ordos block and Sichuan Basin, which extend to 250~300 km depth, may form a transition in tectonic regime from the continental collision control in the west to (oceanic) subduction control in the east and southeast. Indeed, the (direct) influence of the India-Eurasia collision on the tectonic evolution of East Asia may be confined to the Tibetan plateau and

vicinity, whereas the stress field and (3-D) upper mantle processes associated with subduction of lithosphere along (retreating) Pacific, Philippine Sea, Java-Sumatra trenches may be prime drives of the tectonic development of SE Asia, including Indochina.

6.2 Future work

A discrepancy remains between inferences about the upper mantle structure beneath the Tibetan plateau either from shear (surface) wave tomography and *P*-wave travel-time inversion (Chapter 4). In contrast to the surface wave models, which suggest relatively fast *S*-wave propagation at 100-200 km depth beneath the Plateau, we find that in this region the upper mantle is characterized by low *P*-wave velocities. In the future, *S*-wave travel-time data from global (EHB) and regional (CSN) catalogs can be used to provide more constraints on the shear wave velocity beneath the Tibetan plateau. Further research is needed to determine if this discrepancy is an artifact (for instance related to the differences in sampling by and resolution of the data types used) or whether an anomalous *P*-*S* ratio is a real feature of the Tibetan upper mantle, for which an explanation (for instance in terms of temperature and composition) must be sought.

Tomographic inversion of the combined data sets has produced tantalizing images of mantle structure beneath East Asia, but further study is needed to understand the inferred mantle heterogeneity in terms of large scale geology and

tectonics or, vice versa, to use the constraints on structure to overhaul or refine models for the tectonic evolution of this large region over long periods of geological time. For example, quantitative investigation of the fast structures in the mantle transition zone under the Yangtze Craton (Chapter 5), in the context of the regional geological and tectonic framework, could provide new constraints on the evolution of subduction below and accretion to East Asia.

Finally, the newly developed methodology can be applied elsewhere, Whereas our approach toward multi-scale (travel time) tomography was developed in the context of MIT's long-term multi-disciplinary studies of Tibetan tectonics, it can, of course, also be applied to improve upper mantle imaging elsewhere in the world. Indeed, we have begun to apply it toward high resolution imaging of the upper mantle beneath North America using USArray data (Burdick *et al.*, 2007).

Reference:

Burdick S., Li C., Martynov V., Cox T., Eakins J., Astiz L., Vernon F.L., and van der Hilst R. D., Travel time tomography with USArray data, EarthScope Workshop, Monterey, CA, 27-30 March, 2007.

Lev, E., Long, M., and van der Hilst, R.D., 2006. Seismic Anisotropy in Eastern Tibet from Shear-Wave Splitting Reveals Changes in Lithosphere Deformation. *Earth Planet. Sci. Lett.*, 251, 293-304.

Appendix1: Tibetan Arrays

MIT-Chengdu Institute of Geology and Mineral Resource (CIGMR) array in 2003-2004; Lehigh-CIGMR array in 2003-2004; Himalayan Nepal Tibetan plateau (HIMNT) array in 2001-2003; International Deep Profile of Tibet and the Himalayas (INDPTH) II and III arrays in 1994 and 1997-1998; French and Chinese array in 1991-1992.

a) Tibetan plateau Broadband Experiment, Nickname Tibet1991, network XC, 11 Broadband stations in [100.2E 88.9E 36.2N 29.2N], centered [93 33], from 1991/07/03 to 1992/07/01.

b) International Deep Profiles of Tibet and the Himalayas II, Nickname INDEPTH II, network XR, 13 Broadband stations in [91.1E 89.1E 30.8N 27.7N], centered [90 33], from 1994/05/28 to 1994/10/21.

c) International Deep Profiles of Tibet and the Himalayas III, Nickname INDEPTH III, network XR, 49 Broadband stations in [91.7E 86.7E 33.8N 30.4N], centered [90 33], two stations (LUMP and ST09) from 1997/07/11 to 1998/07/11 and 49 stations from 1998/07/12 to 1999/06/07.

d) Himalayan Nepal Tibet Experiment, Nickname HIMNT, network YL, 28 Broadband stations in [88.0E 85.2E 29.5N 26.4N], centered [87 28], from 2001/09/01 to 2003/05/01.

e) 2003MIT-China, Nickname 2003MIT-China, network YA, 25 Broadband stations in [103.9E 99.6E 31.0N 24.2N], centered [102 28], from 2003/09/20 to 2004/09/19.

f) Namche Barwa Tibet, Nickname Namche Barwa Tibet, network XE, 48 Broadband stations in [91E 98.4E 28.9N 32N], centered [95 30], from 2003/07/15 to 2004/10/27.

g) Nepal-Himalaya-Tibet Seismic Transect, Hi-CLIMB, network XF, 173 Broadband stations in [89.7E 83.5E 34.1N 27.0N], centered [87 31], from 2002/09/12 to 2002/12/18, and from 2003/05/01 to 2005/08/29, Data is restricted now and didn't be used in this study.